Fernanda Angélica Sala

Protein-protein interactions involved in copper homeostasis, oxidative aging and neurodegenerative disease

Interações proteína-proteína envolvidas na homeostase do cobre, envelhecimento oxidativo e doenças neurodegenerativas.

Sao Carlos
2020

Fernanda Angélica Sala

Protein-protein interactions involved in copper homeostasis, oxidative aging and neurodegenerative disease

Interações proteína-proteína envolvidas na homeostase do cobre, envelhecimento oxidativo e doenças neurodegenerativas.

Thesis submitted to Chemistry Institute of Sao Carlos of the University of Sao Paulo in accordance with the requirements to obtain the degree of Doctor in Science.

Concentration area: Organic and Biological Chemistry

Thesis director: Professor Richard Charles Garratt

Sao Carlos
2020

Assinatura:
Data:

Ficha Catalográfica elaborada pela Seção de Referência e Atendimento ao Usuário do SBI/IQSC

Sala, Fernanda Angélica
Protein-protein interactions involved in copper homeostasis, oxidative aging and neurodegenerative disease / Fernanda Angélica Sala. — São Carlos, 2020.
160 f.

Tese (Doutorado em Química Orgânica e Biológica) — Instituto de Química de São Carlos / Universidade de São Paulo, 2020.

Orientador: Prof. Dr. Richard Charles Garratt

1. Cristalografia de raios X. 2. hSOD1. 3. hCCS. 4. Heterodímeros. 5. Modificações pós-traducionais. I. Título.

Sonia Alves - CRB: 4280/8

ACKNOWLEDGEMENTS

Thank you first to God and the Virgin Mary for making this journey possible.

Special thank you to my mother Josefina and sisters Bruna and Gabriela for the endless love and support.

Huge thanks to Richard for the directions, encouragement, patience and kindness.

To Samar Hasnain and Svetlana Antonyuk, who received me in their laboratory at University of Liverpool during two years. Thank you both for the guidance, support and for trusting my work. Also thank you to Dr. Gareth Wright for the scientific discussions.

I would like to thank all my friends and colleagues from MBG group, with whom I learned a lot from informal daily discussions in the laboratory and shared amazing moments. People who helped make me feel at home: Jiraporn (Mai), Dr. Thanalai (Yin), Varunya (Ploy), Dr. James, Dr. Mike, Dr. George, Dr. Chai, Dr. Thomas, Dr. Kangsa and Noppon.

I also thanks everyone of the Brazilians colleagues in Liverpool for the warm receptions, for teaching me where to find all kinds of Brazilian products, for the coffees, happy hours and fantastic gastronomic adventures. In special to: Edileuza, Louise, Carina, Tatiana and Patrícia.

I am also grateful to all my colleagues and the technicians from the Laboratory of Structural Biology (LBest) in Sao Carlos, for the scientific discussions and friendship: Dr. Susana, Dr. Humberto, Danielle, Tamiris, Diego, Dr. Evandro and Leonardo. Also thanks to professor Otavio for the opportunity to learn a lot about virus like particles and oversee Tamiris during the development of her undergrad project.

To my friends, who either close or distant made my life easier: Vanessa, Nayara, Paola, Daniel (Chiclete), Ivan and Geraldo. Also, I cannot forget to thank Jonathan, for always being there for me since my second day in Liverpool.

The Soleil team for all the support during all the 23 hours collections at Proxima 1 and for helping us setting the most adequate parameters for data collection. Also to the Diamond teams during the remote data collections.

Finally, Fapesp and Capes for the financial support numbers: 2015/00062-1 and 2016/24686-7. CNPq for the grant 407438/2013-0 which allowed the Science without border Fellowship.

“Science is a way of trying not to fool yourself. The principle is that you must not fool yourself, and you are the easiest person to fool.”

Richard Feynman

ABSTRACT

SALA, F. A. **Protein-protein interactions involved in copper homeostasis, oxidative aging and neurodegenerative disease.** 2020. 160p. Thesis (PhD in Science) - Chemistry Institute of Sao Carlos, University of Sao Paulo, Sao Carlos, 2020.

Despite knowledge of human Cu,Zn Superoxide dismutase (hSOD1) importance in many cellular processes, the final stages of hCCS (human copper chaperone for Superoxide dismutase 1) dependent hSOD1 maturation, have never been fully elucidated. This process involves both copper transfer to hSOD1 and disulfide oxidation and understanding it can be critical in the fight against neurodegenerative diseases, as immature forms of SOD1 are typically identified as more prone to aggregation. The main difficulties are in obtaining the transient human heterocomplexes and the behaviour of full length hCCS which is recalcitrant to crystallization due to its highly flexible structure. The objective of this work was to investigate the recognition processes and sequence of activation events during the maturation of hSOD1 catalyzed by hCCS. Protein-membrane association experiments on different combinations of hCCS and SOD1 mutants suggested that copper acquisition occurs via hCCS, in its homodimeric state, engaging with the lipid bilayer and subsequently forming heterodimers with hSOD1 off the membrane. Additionally, complex stability experiments on combinations of hCCS and hSOD1 mutants confirmed that disulphide formation seems to be both the last step in the hSOD1 maturation and the regulator of complex formation with hCCS. Based on this, we chose a set of complexes suitable for crystallographic assays. Heterodimer crystals were obtained using commercial screens and optimized using different techniques. Crystals of heterodimeric complexes which were either hSOD1 apo or holo for copper in complex with hCCS were obtained, processed and analyzed. The analysis of the structures of the heterodimeric complexes showed a novel conformation for the SOD1 disulphide sub-loop which regulates complex formation and dissociation, communicates the presence of hCCS to the hSOD1 active site and coordinates the timing of copper transfer prior to the disulphide bond formation, minimizing the production of potentially toxic hSOD1 species. Once the disulphide bridge is formed, we suggest that the hCCS Ala231 methyl dictates the heterodimer dissociation by steric effects at the interface. As a consequence, hSOD1 (in its copper loaded and disulphide oxidized form) dimerizes to mitigate this repulsion and thereby generates the mature and catalytically active homodimeric species.

Keywords: hSOD1. hCCS. Heterodimer. Post-translational modifications. ALS. Protein crystallography.

RESUMO

SALA, F. A. **Interações proteína-proteína envolvidas na homeostase do cobre, envelhecimento oxidativo e doenças neurodegenerativas.** 2020. 160p. Tese (Doutorado em Ciências) – Instituto de Química de São Carlos, Universidade de São Paulo, São Carlos, 2020.

Apesar do conhecimento da importância da Cu,Zn Superóxido Dismutase humana (hSOD1) em muitos processos celulares, pouco é entendido sobre os estágios finais do seu processo de maturação. Estudos ressaltam a importância da proteína auxiliar hCCS (chaperona de cobre humana para superóxido dismutase 1), que reconhece especificamente a hSOD1 recém traduzida e a ativa através da inserção do íon cobre e da oxidação da ligação dissulfeto. Entender esse mecanismo pode ser decisivo na luta contra doenças neurodegenerativas, já que formas imaturas de SOD1 são tipicamente identificadas como mais propensas à agregação. As principais dificuldades desse estudo estão na obtenção de heterocomplexos, já que eles apresentam um caráter transitório e, no comportamento da hCCS que é descrito como recalcitrante à cristalização devido à sua estrutura altamente flexível. Neste trabalho, nosso objetivo foi investigar os processos de reconhecimento e a sequência de eventos de modificação pós-traducionais durante a maturação da hSOD1 catalisada pela hCCS. Experimentos de associação proteína-membrana utilizando diferentes combinações de mutantes de hCCS e SOD1 sugeriram que a aquisição de cobre ocorre via hCCS, em seu estado homodimérico, interagindo com a bicamada lipídica e, subsequentemente formando heterodímeros com hSOD1 fora da membrana. Adicionalmente, utilizando diferentes combinações de mutantes de hCCS e hSOD1 monitoramos a estabilidade dos heterocomplexos ao longo do tempo. Os resultados confirmaram a hipótese de que a formação da ligação dissulfeto é o último passo do processo de maturação do hSOD1 e o regulador da formação do complexo com hCCS. Com base nisso, um conjunto de complexos foi escolhido para os ensaios de cristalização. Os cristais para os heterodímeros foram obtidos usando *kits* de cristalização comerciais e otimizados usando diferentes técnicas. As estruturas dos heterocomplexos foram obtidas em diferentes estados de metalação para a hSOD1. Nossos resultados mostraram uma nova conformação para o subloop dissulfeto da hSOD1 responsável por regular a formação e dissociação do complexo, comunicar a presença de hCCS ao sítio ativo de hSOD1 e coordenar a dinâmica das mudanças pós traducionais de modo que a transferência de cobre anteceda a formação da ligação de dissulfeto, minimizando a produção de espécies hSOD1 potencialmente tóxicas. Uma vez que a ponte dissulfeto é formada, o heterodímero se dissocia pela presença do grupo metil da hCCS Ala231 que causa repulsão estérica na interface do complexo. Como consequência, a hSOD1 (com o íon cobre e a ligação dissulfeto oxidada) dimeriza para mitigar essa repulsão e, assim, gera as espécies homodiméricas maduras e cataliticamente ativas.

Palavras-chave: hSOD1. hCCS. Heterodímero. Modificações pós-traducionais. ELA. Cristalografia de Proteínas.

LIST OF FIGURES

LIST OF TABLES

LIST OF ABREVIATIONS

µM – Micromolar

β-ME - 2-Mercaptoethanol

Å - Angstroms

Abs – Absorbance

ALS – Amyotrophic Lateral Sclerosis

AMS - 4-acetamide-4′- amleimidylstilbene-2,2′-disulfonic acid, disodium salt

BL21 (DE3) - Bacterial strain for plasmid expression

C/Cys – Cysteine

CHOL – Cholesterol

Cu – Copper

Cu(I) – Copper(I)

Cu(II) – Copper(II)

Cu,Zn hSOD1 – Copper and zinc loaded human Superoxide Dismutase 1

CuCl2 – Copper chloride

D.O. – Optical Density

Da – Daltons

DNA - Deoxyribonucleic acid

DTT – Dithiothreitol

E,Zn hSOD1 – Apo Copper, zinc loaded human Superoxide Dismutase 1

E. coli – Escherichia coli

E/GLU – Glutamic Acid

EDTA-free - Roche complete™ Protease Inhibitor Cocktail

F/Phe – Phenylalanine

fALS - familiar variants of Amyotrophic Lateral Sclerosis

Fe – Iron

G/Gly – Glycine

hCCS - Human Copper chaperone for Superoxide Dismutase 1

His-tag – Histidine hex peptide

HPLC - High Performance Liquid Chromatography

hSOD1 – Human Superoxide Dismutase 1

$hSOD1^{SH}$ - Human Superoxide Dismutase 1 Cysteine 57 and cysteine 146 reduced

$hSOD1^{SS}$ - Human Superoxide Dismutase 1 Cysteine 57 and cysteine 146 oxidized

IPTG – Isopropyl β- d-1-thiogalactopyranoside

K/Lys – Lysine

Ka – Association Constant

Kd – Dissociation constant

L/Leu - Leucine

LB – Lysogeny Broth

MBG – Molecular Biophysics Group

mM - Milimolar

Mm – millimetre

Mn – Manganese

N/Asp – Asparagine

NaCl – Sodium Chloride

H/his – Histidine

nM – Nanomolar

P/Pro – Proline

PC – 1,2-Dipalmitoyl-sn-glycero-3-phosphocholine

PCTP – sodium propionate, sodium cacodylate, and BIS-TRIS propane in the molar ratios 2:1:2, respectively

PDB – Protein Data Bank

PEG – Polyethylene Glycol

pET14b - Bacterial expression vector

pETM11 – Bacterial expression vector

PMSF - phenylmethylsulfonyl fluoride

POPS – 1-palmitoyl-2-oleoyl-sn-glycero-3-phospho-L-serine

Q/Glu – Glutamine

R/Arg – Arginine

RI – refractive Index

Rosetta (DE3) – Bacterial strain for plasmid expression

S/Ser - Serine

SDS-PAGE – Sodium dodecyl sulphate polyacrilamide gel electrophoresis

SEC – Size exclusion chromatography

SLS – Static Light Scattering

SOD1 – Superoxide Dismutase 1

T – Temperature

T/Tyr – Tyrosine

TCEP - tris(2-carboxyethyl)phosphine

TEV - Tobacco etch virus

Tm - Melting temperature

TRIS – Tris(hydroxymethyl)amino methane

UV – Ultra-Violet

V/Val - Valine

Ve – Elution volume

Wt – Wild type

yCCS – Yeast Copper chaperone for Superoxide Dismutase 1

ySOD1 – Yeast Superoxide Dismutase 1

$ZnCl_2$ – Zinc chloride

λ – wavelength

ρ – Density

SUMMARY

1 The Superoxide Dismutases (SODs)

The superoxide dismutases (SODs) are divided in three classes which present different folds and metal ion content. The first is the MnSODs/ FeSODs, also known as SOD2, found in the mitochondria matrices of eukaryotes and cytoplasm of bacteria (SMITH; DOOLITTLE, 1992). Another evolutionary distinct form only recently discovered is the Nickel SODs, which is largely prokaryotic (YOUN *et al.*, 1996). The last one is the Cu,Zn SODs, also termed SOD1, which occurs in eukaryotes and some prokaryotes.

All these classes share in common as their enzymatic activity the disproportionation reaction of the superoxide radical. However, they are very different in terms of amino acid sequence and three-dimensional structure and can be found in both intracellular and extracellular locations (ROBINETT; PETERSON; CULOTTA, 2018).

Over the 80 years, since the first report, SODs have been attracting extensive interest. Almost 500 new publications come out every year, reflecting their relevance (WRIGHT; ANTONYUK; HASNAIN, 2019). Here, we will focus our work on the human Cu,Zn SOD, which is expressed in almost all cells. The enzyme is well-characterized and found predominantly in the cytosol with a smaller fraction in the mitochondrial periplasmic spaces, but also in lysosomes, peroxisomes and nuclei. It is expressed in almost all human cells and comprises 0.5% of total protein in some tissues, underscoring its biological importance (CHANG *et al.*, 1988; OKADO-MATSUMOTO; FRIDOVICH, 2001; WEISIGER; FRIDOVICH, 1973).

We will start this work describing its story, structure-based breakthroughs, maturation mechanism and linkage with ALS (Amyotrophic Lateral Sclerosis).

1.1 Ubiquitous Cu,Zn SOD

In 1938, Thaddeus Mann and David Keilin described the isolation of a bovine erythrocyte protein which displayed a blue colour. The protein was around 31.5 kDa in size and contained two copper ions and was called hemocuprein (MANN; KEILIN, 1938). During the 1950s homolog proteins were purified from human erythrocytes

and brain, but no function could be ascribed, thus it was thought to act as a copper storage molecule (MOHAMED; GREENBERG, 1954). Only in 1969, after almost 30 years of its discovery, McCord and Fridovich (MCCORD; FRIDOVICH, 1969) renamed the protein as Superoxide dismutase (SOD) after proposing that SOD1 catalysed the dismutation of the superoxide anion into hydrogen peroxide and oxygen by redox cycling of copper, according to the two step reaction shown below:

$$O_2^{\bullet-} + \text{SOD-Cu(II)} \rightarrow \text{SOD-Cu(I)} + O_2 \quad (1)$$

$$O_2^{\bullet-} + \text{SOD-Cu(I)} + 2H^+ \rightarrow \text{SOD-Cu(II)} + H_2O_2 \quad (2)$$

The metal cofactors catalyze both an oxidation and a reduction of superoxide molecules (see first and second step, respectively) turning two separate superoxide anions into O_2 and H_2O_2. The redox cycling reaction is accompanied by a change in metal coordination at the metal binding site. Even though the disproportionation of superoxide is a fast reaction under typical conditions (5x 10^5 $M^{-1}s^{-1}$), SOD1 accelerates the reaction by four orders of magnitude (FETHEROLF *et al.*, 2017a), reaching rates that approaches the diffusion limit (~10^9 $M^{-1}s^{-1}$) (MCCORD; FRIDOVICH, 1969).

Not long afterwards, zinc was described to be also present in the cuproprotein, establishing the Cu,Zn SOD as a bimetallic enzyme (CARRICO; DEUTSCH, 1970). The biochemical and biophysical characterization of human and bovine SOD1 started in the early 1970s and indicated that SOD1 was a dimer composed of two identical sub-units of 16 kDa with high dimer association affinity (HARTZ; DEUTSCH, 1972; KEELE; MCCORD; FRIDOVICH, 1971).

In 1982 the first crystallographic structure was obtained for the enzyme from bovine erythrocytes at 2.0 Å resolution, PDB ID 2SOD (TAINER *et al.*, 1982). For wild-type human hSOD1 (hSOD1), the first structure was described at 2.5 Å resolution in 1992 (PDB ID 1SOS) (PARGE; HALLEWELL; TAINER, 1992) followed years later by a 1.07 Å atomic resolution structure of wild-type native human hSOD1 (PDB ID 2C9V) (STRANGE *et al.*, 2006). The following section will discuss in detail the structure of hSOD1.

1.1.1 Human SOD1 structure and mechanism

The superoxide radical ($O_2^{\bullet -}$) is a physiological by-product of the electron transport chain. In mammals, around 2% of the daily consumed oxygen is released to the intracellular environment as oxidative species, such as: peroxides, hydroxyl radical, singlet oxygen and alpha-oxygen. The superoxide is the precursor of most of the other oxygen species and leads to cell dysfunction and necrosis, without the participation of the human superoxide dismutase neutralizing it (TYLER, 1975). The mature form of hSOD1 is a homodimer with a dissociation constant of 2.2 nM (BROOM *et al.*, 2015; WILCOX *et al.*, 2009) and is 32 kDa in size. Each monomer has 153 amino acid residues, one copper and one zinc ion bound.

Structurally it is composed of seven loops and eight antiparallel beta-sheet strands which fold together to form a Greek-key β-barrel motif. Two loops are particularly important: the zinc loop or loop IV (amino acid residues 50-83) and the electrostatic loop or loop VII (amino acid residues 121-142). The first contains all residues responsible for coordinating the zinc ion and Cys57 which anchors this loop to the β-barrel via a disulphide with Cys146. The second contains charged amino acids residues responsible for the guidance of the substrate towards the active site (Figure 1). These two loops have been described as the protective loops safeguarding the beta sheet structure from self-association (BERTINI; MANGANL; VIEZZOLI, 1998; PARGE; HALLEWELL; TAINER, 1992; TAINER *et al.*, 1982).

Figure 1 - The structure of human SOD1 - PDB ID 2C9V. Loop VII and loop IV are coloured in blue and red, respectively. Disulphide bond between Cys57-Cys146 is depicted as yellow sticks. The zinc and copper are shown with gray and orange spheres, respectively. The structure shows double occupancy at the copper site, copper is coordinated as Cu(I) and Cu(II).

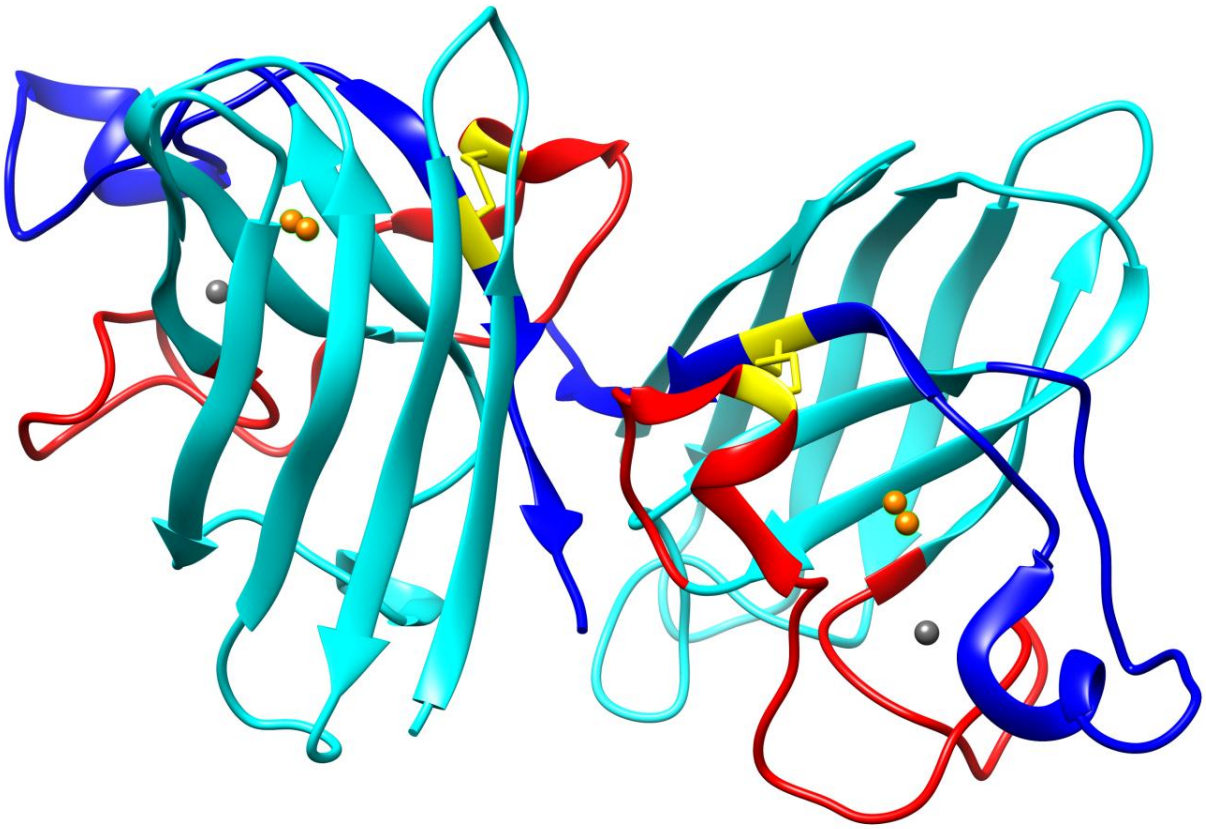

Source from: Own authorship.

The presence of an intra-disulphide bond between Cys57 and 146 (highlighted in Figure 1 as yellow in sticks) is critical for the integrity of the dimer interface, via stabilization of loop IV (the zinc loop, in red) and thereby shifting the equilibrium toward stable dimer. (CULIK *et al.*, 2018; HÖRNBERG *et al.*, 2007; LINDBERG *et al.*, 2004). Moreover, it is conserved among all wild type SOD1 structures published to date; highlighting its importance. Copper and zinc bind sites are in close proximity (6 Å) and bridged by the imidazole ring of Histidine 63 (Figure 2).

Figure 2 - Copper and zinc binding sites in hSOD1. Copper and zinc are represented as spheres in orange and gray, respectively. (A) The active site in oxidized hSOD1 (Cu(II)) shows copper bound in a distorted pyramidal tetragonal geometry. (B) hSOD1 active site in the reduced state (Cu(I)) where copper is no longer bound by the His63 and assumes a planar trigonal geometry (PDB ID 2C9V).

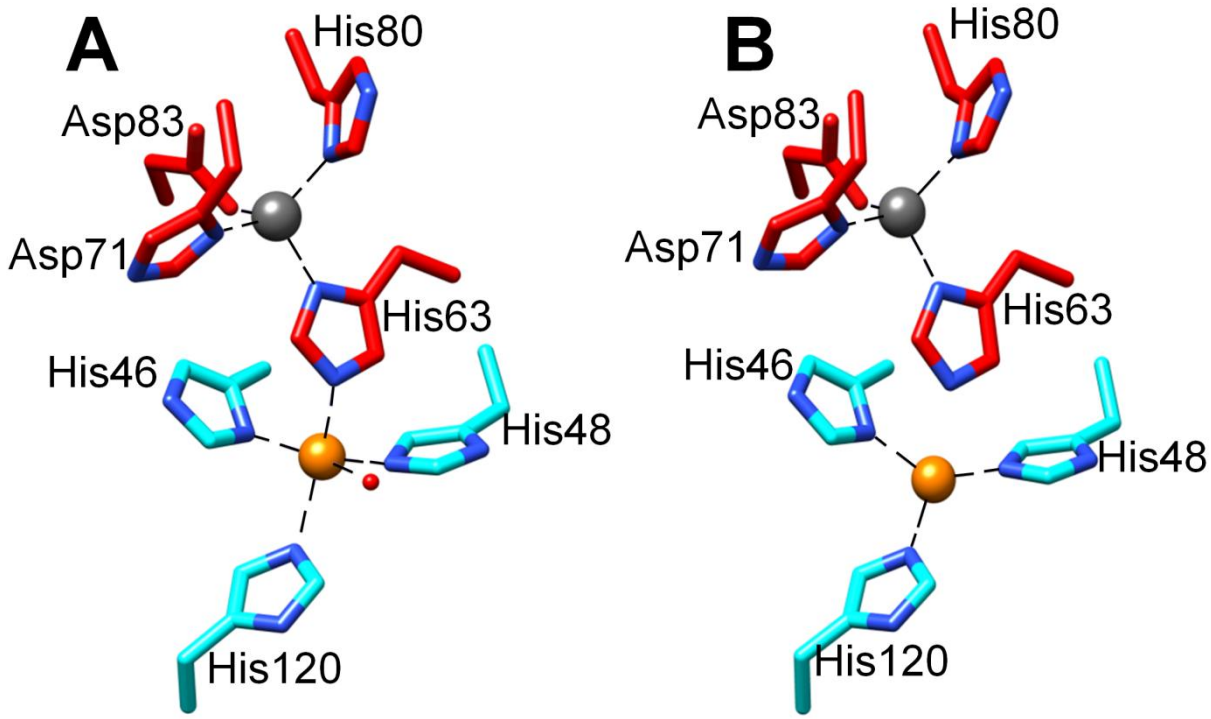

Source from: Own authorship.

Copper can be found in two different coordination and geometries depend on its oxidative state (Figure 2 A and B). Cu(II) is bound in a square pyramidal structure coordenated to His46, 48, 63, 120 and a water molecule in the axial position. Once reduced, after the first step of superoxide catalysis, the reduced copper, Cu(I), moves 0.9 Å towards His120, breaking the bridge with His63 and resulting in a triangular planar conformation with His46, 48 and 120.

In spite of copper oxidation state, zinc remains bound by His71, His80, Asp83 and His120 in a distorted tetrahedral geometry. Although the zinc cofactor is not essential as is copper for hSOD1 activity, its coordination with the histidyl imidazole, of residue 63, assists in the proton transfer during the second step of catalytic mechanism and accounts for the large pH independence of hSOD1 activity (PANTOLIANO *et al.*, 1982). The zinc also plays a structural role increasing thermal stability (ROBINETT; PETERSON; CULOTTA, 2018). This coordination geometry of

the two metals which are spatially close and bridged by a single side chain appears to be unique in metalloproteins (RAKHIT; CHAKRABARTTY, 2006).

The active site in hSOD1 is outside the β-barrel, located between loops IV and VII. Arg143 projects toward the active site channel and is critical in guiding the superoxide anion towards the copper site. The mutation Arg143Lys causes a decrease in hSOD1 activity by half, despite preserving the formal charge on the side chain. On the other hand the substitution by negatively charged residues at this position caused a 100 fold decrease. Together with Arg143, Thr137, Glu133 and Glu132 on the other side of loop IV generate a mixture of positive and negative charges responsible for the electrostatic guidance of superoxide to the active site (GETZOFF et al., 1983) (Figure 3).

Figure 3 - hSOD1 catalytic site. (A) Structure of human hSOD1- PDB ID 2C9V. The residues considered important for enzymatic activity are coloured in yellow and represented in full as sticks. Zinc and copper are in spheres coloured as gray and orange, respectively. Loop IV and loop VII are coloured in blue and red, respectively. (B) The dimer is shown with the same orientation as in (A). The columbic surface was generated with Chimera. Negatively and positively charged areas are coloured in red and blue, respectively. The active site positive charge enhances electrostatic guidance of superoxide to the copper centre, as indicated by the yellow arrows.

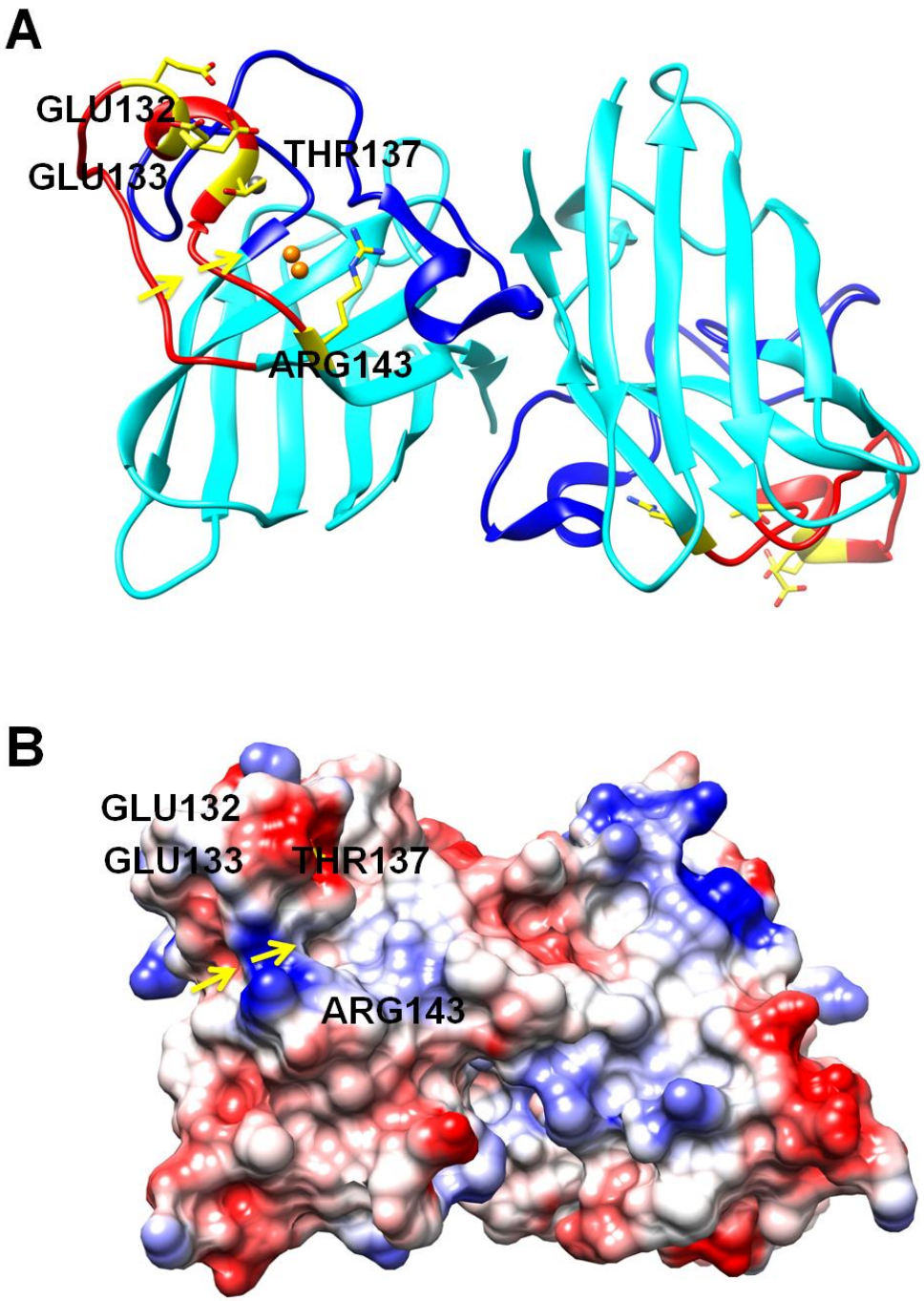

Source from: Own authorship.

The Zinc is completely buried, and copper has a solvent-exposed surface of roughly 5 $Å^2$. The residues Thr137 and Arg143 in the bottom of the active site sterically block any large particle incoming to the catalytic site (Figure 3). The shape of the active site cavity is such that the only access is via the lateral positively charged open channel (Figure 3 B). The residues that form the border of this cavity are highly conserved amongst Cu,Zn SOD1 (TAINER *et al.*, 1983).

However, even though the Zn, Cu hSOD1 disulphide oxidized form is a homodimer, each subunit works independently, so why is the enzyme a dimer? Studies have shown that mutations of Phe50 and Gly51 to Glu are efficient in disrupting the dimer interaction and produce a monomeric, soluble hSOD1. This species has a decrease in its enzyme activity, most likely due to reorientation of charged amino acids surrounding the active site channel, which decreases its positive charge, therefore affecting its electrostatic potential and ability to attract de superoxide radical (BANCI *et al.*, 1998).

Biophysical experiments have demonstrated that the full mature hSOD1 homodimer, which means copper and zinc metalated and disulphide oxidized (^{SS}), is one of the most stable enzymes known, with a melting temperature (Tm) higher than 92 °C. Interestingly, once the copper is lost the E,Zn-hSOD1^{SS} its melting temperature is decreased to 74 °C. Moreover, when the disulphide is reduced (^{SH}) the Tm drops to a value of 58 °C probably due to an increase in the entropy of loop IV from residues 50-61, which favours the monomerization (FURUKAWA; O'HALLORAN, 2005; STATHOPULOS *et al.*, 2006; VASSALL *et al.*, 2011). As a result, metallation, disulphide oxidation or both act by shifting the equilibrium towards the formation of the dimeric species (CULIK *et al.*, 2018; HÖRNBERG *et al.*, 2007; LINDBERG *et al.*, 2004).

In this way, to reach the mature form hSOD1 requires: copper and zinc binding, disulphide formation and dimerization. Disruption of any step results in enzyme inactivation. The first step in hSOD1 maturation appears to be the zinc incorporation. This metal is not considered to be as harmful to cells as copper or iron, and its concentration is of the order of 10^5-10^8 molecules per cell and there is a vast abundance of zinc metalloproteins. Thereby zinc ions are not expected to be delivered by metallochaperones. Even though its incorporation into hSOD1 is still unknown, it is presumably via a free diffusion process (BANCI *et al.*, 2012a, 2013a; MACDIARMID, 2000; OUTTEN; O'HALLORAN, 2001; SUHY *et al.*, 1999).

On the other hand, in general, metalloproteins that require copper and/or the oxidation of a disulphide bond usually acquire them through interactions with accessory proteins. For human hSOD1, the human copper chaperone for hSOD1 (hCCS) facilitates this process. Although the CCS-dependent mechanism for hSOD1 maturation has been extensively studied, many of the details are still not well understood (BANCI *et al.*, 2012b; CULIK *et al.*, 2018; FETHEROLF *et al.*, 2017b; FURUKAWA; O'HALLORAN, 2006). In the following sections, we will examine the importance of copper homeostasis, the hCCS structure and what is currently known about the mechanism of maturation of hSOD1 as catalyzed by its metallochaperone.

1.2 hCCS catalysis hSOD1 maturation

1.2.1 Copper metabolism and the copper transporter

The evolutionary shift to aerobic respiration resulted in the need for organisms to employ an element with high redox potential. As the atmosphere became more oxidising this require could not be filled by iron, which was converted into the insoluble Fe(III). As a consequence of this change and the following proliferation and evolution of aerobic organisms, copper became an essential element for the vast majority of species including humans (FESTA; THIELE, 2011).

Even though absolutely necessary for life, copper could be toxic if freely dispersed in the cell, because it generates reactive oxygen species through Fenton chemistry. As a consequence, the intracellular cell-free copper concentration is maintained at a low level and regulatory mechanisms involving transporters and chaperones control its homeostasis ensuring that the metal is provided to the correct proteins and cellular compartments necessary for normal activity (O'HALLORAN; CULOTTA, 2000; ROBINSON; WINGE, 2010).

A central player in this process is the human copper transporter (hCTR1), a high-affinity integral membrane protein which imports copper into eukaryotic cells in the form of Cu(I) (LEE; PETRIS; THIELE, 2002). This transporter is the only known system for cellular copper uptake in eukaryotes and imports copper similarly to other channel proteins (ALLER; UNGER, 2006).

It has been hypothesized that once the soluble Cu(I) has been transferred to the cytosol through hCTR1, glutathione or recipient proteins such as copper chaperones will bind the metal immediately and deliver it to target proteins via direct protein-protein interaction (AMIE; ROSENZWEIG, 2009).

Human Cu,Zn superoxide dismutase (hSOD1) is one of the proteins which requires copper as a cofactor for enzymatic activity. However, hSOD1 does not acquire copper via direct interaction with hCTR1 (SKOPP *et al.*, 2019). It is well known that a copper chaperone for Superoxide Dismutase 1 (hCCS) is the protein responsible for copper transfer to hSOD1, through the formation of stable heterodimers (Banci et al., 2012).

Albeit the mechanism behind how the copper chaperone itself initially acquires its cargo remains an open question, its importance in maintaining the concentration of free copper at a minimal level and in transferring it to hSOD1 is widely accepted (CASARENO; WAGGONER; GITLIN, 1998; POPE; DE FEO; UNGER, 2013). Therefore, a brief description about the structure of hCCS and its complex formation with hSOD1 will be presented in the following section.

1.2.2 hCCS structure

The CCS1 was first described in yeast by Culotta and co-workers who observed that cells lacking the LYS7 gene displayed the same phenotype as hSOD1 null cells. LYS7 was renamed as CCS1 and not long after, a human homologue was reported. The human copper chaperone for Superoxide Dismutase 1 (hCCS) is ubiquitously expressed in multiple tissues and is primarily found in the cytosol, but also present in the nucleus and inter membrane space of mitochondria, like hSOD1 (CULOTTA *et al.*, 1997; WONG *et al.*, 2000).

The hCCS protein belongs to the family of copper transfer proteins with a role in hSOD1 maturation. Structurally, it is a homodimeric protein in which each monomer have a molecular weight of 28 kDa and is made up of 3 domains: Domains I, II and III. Amino acid sequence alignments display clear homology of hCCS with the hSOD1 and others copper chaperones related to metal distribution: Atx1 (antioxidant 1 copper chaperone) and yCCS (Figure 4).

Figure 4 – Multiple sequence alignment of the Atx1, yCCS, hCCS and hSOD1 proteins. *S. Cerevisiae* Atx1 (NCBI accession: P38636), yCCS (NCBI accession: P40202), hCCS (NCBI accession: O14618), hSOD1 (NCBI accession: P00441) generated using Clustal X. The numbers correspond exclusively to the hCCS sequence. The amino acids residues corresponding to DI, DII and DIII are coloured in green, orange and blue respectively. In pink is highlighted the MXCXXC motif responsible for copper acquisition, in yellow the cysteines involved in disulphide formation and in red the ones pointed out as fundamental for disulphide transfer from CCS to hSOD1.

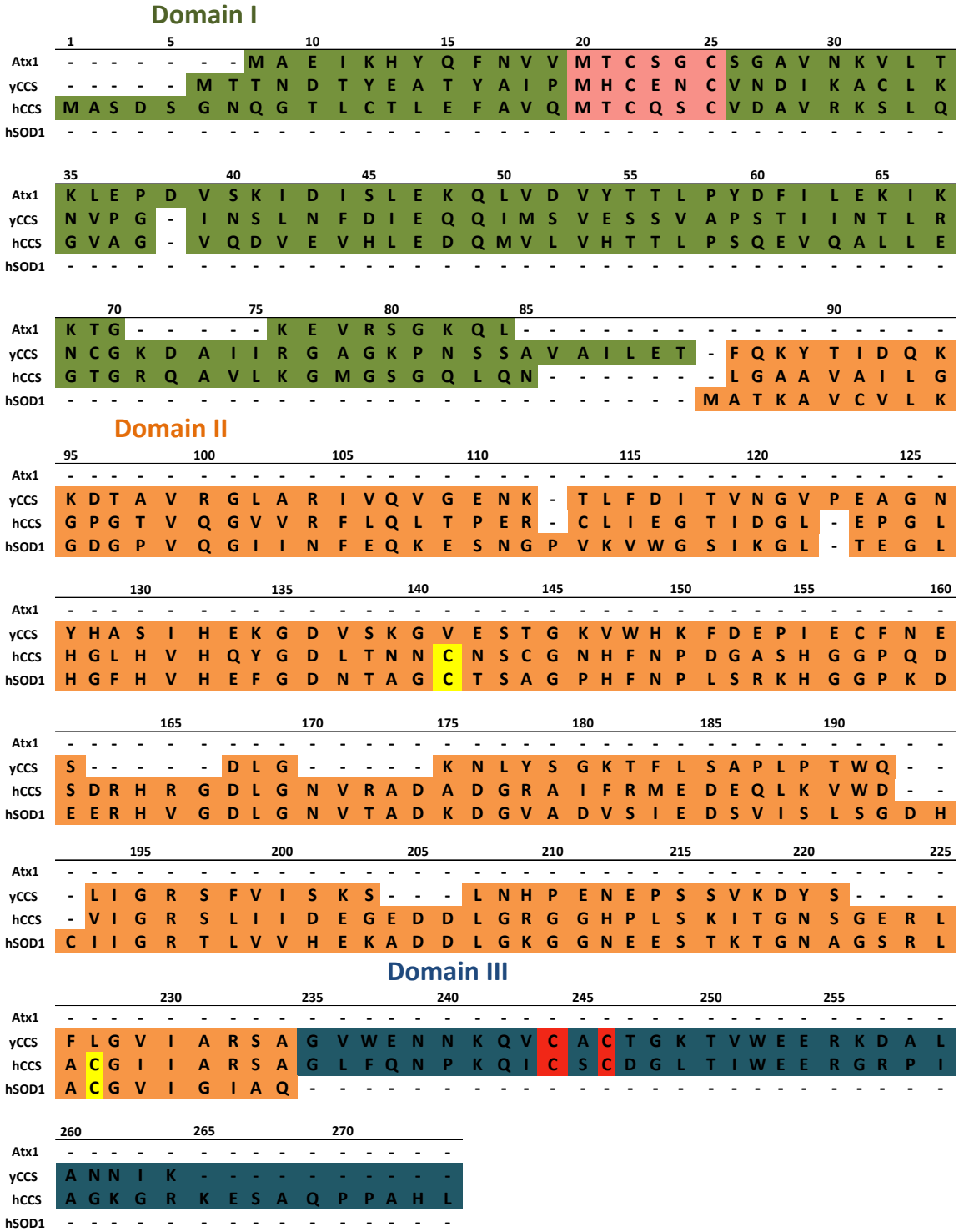

Source from: Own authorship.

The full length human CCS is just 26% identical to yCCS. Analysing the domains separately, it is possible to observe homology between the N-terminal domains of hCCS and the others copper chaperones. All sequences conserve in domain I (green) the MXCXXC motif typically present in family of copper-storage proteins. The central region in hCCS, Domain II (orange background in Figure 4), shares 47% identity with hSOD1 and, differently from yCCS, conserves the Cys141-Cys227 disulphide which is analogous to that formed between, Cys57-Cys146 in homodimeric hSOD1 (residues highlighted in yellow Figure 4). Domain III from yCCS and hCCS display the motif CXC (in red), possibly linked to disulphide transfer (WRIGHT; HASNAIN; GROSSMANN, 2011).

Although full-length yCCS has been structurally characterized (PDB ID 1QUP) (LAMB *et al.*, 1999) the human homolog is still relatively unknown, and described as recalcitrant to crystallization (WRIGHT; HASNAIN; GROSSMANN, 2011). Nevertheless, studies with truncated hCCS constructs have provided important insights into their structure and function.

The N-terminal domain of human CCS (domain I) has been structurally studied by NMR, in both its apo (PDB ID 2CRL) and Cu(I) loaded (PDB ID 2RSQ) forms, Figure 5 A and B, respectively. Similar structures are also available for yCCS DI copper loaded (Figure 5 C) and Atx1 (apo-copper) (Figure 5 D) (PDB ID 1QUP and 1FD8, respectively).

Figure 5 - The structure of hCCS domain I. The motif MXCXXC is show in blue and the cysteines responsible for copper binding, are displayed as sticks. The copper ions, present only in structures B and C, are shown with orange spheres. The PDB IDs for the structure are: (A) 2CRL. (B) 2RSQ. (C) 1QUP. (D) 1FD8.

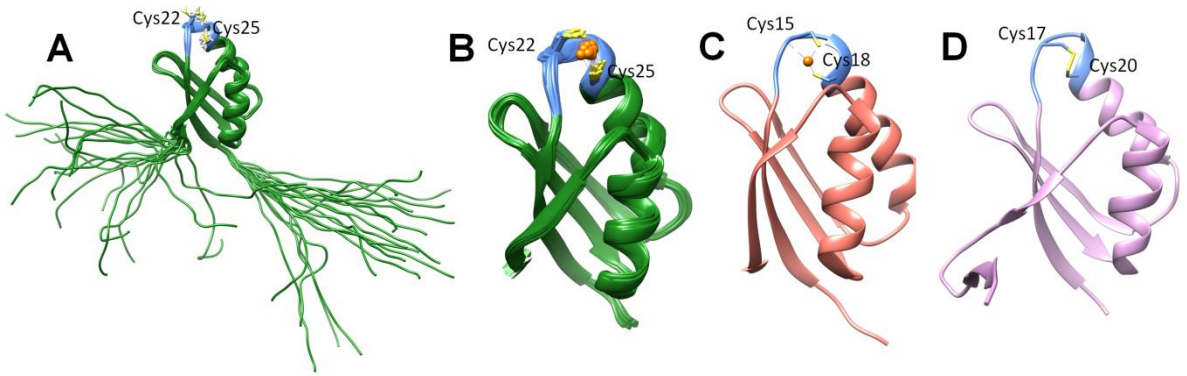

Source from: Own authorship.

All the structures conserve the βαββαβ ferredoxin fold independent of the presence of copper or not. Overall hCCS DI is very similar to Atx1 (Figure 5 D) and yCCS DI (Figure 5 C), as indicated by the RMSD of 0.92 and 1.24 Å (over 55 Cα carbons), respectively. The motif MXCXXC (coloured in blue), capable of binding one Cu(I), is present in all structures. The cysteines involved in copper acquisition are shown in blue and yellow as sticks (BANCI *et al.*, 2013b; LAMB *et al.*, 2000). In the absence of copper the cysteines can form a disulphide bond, as displayed in Figure 5 D. The Atx1 like domain reinforce the role of hCCS DI in copper delivery to hSOD1.

The central region of hCCS, Domain II, is structurally similar to hSOD1 with 47% sequence identity, and an overall RMSD of 0.60 Å. This domain plays a role in protein-protein recognition during the heterodimer formation necessary for hSOD1 maturation, most likely mimicking the dimerization observed in mature hSOD1. To date, just a 2.75 Å resolution crystal structure of the central hSOD1-like domain of hCCS is available (PDB ID 1DO5). The structure comprises an eight-stranded β-barrel that strongly resembles that of hSOD1 and also has the conserved disulphide bridge found in hSOD1 which connect loop IV to the central β-barrel (Figure 6).

Figure 6 – The hCCS domain II dimer (PDB ID 1DO5). Cys141 and Cys227 are shown in yellow as sticks. Zinc is displayed as a grey sphere and the residues coordinating it are highlighted in green. In orange are displayed the residues that are expected to coordinate a copper ion. Arg232 and Arg196 are shown in red.

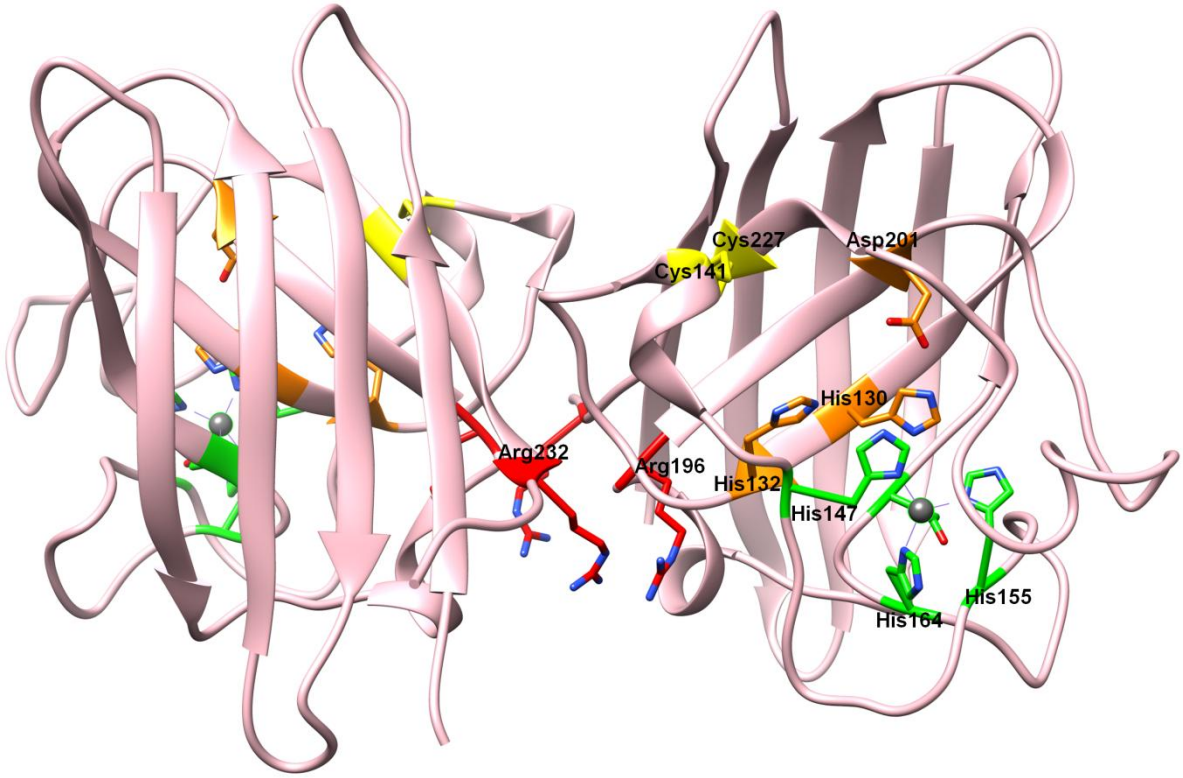

Source from: Own authorship.

The hCCS conserves the zinc binding site, the metal itself and the electrostatic loop, which together forms the active-site in hSOD1. Furthermore, hCCS displays one Zn(II) per monomer, which is coordinated by His147, His155, His164 and Asp167 in a distorted tetrahedral geometry (Figure 6 shown in green as sticks), the same as that observed in hSOD1 (Figure 2).

However, the hCCS domain II does not have a Cu(II) ion, as observed in hSOD1. Three of the four residues responsible for copper coordination are conserved (His130, His132 and His147) but the fourth histidine residue is replaced by Asp201 (displayed in orange Figure 6), the hCCS is thus unable to coordinate copper ions. The structure is also lacking some central residues responsible for driving the superoxide towards the active site. These include Glu132 and Glu133 (in hSOD1) which in hCCS correspond to Pro213 and Leu214, respectively. Together, these differences presumably explain why hCCS is not catalytically active.

It is noteworthy that, while the zinc is essential to human CCS stabilization, it is absent in the yeast counterpart. These structural differences in domain II may lead to specificity in protein-protein recognition between species.

Although structurally very similar, one key difference among hCCS domain II and hSOD1 is the absence of three residues in the former, between Asp192 and Val193 (Figure 4). As a consequence, Arg196 and Arg232 in hCCS (Figure 6, represented as red sticks) are in close proximity and create an electrostatic repulsion between the monomers of the dimer, decreasing their affinity in comparison to the hSOD1 dimer and facilitating heterodimer formation, since Arg232 has an isoleucine as its counterpart residue in hSOD1 (LAMB *et al.*, 2000).

Finally, the C-terminal domain in hCCS consists of only 40 residues and is called domain III. It is the least characterized of the hCCS domains and is a highly conserved short segment in a diversity of species and contains the motif CXC (C244 and C246) that has been proposed to be essential for disulphide transfer to hSOD1. However, no structure is available for hCCS DIII up to date (BANCI *et al.*, 2012b; WRIGHT; HASNAIN; GROSSMANN, 2011).

In order to accomplish the copper transfer process, hSOD1 chaperones form stable heterodimers with hSOD1. The proposed mechanism for hCCS-dependent hSOD1 maturation will be discussed in details below.

1.2.3 hCCS-hSOD1 heterodimer formation and the hSOD1 maturation mechanism

The currently accepted mechanism for maturation of hSOD1 is shown in Figure 7, and depicts the CCS, as a homodimer, interacting with the membrane and sequestering copper(I) from hCTR1. Off the membrane the Cu(I)-hCCS forms a heterodimer via contacts between the hCCS DII and the immature hSOD1. This interaction suggests subsequent amendments which involve reorientation of hCCS DI and copper transfer (BANCI *et al.*, 2012b).

Figure 7 - Schematic mechanism for hCCS-dependent hSOD1 maturation. Copper ions are imported into the cytoplasm by the transmembrane protein hCTR1, via direct protein-protein interaction. The copper is thereby transferred from the HCH copper binding motif present in its C-terminal tail to the cytosolic hCCS domain I motif. During this process the copper chaperone is tethered to the cell membrane. Subsequently Cu(I) loaded hCCS, once off the membrane, interacts with a nascent hSOD1 monomer. hCCS domain I transfers its cargo to hSOD1 and the hSOD1 Cys57-Cys146 disulphide bond is oxidized by hCCS domain III. The heterodimer thus dissociates into its components and hSOD1 forms a mature and enzymatically active homodimer whilst hCCS is released to bind another copper ion.

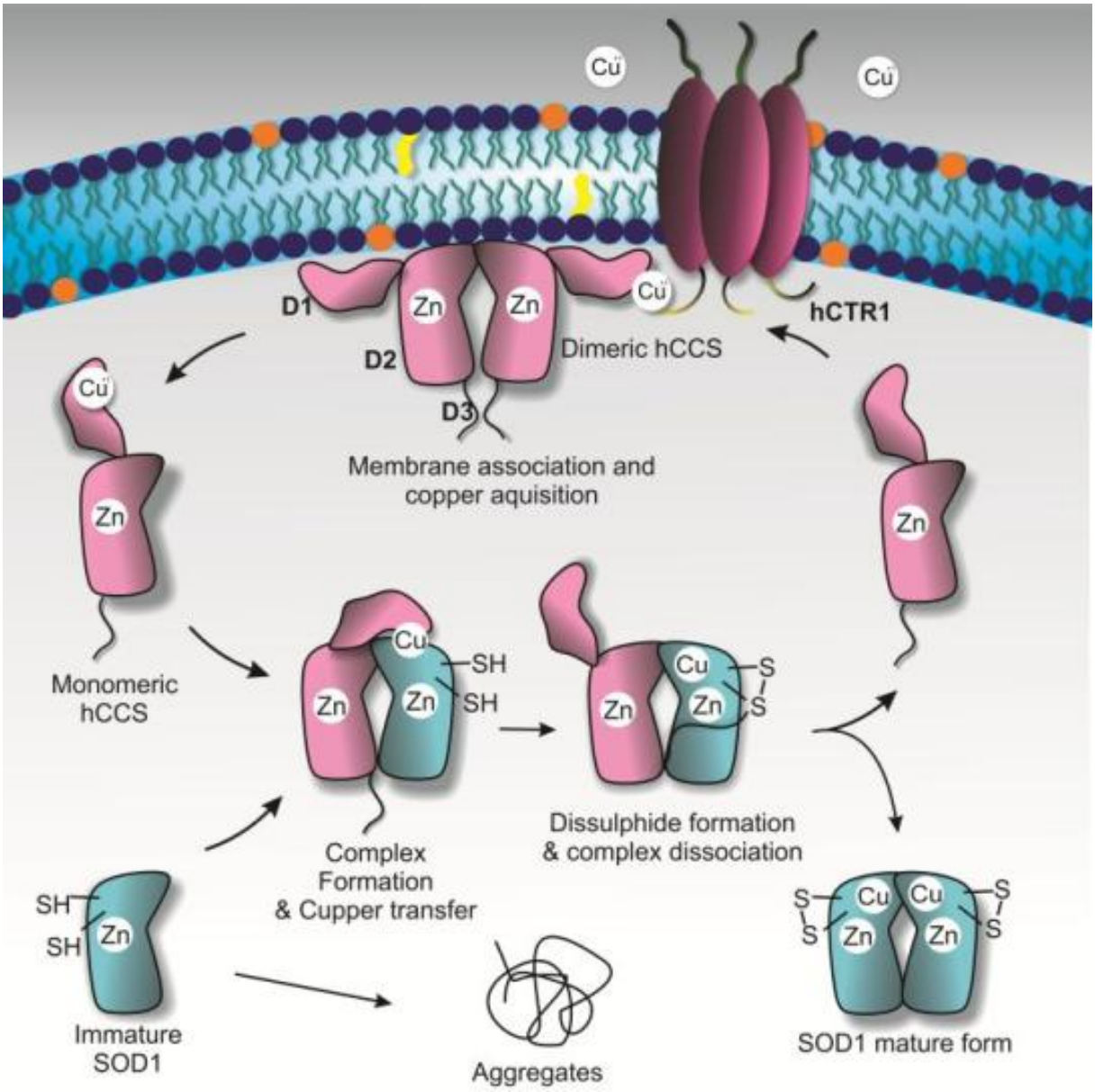

Source from: Own authorship.

The hCCS also participates in the oxidation of the disulphide bond in hSOD1 most likely via Cys244-hCCS and Cys57-hSOD1 interactions. Subsequent reorganisation of this disulphide, in the presence of oxygen, creates the hSOD1 internal disulphide and enables separation of the heterocomplex. The copper-free

hCCS is able to restart the cycle and the copper-loaded and disulphide oxidized hSOD1 is released as a stable and catalytically active enzyme (BANCI *et al.*, 2012b; LAMB *et al.*, 2001).

However, due to the reducing cytosolic environment, most pairs of exposed cysteines residues are not expected to be persistently oxidized. Thus, how can the physiological stability of the disulphide bound in hSOD1 structures be explained? The reduction potential for Cys57-Cys146 is -234 mV, while the redox state of the cytoplasm varies from -290 mV to -310 mV. Thus the hSOD1 is expected to be reduced in the cytoplasm (FURUKAWA; TORRES; O'HALLORAN, 2004). The unusual robustness is not due its thermodynamic stability, but rather is likely to be due to the disulphide formation near the dimer interface, which has a reduced exposed solvent accessible area, limiting the access of cellular reductants (FURUKAWA; O'HALLORAN, 2006).

Structurally, the first heterodimeric complex between hSOD1 and its chaperone was published for *Saccharomyces cerevisae* in 2001 (PDB ID 1JK9) (LAMB *et al.*, 2001). More recently, a chimeric structure between human hSOD1 and yeast CCS was published (FETHEROLF *et al.*, 2017b). However, prior to this thesis, no success has been reported for the human orthologous protein, almost certainly due the human CCS flexibility.

Despite considerable effort, the mechanisms of these post-translational modifications remain somewhat obscure. It is well known that hSOD1 in its immature form has a higher affinity for hCCS, which is lost upon hSOD1 maturation. But the question is what drives it? To comprehend in depth the atomic details underscoring these preferences, a heterodimeric complex formed between human hSOD1 and human CCS is needed. This knowledge could be critical in the fight against neurodegenerative diseases, as demetallation, disulphide reduction or a combination of both, destabilise hSOD1 homo and heterodimers and this appears to be a central characteristic of lateral amyotrophic sclerosis (ALS) associated mutants (HOUGH *et al.*, 2004; VEHVILÄINEN; KOISTINAHO; GOLDSTEINS, 2014).

1.3 hSOD1 and Amyotrophical Lateral Sclerosis

Lateral amyotrophic sclerosis is the most common neurodegenerative disease. Its hallmark is the degeneration of motor neurons in the brain and spinal cord, paralysis and death within 3-5 years after diagnosis, mostly due respiratory failure (TRUMBULL; BECKMAN, 2009). The majority of the cases, 80-90%, are sporadic, and the remainder are termed familiar (fALS); of these, roughly 20% are related to mutations in the gene encoding the hSOD1 protein (CLEVELAND; ROTHSTEIN, 2001).

As already described, native hSOD1 is one of the most stable enzymes known with respect to its biophysical properties, and thus, *a priori*, one of the least likely proteins to be involved in a neurodegenerative disease. However, a large number mutations associated with fALS, more than 140, have been identified (Figure 8), most of which are due to the substitution of a single amino acid of the 153 residues present in the polypeptide, even though insertions, deletions and C-terminal truncations also occurs (CHATTOPADHYAY; VALENTINE, 2009; SACCON *et al.*, 2013). The mutations are distributed along the entire length of the protein and vary in terms of their impact on the enzyme´s properties as well as on the ALS symptoms themselves in afflicted individuals, e.g. the onset, duration, and severity (MÜNCH; BERTOLOTTI, 2010).

Figure 8 - Diagram of Human hSOD1 mutations described in patients with ALS. Only mutations that affect the amino acid sequence have been included.

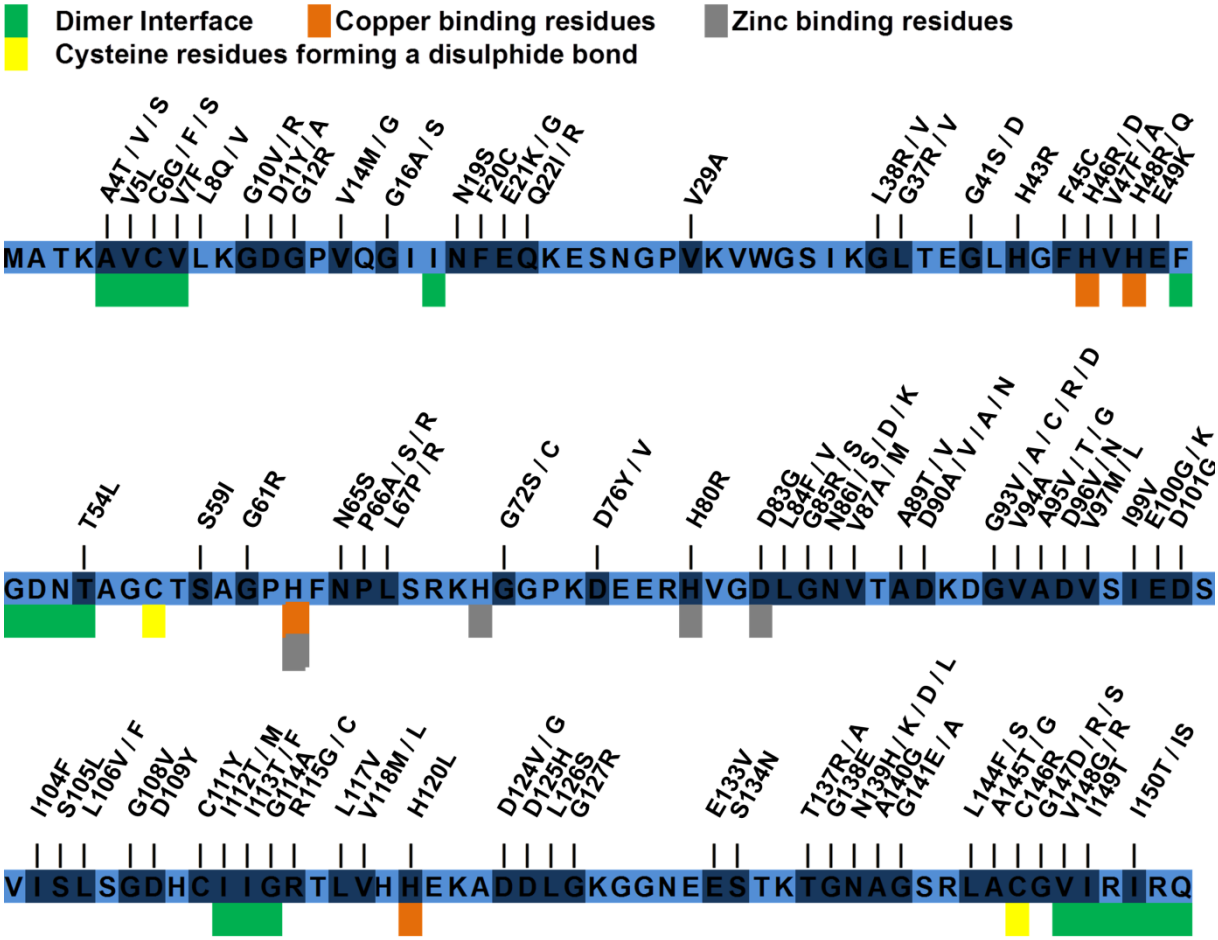

Source from: Figure adapted from (SACCON *et al.*, 2013).

The mutations can be divided into groups: 1) mutations that affect the coordination of the metal ions, affecting directly the enzymatic activity, thermal stability and maybe also compromising the in vivo folding (e.g., mutants H48Q, H46R, H80R or D83G); 2) Mutations in amino acids relating to the intramolecular disulphide bond formation causing a reduction in stability and favouring monomerization (C146R, for instance) 3) Mutations spread throughout the protein that do not affect the regions responsible for enzymatic activity or metal acquisition, but remains less active and stable compared to wt hSOD1 (e.g., A4V and L38V) (HAYWARD, et al., 2002; RODRIGUEZ et al., 2002) 4) Finally, the mutant which are remarkably similar to wt hSOD1 in stability and activity (e.g., D101G, N139K and E100K).

Several experimental approaches have demonstrated that fALS is not only caused by a reduction in hSOD1 activity (SACCON *et al.*, 2013) and stability

(MÜNCH; BERTOLOTTI, 2010), but by exposing hydrophobic amino acid residues in almost all the ALS related mutants, providing cohesive surfaces for interactions with other proteins, or membranes, resulting in proteinaceous inclusions, a hallmark of ALS (HIPP; PARK; HARTL, 2014; MÜNCH; BERTOLOTTI, 2010).

Furthermore, hSOD1-ALS mutants have also been reported to be linked with a faulty interaction with wild-type hCCS. This is most likely due to loss of hSOD1 affinity for zinc and perturbation to loop IV, therefore impairing heterodimer formation, which causes an increase in the number of immature and monomeric hSOD1 species, more prone to aggregation (WRIGHT; ANTONYUK; HASNAIN, 2016).

Although the hSOD1-rich inclusions have been detected in the spinal cord and neurons of ALS patients, it is still unclear how the hSOD1 amyloidal fibrils provoke the motor neurone degeneration, as their relative abundance is not always correlated with the severity of the disease (RODRIGUEZ *et al.*, 2005). Interestingly, studies have shown that small misfolded aggregated hSOD1 species are directly involved in cell death, and the formation of amyloidal fibrils, therefore, could be a protective mechanism, possibly by reducing the solvent exposed area of the aggregates. This raises the question of whether the formation of inclusions is the cause or consequence of neurodegenerative diseases (YERBURY *et al.*, 2016).

In spite of the uncertainty, all the observations indicate that hSOD1 metal deficiency, instability, disulphide reduction and local or global unfolding act in concert towards hSOD1 monomerization and thus aggregation, amyloid formation and toxicity (BANCI *et al.*, 2008; CHATTOPADHYAY; VALENTINE, 2009; KARCH *et al.*, 2009; SEA *et al.*, 2015; TOKUDA; FURUKAWA, 2016). However it is still obscure how the ALS-hSOD1 mutations may interfere in the mechanism of hCCS-dependent hSOD1 maturation. Understanding this may help us to restore the maturation pathway and hopefully rescue the proteins from becoming toxic to the cell.

2 Aims

The objective of this project is to understand how hCCS activates hSOD1 and why this process is ineffective in hSOD1-related amyotrophic lateral sclerosis. Currently a central part of our understanding of hSOD1 maturation is missing; the structure and function of the hCCS-hSOD1 complex. This project aims to:

- Address the role of the lipid bilayer in initial copper acquisition by hCCS or hCCS-hSOD1 through binary (hCCS-hCTR1) or ternary complexes hSOD1-hCCS-hCTR1);
- Characterize the oligomeric state of wt hCCS & mutants in solution using biophysical techniques;
- Observe and characterize the ability of disease related hSOD1 mutants to complex with hCCS;
- Define the sequence of events involved in hCCS catalyzed SOD1 maturation which includes: complex formation, copper loading and disulphide transfer;
- Describe the role of the cysteines in hCCS domains I and III in SOD1 disulphide oxidation by studying their mutations, e.g., hCCS C22,25S or hCCS C244,246A, using SDS-PAGE under non-reducing conditions;
- Crystallize and solve the structure of reaction precursors, such as immature hSOD1 and hCCS homodimers;
- Trap reaction intermediates of the of hSOD1 maturation pathway *in crystallo*, through direct mutagenesis of the hSOD1 cysteines involved in disulphide bond formation as well as hCCS mutations and truncations to decrease aggregation and/or reduce flexibility;
- Dissect the molecular recognition event and conformational rearrangements that facilitate hCCS-catalysed SOD1 activation.

3 Methods

3.1 Protein expression and purification

The wild type hCCS and hSOD1 constructions were already available in the Molecular Biophysics Group (MBG) at the University of Liverpool, Liverpool - UK. Further mutants required for this work were commercially ordered from GenScript. Figure 9 shows the sequence of the proteins used in this work:

Figure 9 - Primary structure of wt hCCS, hCCS domain truncations and wt hSOD1 proteins. Based on these constructs, site-directed mutations were performed, as will be described in details in table 1. All residues that were mutated and originated in a new constructs based on the existent one, are highlighted in bold red. The initial methionine is in orange, the 6xHis-tag in blue and the cleavage site for the TEV protease in green.

wt hCCS

MHHHHHHENLYFQSMASDSGNQGTL**C**TLEFAVQMT**C**QS**C**VDAV**RK**SLQGVAGVQ
DVEVHLEDQMVLVHTTLPSQEVQALLEGTGRQAVLKGMGSGQLQNLGAAVAILGG
PGTVQGVV**R**FLQLTPERCLIEGTIDGLEPGLHGLHVHQYGDLTNNCNSCGNHFNPD
GASHGGPQDSDRHRGDLGNVRADADGRAIFRMEDEQLKVWDVIGRSLIIDEGEDD
LGRGGHPLSKITGNSGERLACGII**AR**SAGLFQNPKQI**C**S**C**DGLTIWEERGRPIAGKG
RKESAQPPAHL

hCCS Domain I

MHHHHHHENLYFQSMASDSGNQGTLCTLEFAVQMTCQSCVDAVRKSLQGVAGVQ
DVEVHLEDQMVLVHTTLPSQEVQALLEGTGRQAVLKGMGSGQLQN

hCCS Domain II

MHHHHHHENLYFQSLGAAVAILGGPGTVQGVVRFLQLTPERCLIEGTIDGLEPGLH
GLHVHQYGDLTNNCNSCGNHFNPDGASHGGPQDSDRHRGDLGNVRADADGRAIF
RMEDEQLKVWDVIGRSLIIDEGEDDLGRGGHPLSKITGNSGERLACGIIA**R**S

hCCS Domain I,II

MHHHHHHENLYFQSMASDSGNQGTLCTLEFAVQMTCQSCVDAVRKSLQGVAGVQ
DVEVHLEDQMVLVHTTLPSQEVQALLEGTGRQAVLKGMGSGQLQNLGAAVAILGG
PGTVQGVVRFLQLTPERCLIEGTIDGLEPGLHGLHVHQYGDLTNNCNSCGNHFNPD
GASHGGPQDSDRHRGDLGNVRADADGRAIFRMEDEQLKVWDVIGRSLIIDEGEDD
LGRGGHPLSKITGNSGERLACGIIAR

hCCS Domain II,III

MHHHHHHENLYFQSLGAAVAILGGPGTVQGVVRFLQLTPERCLIEGTIDGLEPGLH
GLHVHQYGDLTNNCNSCGNHFNPDGASHGGPQDSDRHRGDLGNVRADADGRAIF
RMEDEQLKVWDVIGRSLIIDEGEDDLGRGGHPLSKITGNSGERLACGIIARSAGLFQ
NPKQICSCDGLTIWEERGRPIAGKGRKESAQPPAHL

wt hSOD1

ATK**A**VCVLKGDGPVQGIINFEQKESNGPVKVWGSIKGLTEGLHGF**H**V**H**EFGDNTAG
CTSAGPHFNPLSRKHGGPKDEERHVGDLGNVTADKDGVADVSIEDSVISLSGDHCII
GRTLVVHEKADDLGKGGNEESTKTGNAGSRLA**C**GVIGIAQ

Source from: Own authorship.

During the course of this work it was necessary to construct many site-directed mutations affecting a single (e.g. hCCS DII R232A), two (e.g. hCCS C22,25S) or more residues (hCCS C12,22,25,244,246A). These were based on constructs already available, shown in Figure 9, and were also ordered from GenScript. Table 1 summarizes all the constructs, vectors and corresponding computed parameters for them.

Table 1 - Proteins constructions in expression plasmids and physical chemical parameters.

Constructions	Vectors	Molecular Weight (Da)	Extinction coefficients (M^{-1} cm^{-1})
wt hCCS	pETM11	29127.68	12490
hCCS C22A	pETM11	29095.62	12490
hCCS C25A	pETM11	29095.62	12490
hCCS C22,25S	pETM11	29095.56	12490
hCCS C244,246A	pETM11	29063.56	12490
hCCS C12,22,25,244,246A	pETM11	28967.38	12490
hCCS DI	pETM11	9061.25	0
hCCS DII	pETM11	15728.44	6990
hCCS DI,II	pETM11	24597.52	6990
hCCS DII,III	pETM11	20171.52	12490
hCCS DII R232A	pETM11	15643.33	6990
hCCS A231G	pETM11	29113.65	12490
hCCS R30A,K31A	pETM11	28942.45	12490
wt hSOD1	pET14b	15804.55	5500
hSOD1 A4V	pET14b	15832.60	5500
hSOD1 H46R	pET14b	15823.60	5500
hSOD1 H46R/H48Q	pET14b	15814.59	5500
hSOD1 C57,146A	pET14b	15740.43	5500
hSOD1 C57A	pET14b	15772.49	5500
hSOD1 C146A	pET14b	15772.49	5500

Source from: Own authorship.

Expression and purification were carried out based on well established protocols available at MBG (WRIGHT *et al.*, 2013; WRIGHT; HASNAIN; GROSSMANN, 2011), with slight modifications. DNA fragments were used to

transform *E. coli* BL21 (DE3) competent cells, except for hSOD1 C146A which were transformed in Rosetta (DE3). Cells from a single colony were grown overnight at 37 °C on LB medium supplemented with 50 $\mu g.mL^{-1}$ kanamycin for hCCS and its mutants and 75 $\mu g.mL^{-1}$ ampicillin for hSOD1 & mutants. 100 $\mu g.mL^{-1}$ chloramphenicol were used for transformations using Rosetta (DE3).

After cell growth, 10 mL of these samples were inoculated into 1 litre of liquid culture medium, while shaking at 37 °C until reaching an optical density value of 0.6, measured at a wavelength of 600 nm in a spectrophotometer. Induction for hCCS and mutants were performed with 0.4 mM of IPTG and 0.25 µM of $ZnCl_2$, and incubated at 25 °C for 16 hours. hSOD1 and mutants were induced using 0.5 mM of IPTG, 0.25 µM of $ZnCl_2$ and 0.25 µM of $CuCl_2$ when copper was required. The exceptions were: hSOD1 C57,146A, for which the expression was conducted at 37 °C during 6 hours, and hSOD1 A4V and hSOD1 C146A for which the incubation temperature was decreased to 16 °C for 16 hours.

Subsequently, cells were harvested by centrifugation at 5000 xg for 15 minutes at 4 °C, and the pelleted cells ressuspended in 20 mM Tris buffer, pH 7.4, 150 mM NaCl and 5 mM DTT (dithiothreitol) or 20 mM Tris buffer, pH 8.0, for hCCS and hSOD1 (and their mutants), respectively. Due to protein proteolysis, Roche complete™ Protease Inhibitor Cocktail EDTA-free tablets and/or phenylmethylsulfonyl fluoride (PMSF) at 0.2 mM concentration were added to the lysis buffer in all cases. Cells were lysed by sonication for 10 cycles, where each cycle corresponds to a 30 second ultrasound pulse followed by a 1 minute interval. Thereafter, proteins were centrifuged at 14,000 xg for 30 minutes at 4 °C.

The hCCS & mutants were fused with a hexa-histidine tag and a TEV (Tobacco etch virus) cleavage site (Glu-Asn-Leu-Tyr-Phe-Gln-Ser) prior to its N-terminus. The first step in the purification was an affinity chromatography, in which the supernatants were applied to a nickel metal affinity resin column (HisTrap HP, GE Healthcare) pre-equilibrated with lysis buffer and eluted with an imidazole gradient from 0 to 500 mM.

After elution, protein solutions were dialyzed to remove the imidazole, and the 6xHis-tag of the recombinant proteins was cleaved overnight at 4 °C with TEV, protease produced at the University of Liverpool, added to a final concentration of 110 µg/ml. The cleavage takes place between the GLN and SER residues of the

recognition sequence, leaving only a serine residue at N-terminus prior to the initial methionine. Subsequently, the proteins were re-applied to the metal affinity column to remove the released His-tag and the proteolytic enzyme.

The protocol for wild type and mutants hSOD1 were the same. Supernatants were dialyzed overnight with the lysis buffer for wt hSOD1, at 4 °C. Subsequently, they were applied to an anion exchange resin column (DEAE Sepharose Fast Flow, GE Healthcare) pre-equilibrated with the same buffer, and proteins were eluted using an increasing sodium chloride gradient in the range of 0 to 1 M.

All protein steps were analyzed on denaturing gel (SDS-PAGE 15%), stained with 0.010% comassie brilliant blue and distained with water or distaining solution composed of water, methanol and acetic acid in the ratio 5: 4: 1, respectively. The purified samples were concentrated at 2,000 xg and 4 °C by ultra filtration using a 10 to 30 kDa cutoff Millipore membrane (Merck) according to the protein size.

The protein concentration of the resulting samples was measured using the Nanodrop^{TM} 2000 spectrophotometer (Thermo scientific) from the theoretical molar extinction coefficient for each protein, with exception of hCCS DI in which Bradford assay was used for protein quantification, due absence of tryptophan residues in the sequence.

Finally, all proteins were purified by size exclusion chromatography (Superdex 200 16/60 GL column, GE Healthcare) using 20 mM Tris buffer, pH 7.4, and 150 mM NaCl at flow rate of 0.5 mL/min. Protein elutions were monitored in 222 nm and 280 nm, the protein purity were analyzed by SDS-PAGE, DTT was added when required.

3.2 Complex formation

hSOD1 - hCCS complex formation was made by reduction of hSOD1 with 40 mM dithiothreitol (DTT) at 4 °C overnight and mixing at 1:1 molar ratio with hCCS. Subsequently, complexes were applied to an ÄKTA Purifier system (GE Healthcare) coupled to a Superdex 75 10/300 GL (GE Healthcare) column equilibrated with 20 mM Tris, pH 7.4, and 150 mM NaCl. All fractions eluted were analysed by SDS-PAGE and solely the fraction corresponding to the heterodimeric species were selected.

When copper was required, it was incorporated into hSOD1 by addition to the expression medium or by dialysing the protein with 20 mM Tris, pH 7.4, 150 mM

NaCl and 0.2 mM $CuCl_2$ overnight. Excess copper was removed by desalting chromatography using the prepackaged gravity PD MidiTrap G-10 column (GE Healthcare) and heterodimer formation was carried out as previous described.

3.3 Dissociation over a time course

hCCS dependent hSOD1 maturation was investigated in order to outline the importance of the cysteines in hCCS domains I and III on the oxidation of the hSOD1 disulphide bond and, consequently, the dissociation of the heterodimer complex. To address this question, the hSOD1 and hCCS wild types and mutants were mixed in equimolar proportions and loaded onto a Superdex 75 10/300 GL column (GE Healthcare) coupled to an ÄKTA Purifier (GE Healthcare). Only the fractions corresponding to the heterodimer were subsequently loaded after different time intervals onto an Agilent 1260 series HPLC (High performance liquid chromatography) using Bio SEC-3 4.6 x 300 mm column with 3 µm bead size and 300 Å pore size equilibrated with 20 mM Tris, pH 7.4, and 150 mM NaCl nitrogen purged buffer at a flow rate of 0.25 ml/min. The experiment was performed in triplicate.

The complexes analyzed were: E,Zn wt hSOD1 - hCCS; E,Zn wt hSOD1 - hCCS C22A; E,Zn wt hSOD1 - hCCS C25A; E,Zn wt hSOD1 - hCCS C22,25S; E,Zn wt hSOD1 - hCCS C244,246A. All samples were at an initial concentration of 120 µM, and were monitored at time intervals of 0 hour, 2 days, 5 days and 10 days. The fraction of heterodimer remaining in solution was determined over time and plotted as a function of the area under the relevant SEC elution peak height monitored at 280 nm.

Finally, the ability of wild-type hCCS to form a heterodimer with hSOD1 copper holo (Cu,Zn hSOD1 C57,146A) and apo (E,Zn hSOD1 C57,146A) was determined by mixing equimolar proportions of hCCS and E,Zn hSOD1 C57,146A or Cu,Zn hSOD1 C57,146A followed by thirty minutes incubation and analysis as described above. The mutant was used in order to guarantee that the experiment probed only the influence of the copper and not the presence of the disulphide bridge. Moreover, the heterodimers were also investigated over time (0, 2, 5 and 10 days) to analyze their stability.

3.4 AMS

The disulphide status of hSOD1 in all heterodimers, described above, was evaluated at day 1 and day 10 by the selective reaction of free thiol groups with 4-acetamido-40-maleimidylstilbene-2,20-disulfonic acid (AMS) which results in an increase in protein molecular weight of approximately 0.5 kDa per free cysteine. Heterodimers were incubated at 37 °C for 2 hours with 100 mM AMS following manufacturer's instructions (Thermo Fisher Scientific). Subsequently, samples were boiled at 95 °C with loading page buffer without β-ME and loaded onto SDS-PAGE under non-reducing conditions and bands were stained by comassie blue.

3.5 Derived molecular weights by size exclusion chromatography and light scattering

The Agilent 1260 Infinity Multi-Detector Bio-SEC/LS system combines size exclusion chromatography (SEC) and an advanced light scattering detector which combines: static light scattering (SLS), refractive index (RI) and ultraviolet (UV). It is an accurate tool to determine the molecular weights and sizes of proteins in solution. The advantage of the light-scattering detectors is that there is no need for calibration; they determine the molecular masses of all scattered particles eluted in the course of an SEC run.

The SLS is based on the interaction of the light and matter. Light can be described as an oscillating electro-magnetic field. Upon interaction with a molecule, the oscillating field induces an oscillating dipole. The induced dipole itself now also emits electro-magnetic waves with properties which depend on the molecular properties.

The detectors, set at some angle to the incident beam, collect the resulting scattered light from the molecule. The intensity of the scattered light is measured as the Rayleigh ratio, R_θ, which is defined as the total intensity scattered by the particles (I_θ) and by the solvent ($I_{sol\theta}$) observed at an angle θ normalized by the incident light intensity (I_0) and the absolute calibration constant (f). This allows the determination of the molecular weight of the protein by analyzing the scattered light (MURPHY, 1997; WYATT, 1993; ZIMM, 1948). The equation is complex and takes the following form:

$$\frac{K^* c}{R_\theta} = \frac{1}{M_w P_\theta} + 2A_2 c \quad (3)$$

Where, c denotes the concentration of protein in mg/mL, M_w is the weight-averaged molecular mass, A_2 is the second virial coefficient which accounts for interparticle interactions, but which can be neglected for dilute solutions (1-5 mg/mL).Thus equation (3) can be simplified to

$$\frac{K^* c}{R_\theta} = \frac{1}{M_w P_\theta} \quad (4)$$

$P(\theta)$ is the particle shape factor which is defined by:

$$P_\theta = 1 + \frac{16\pi^2 n_0^2 R_g^2}{3\lambda_0^2} \sin^2\left(\frac{\theta}{2}\right) \quad (5)$$

$P(\theta)$ is related to the wavelength of the light in the vacuum λ_0^2, R_g the radius of gyration of the particle, the refractive index of the solvent (n_0) and the angle between the incident light and the scattered light (θ). However for small particles (below 10 nm) there is no angular dependence due to isocratic light scattered by the particles, thus $P(\theta)$ approaches 1 (TARAZONA; SAIZ, 2003). Under these circumstances, equation (4) further reduces to:

$$\frac{K^* c}{R_\theta} = \frac{1}{M_w} \quad (6)$$

Where the K* is:

$$K^* = \frac{4\pi^2 \left(\frac{dn}{dc}\right)^2 n_0^2}{\lambda_0^4 N_A} = (dn/dc)^2 K \quad (7)$$

where, dn/dc is the refractive index increment of the scattered particle. For the majority of the proteins this value is approximately 0.187 ml/g. N_A is Avogadro's number. From the equation, it is clear the importance of the dn/dc value in light

scattering calculations (SLOTBOOM *et al.*, 2008; WYATT, 1993). Substituting of eq. 7 in eq. 6 results in:

$$R_\theta = M_w K \left(\frac{dn}{dc}\right)^2 c \quad (8)$$

R_θ is the experimentally measured quantity, K can be easily determined based on the equation 7, dn/dc is a constant and the c is the concentration which is already known. From (6) it is evident that the response of the detector is directly proportional to the molecular weight and concentration, so low molecular weight samples or diluted samples will lead to poor scattering.

We used the size exclusion chromatography technique coupled with light scattering to accurately determine the molecular weight of the proteins studied here. The constructs: hCCS DI, hCCS DII, hCCS DI,II were loaded onto the AdvanceBio SEC 300Å, 4.6 x 300 mm column with 2 µm bead size (Agilent) while the hCCS, hCCS DII,III and wt hSOD1 were loaded onto a Superdex 75 10/300 GL column (GE Healthcare) both coupled to the Agilent 1260 Infinity II Bio-SEC multi Detector (Agilent). All proteins were tested at 60 µM, except for the hCCS domain I which was 5 mg/mL.

3.6 Monomer-dimer equilibrium for hCCS and hCCS truncations

The copper chaperone domains: II, I,II and II,III were loaded again onto the Agilent 1260 Infinity II Bio-SEC using the same column and parameters described in section 3.5, but with concentrations of 200 µM for hCCS DI,II and hCCS DII,III and 300 µM for hCCS DII. The aim was to investigate the oligomerization effects as a function of concentration.

Moreover, mutation of the charged residue Arg232 to alanine was conducted for hCCS DII to assess whether the monomer-dimer equilibrium is affected on decreasing the interface charge repulsion. The peaks observed in the chromatogram profile during the last purification step, the SEC using the Superdex 200 16/60 GL (GE Healthcare), were loaded onto the SEC-LS to determine their oligomeric state, as described for hCCS DII in section 3.5. The samples were also tested after two days to inspect a possible slow equilibrium between species.

Finally, in an attempt to determine the dissociation constant for the wt hCCS we measured the retention volumes over the range of 0.7 – 750 µM using SEC for the peak corresponding to the dimeric wild type copper chaperone. The column used was the AdvanceBio SEC 300Å, 4.6 x 300 mm column with 2 µm bead size (Agilent). The measurements were taken at 220 nm and 20 °C.

3.7 Disulphide transfer

In an attempt to determine the role of the cysteines in hSOD1 (i. e., Cys57 or Cys146) and the hCCS domains (Cys22, Cys25 from domain I and Cys244, Cys246 from domain III) involved in thiol oxidation for the human orthologous the complexes shown in Table 2 were analyzed.

Table 2 – Complex investigated to underscore the role of cysteines in hSOD1 and in the hCCS DI and III involved in disulphide transfer.

	hCCS DI Cys mutated	**hCCS DIII Cys mutated**	**Expectation**
hSOD1 Cys57 and Cys146 mutated	hSOD1 C57,146A - hCCS C22,25S	hSOD1 C57,146A - hCCS C244,246A	Negative Control – no complex formation
hSOD1 Cys57 mutated	hSOD1 C57A - hCCS C22,25S	hSOD1 C57A - hCCS C244,246A	Interaction of hCCS DI and/or DIII with hSOD1 cys146
hSOD1 Cys146 mutated	hSOD1 C146A - hCCS C22,25S	hSOD1 C146A - hCCS C244,246A	Interaction of hCCS DI and/or DIII with hSOD1 cys57

Source from: Own authorship.

Initially, the copper chaperone and hSOD1 were mixed equimolar. Afterwards, all complexes were loaded onto a Superdex 75 GL 10/300 column (GE Healthcare) and just the peak corresponding to the heterodimer in equimolar proportions were used to avoid the formation of oligomers of the same species that could impair further analysis. The complexes were maintained at 20°C and were analyzed at day 0, day 3 and day 7 by SDS-PAGE under reducing and non-reducing conditions. The experiment was conducted in triplicate.

3.8 Crystallization

The process of crystallizing a protein is a crucial step for determining its atomic structure by X-ray diffraction. The procedure is based on the controlled reduction of a protein's solubility, so that the molecules organize themselves periodically into well ordered and diffracting crystals. The growth of protein crystals is influenced by several parameters such as sample concentration, temperature, pH value, thermal stability, and precipitant among others. Due to the chemical complexity of a protein and the many parameters involved, the theoretical determination of crystallization conditions is still an unsolved problem making the discovery of the optimal parameters an unpredictable process. In this sense, a systematic variation of the conditions of variables involved in crystallization becomes necessary (JEN; MERKLE, 2001; KRAUSS *et al.*, 2013; RUPP, 2010).

Usually crystals grow when the concentration of a protein solution is above its solubility limit, a so-called supersaturated solution. Numerous methods have been employed for bringing a protein solution into this state, for example: vapor diffusion, free interface diffusion, batch and dialysis. In the crystallization of macromolecules, vapour diffusion is by far the most common technique used, and can be divided in the two most common methods: hanging drop and sitting drop (OCHI *et al.*, 2009; RUPP, 2010).

Both methods utilize the evaporation and diffusion of volatile species between two solutions - a small droplet containing protein, buffer and precipitant and a reservoir containing the precipitant. The process occurs in a closed environment, usually created by grease or sealing tapes over the reservoir or wells. Initially the droplet contains a less concentrated solution of precipitants than the reservoir. The diffusion of volatile compounds from the drop to the reservoir occurs until both solutions are in equilibrium. During this time, there is a slow increase of both protein and precipitant concentration in the droplet, which can cause supersaturation and hopefully crystal growth. A schematic illustration of this process and the phase diagram are reported in Figure 10 A and B, respectively (KRAUSS *et al.*, 2013; RUPP, 2010):

Figure 10 – The vapor diffusion method and phase diagram. (A) Schematic representation of the hanging drop vapor diffusion method. The drop is shown in green and the precipitant in blue. The protein + precipitant solution in the drop is allowed to equilibrate in a closed container with a larger aqueous reservoir solution. Crystals are predicted to grow when equilibrium is reached and if the conditions are favourable. (B) The phase diagram shows the undersaturation, metastable, nucleation and precipitation zones. Initially the protein-precipitant droplet is in the soluble zone (undersaturation). When the drop starts to shrink due to evaporation, both precipitant and protein concentration increases moving the conditions to the nucleation zone [step numbered as 1]. As nuclei form, the protein concentration decreases, moving the conditions vertically into de growth zone [steps 2-3]. The crystal grow until the supersaturated solution equilibrates with the crystals [step 4].

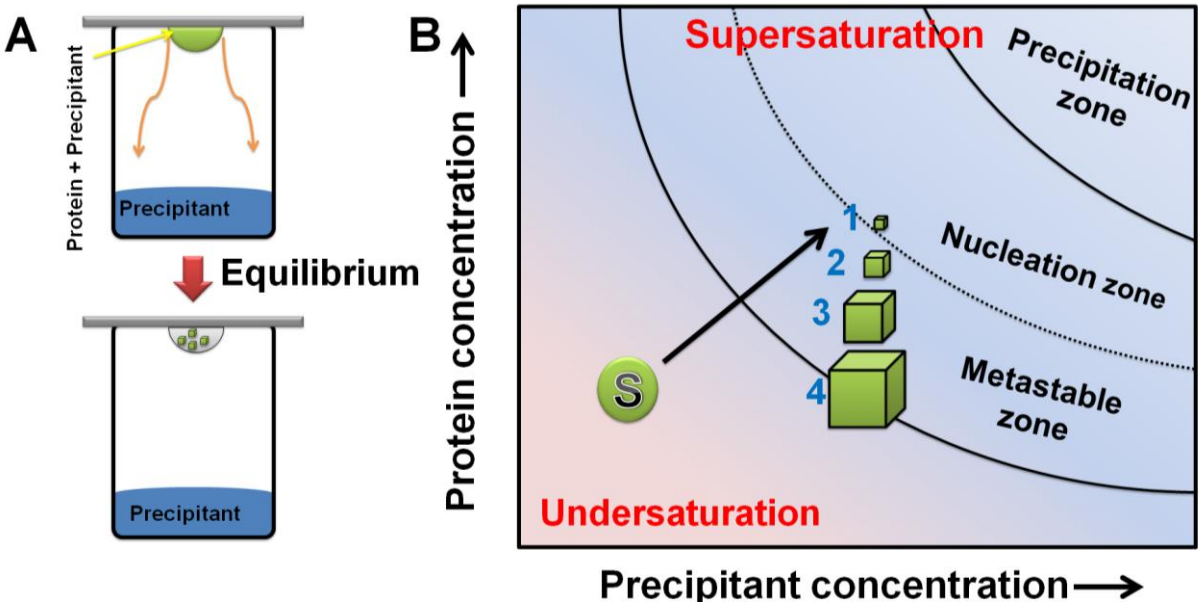

Source from: Adapted from (RUPP, 2010).

The supersaturated zone of the diagram is divided into three regions: very high supersaturation, where molecules form amorphous aggregates known as precipitates, intermediate supersaturation where both nucleation and growth can occur, and lower supersaturation, the metastable zone, where only growth is supported. For a successful crystallization experiment, the protein and precipitant concentration increases until they reach the region of spontaneous nucleation, numbered as 1 in Figure 10 B, where nucleation can occur and a crystal may start to grow. As the crystals grow, the solution becomes depleted of protein and a few of the crystal may grow into large ones in the metastable phase. The crystals reach their final size when they and the saturated protein solution are in equilibrium (number 4 in in Figure 10 B) (JEN; MERKLE, 2001; OCHI *et al.*, 2009; RUPP, 2010).

Nucleation and crystal growth are therefore uncoupled events, usually the optimal solution condition for spontaneous nucleation is not ideal for subsequent

crystal growth. Seeding is for this reason a powerful tool for the separation of these events. The technique can be classified into two categories based on the size of the crystalline material utilized: microseeding which uses sub microscopic fragments of crystalline material and macroseeding which implies the transfer of one single well formed crystal into a new equilibrated drop. Seeding removes the need for new nucleation and, in some cases, facilitates the growth of bigger and well-ordered crystals (BERGFORS, 2003; D'ARCY *et al.*, 2014; RUPP, 2010).

The main challenge of this project was to produce a heterodimer of hSOD1 and its cognate chaperone that remains as a stable complex over periods long enough to facilitate crystallization. Using different mutants combinations of hCCS and hSOD1 we monitored complex dissociation at time intervals of 8 days, 20 days and 50 days using an Agilent 1260 series HPLC using Bio SEC-3 4.6 x 300 mm column with 3 µm bead size and 300 Å pore size equilibrated with 20 mM Tris, pH 7.4, 150 mM NaCl and 1mM DTT at a flow rate of 0.3 ml/min. Here the objective was to trap a monodisperse complex suitable for crystallization experiments. The heterodimers studied were: wt hCCS – wt hSOD1, hCCS C22,25S – wt hSOD1, wt hCCS – hSOD1 A4V, wt hCCS – hSOD1 H46R, wt hCCS - hSOD1 H46Q/H48R, wt hCCS - hSOD1 C57,146A, hCCS C22,25S - hSOD1 C57,146A and hCCS DII,III – wt hSOD1**.**

From the time course experiment using SEC, the most stable heterodimers were analyzed and new combinations for heterocomplexes with potential stability were rationalized. All the promising complexes were conducted to high-throughput screens. Sitting drop, vapor diffusion crystallization trials were set up at 4 and 20 °C in 96-well plates with commercial screens (Morpheus I/II, PACTpremier and Structure HT - Molecular dimensions; JCSG+ - Qiagen; SaltRX, Index, Natrix, PEGRx HT – Hampton Research) using an Innovadyne Screenmaker 96+8 crystallization robot. Protein concentration as well as reducing agents, e.g. TCEP, DTT and β-Mercapto ethanol, were tested. The complexes were tested by mixing 200 nL of sample with 200 nL of precipitant, i.e., using a 1:1 ratio. A total of over 19200 conditions were screened. Temperature of both 4 °C and 20 °C were tested.

Optimization screens were carried out manually in 24-well plates using the hanging-drop vapour-diffusion method by mixing equal volumes (1 to 2 µL) of protein and reservoir solutions, and also by changing the protein: precipitant ratio from 1:1 to 1:2 and 2:1. Microbatch trays were also tested in order to attempt to improve crystal quality, as well as macro- and microseeding methods.

Microseeding experiments were carried out using a "seed soup". To prepare this we selected a drop containing many crystals and added 10 µL from the reservoir solution to it. The mixture was then transferred to an eppendorf tube. The procedure was repeated until there was a total of 50 µL of the mixture containing crystals in the tube. A glass bead was then added to the eppendorf and the solution was vortexed for 2-3 minutes to crush the crystals. The seed soup was diluted serially: 1:5, 1:25, 1:125 and 1:625 in 20 % (w/v) PEG 3350 and 0.2 M Sodium malonate, frozen in liquid nitrogen and stored at -80 °C (D'ARCY *et al.*, 2014). The seeds were tested in commercial screens and in manual optimizations.

The first complex to be crystallized was that of hCCS DII,III – wt hSOD1 at a concentration of 10 mg/mL of protein mixed with 14% (w/v) PEG 3350 and 0.2 mM sodium malonate at a ratio of 1:1 (1µL sample and 1µL precipitant). 10 mM DTT and 20 mM TCEP were also added. To verify the actual proteins present in the asymmetric unit, the crystals were washed in the reservoir solution 5 times and then dissolved in the protein buffer and loaded onto a 15% SDS-PAGE.

hCCS C244,246A at 25 mg/ml and hCCS C22,25S at 40 mg/ml were also crystallized by mixing 0.25 µL protein and 0.25 µL precipitant, in the automatic screening. The conditions were: 1) 0.2 M Magnesium Chloride, 20% (w/v) polyethylene glycol 6000, 0.1 M tris, pH=8.0, and 2) 0.002 M Zinc Chloride, 20% (w/v) polyethylene glycol 6000, 0.1 M tris, pH=8.0, respectively.

For the E,Zn hSOD1 C57,146A (apo copper and zinc loaded hSOD1 mutant) 1.0 µL of protein at 15 mg/mL were mixed in equal proportions with 0.2 M Lithium sulphate; 0.1 M Tris, pH 8.0, and 24% (w/v) PEG 4000. Crystals appeared after 10 days incubation.

E,Zn hSOD1 C57,146A - hCCS DII at 15 mg/mL was crystallized in 25% (w/v) PEG 1500; 0.1 M PCTP buffer, pH 7.0, (sodium propionate, sodium cacodylate, and BIS-TRIS propane in the molar ratios 2:1:2, respectively) by mixing 1µL protein and 1µL reservoir solution in a 24 well plate with well volume of 500 µL. Crystals grew after 15 days.

Heterocomplexes: hCCS C12,22,25,244,246A – E,Zn wt hSOD1; hCCS C22,25S – E,Zn wt hSOD1; hCCS C22,25S - E,Zn hSOD1 C57,146A; hCCS C12,22,25,244,246A - E,Zn hSOD1 C57,146A and Cu,Zn hSOD1 C57,146A – hCCS C12,22,25,244,246A were crystallized from non-diffracting seeds prepared from

hCCS C22,25S – E,Zn hSOD1 C57,146A crystals grown in 0.2 M Sodium malonate, 20% (w/v) PEG 3350, frozen in the same solution in liquid nitrogen and stored at -80 °C. The drop volume ratio of 3 parts protein: 2 parts reservoir solution:1 part seed stock were used (protein volume varied from 0.6 to 2.4 µL).

For the hCCS C12,22,25,244,246A – E,Zn wt hSOD1 trays were set using 1.2 µL of protein at 25 mg/mL and crystals grew in 6 months in the condition 20% (w/v) PEG 3350, 0.2 mM Sodium Nitrate and 0.1 M Bis-tris Propane (pH=8.0). The crystals were analyzed by SDS-Page and X-ray diffraction.

The hCCS DII homodimer grew from 1.2 µl of 15 mg/mL full-length hCCS C22,25S – wt hSOD1 with the addition of 0.2M Sodium chloride, 20% (w/v) PEG 6000, 0.1 M HEPES (pH 7.0) reservoir solution after roughly 8 months. Crystal content was also checked by SDS-PAGE.

For E,Zn hSOD1 C57,146A – hCCS C22,25S the complex was crystallized at 20 mg/ml in 0.1 M MES (pH 6.0), 0.2 M Magnesium chloride, 20 % (w/v) PEG 6000, with a protein initial drop size of 0.6 µL. Matrix seeding technique and seeding serial dilution was employed during optimization. Crystals appeared within 45 days.

E,Zn hSOD1 C57,146A – hCCS C12,22,25,244,246A and Cu,Zn hSOD1 C57,146A – hCCS C12,22,25,244,246A at 8 and 6 mg/mL, respectively, were crystallized in 0.1 M PCTP buffer, pH 9.0, 20% (w/v) PEG 3350. For these crystals the seeding dilution optimization was varied from 1:5 to 1:25, moreover the best results were obtained increasing the drop size to 2.4 µL of protein. Crystals appeared within 25 days.

Finally, hCCS C244,246A – E,Zn hSOD1 C57,146A at 30 mg/ml and wt hCCS – E,Zn hSOD1 C57,146A at 15 mg/ml were crystallized by mixing 0.25 µL protein and 0.25 µL of precipitant. The crystals grew after roughly 6 months under the following conditions: 1) 0.2 M ammonium chloride, 20% (w/v) PEG 6000, 0.1 M MES pH=8.0 and 2) 0.002 M zinc chloride, 20% (w/v) PEG 6000 and 0.1 M Tris, pH=8.0, respectively.

3.9 Data collection, reduction, scaling & merging

All crystals were transferred into cryoprotective solution consisting of the respective reservoir solution and 20% glycerol and then flash frozen in liquid nitrogen. All crystals were tested at the Synchrotron Soleil Proxima 1 beamline, which

had a Pilatus 6M detector or at the *Diamond Light Source*. The data were collected with a transmission of 20%, exposure time of 0.2 seconds, oscillations of 0.25°, T= 80 K and a wavelength of 0.9795 Å. The exceptions were E,Zn hSOD1 C57,146A data which was collected on Diamond beamline IO3 and Cu,Zn hSOD1 C57,146A - hCCS C12,22,25,244,246A data collected on Diamond beamline I24 both using a wavelength of 0.97626 Å and Pilatus 6M detectors.

A diffraction experiment involves measuring numerous reflection intensities. Each reflection contains an amplitude and phase, but no directed information about the phases is measureable. The first stage in the process of creating a model of a biomolecule by X-ray diffraction crystallography is indexation. In this process, once the cell constants (a, b, c, α, β and γ) and the orientation of the unit cell is defined, it is possible to assign the reflections to their correct Miller indices (*h*, *k* and *l* values) corresponding to its coordinates in the reciprocal lattice.

Thereafter integration consists of counting how many diffracted X-ray photons corresponding to each diffraction maximum (reflection) have been measured by the detector for each set of Miller indices (hkl) (RHODES, 2006; RUPP, 2010; WLODAWER *et al.*, 2008). Throughout this work data processing was performed with iMOSFLM (BATTYE *et al.*, 2011), XDS (KABSCH, 2010) or DIALS (CLABBERS *et al.*, 2018).

The raw intensity of each reflection can be affected by the variability in the beam's path length through the crystal as it is moved into different orientations, the intensity of the incident X-ray beam, geometrical factors and beam polarization. It cannot be assumed therefore, that the intensities measured directly from the diffraction image are consistent across the whole data set. This problem is eliminated by observing reflections with the same index across more than one frame and rescales the intensities of the data so that identical reflections have identical intensity throughout. Once finalized this process, the Miller indices of each reflection (*hkl*), its intensity (I_{hkl}) and the standard uncertainty (σI_{hkl}) are obtained (RHODES, 2006; RUPP, 2010). This task is called scaling and merging and were performed here using the programs SCALA and or AIMLESS (EVANS, 2006).

The redundancy (or multiplicity) of the data set corresponds to the number of total reflections measured divided by the number of total unique reflections, already considering the symmetry of the crystal. It therefore corresponds to the mean number

of times a given reflection (or its symmetry equivalents) has been measured. The accuracy of the averaged intensities can be judged from the spread of the individual measurements of equivalent reflections by the R_{values}, in which R_{merge} is by far the most commonly used, but it does not take into account the multiplicity of the data. More elaborated R_{values} such as the R_{rim} or R_{meas} (redundancy-independent merging R-values) have been proposed (RHODES, 2006; RUPP, 2010).

In addition, the quality of the collected diffraction data was also evaluated by the signal to noise ratio calculated as the average $\langle |I|/\sigma(I) \rangle$ for all reflections in a given resolution layer. Usually, a signal to noise ratio between 1.5 and 2.0 is an acceptable value for a low-resolution cutoff during data processing (RUPP, 2010).

An alternative is to use $CC_{1/2}$, which takes into account the variance of the average intensities, and is defined as the linear correlation between two halves of a randomly separated experimental data set. A $CC_{1/2}$ value of 0.3 has become the recommended criterion for selecting the high-resolution cut-off of the data (ASSMANN; BREHM; DIEDERICHS, 2016; DIEDERICHS; KARPLUS, 2015).

3.10 The phase problem

Because $\boldsymbol{F_{hkl}}$ (the structure factor) is a periodic function, it possesses amplitude and phase. Each structure factor is described as:

$$\boldsymbol{F_{hkl}} = F_{hkl} \exp(i\emptyset_{hkl}) \tag{9}$$

where, F_{hkl} is the structure factor amplitude, and $\emptyset_{hkl}$ is the phase of the electromagnetic wave. For each of the reflections it is only possible to calculate the observed value of the amplitude of the structure factor:

$$F_{hkl} \propto \sqrt{I_{hkl}} \tag{10}$$

where, I_{hkl} is the total intensity scaled for each (hkl). From this equation if we know the I_{hkl} of each reflection, we can obtain the amplitude. The frequency is the same as the inverse of the spacing distance between the planes, $1/d_{hkl}$ but the phase, $\emptyset_{hkl}$ is not directly obtained (RHODES, 2006).

In fact, the phase problem is a major hurdle when the structure of a new protein is being experimentally determined. By adding the electrons at each point in space, the combined waves (structure factors) provide the complete image of the electron density ρ(xyz), calculated at each point xyz and displayed as a map, according to the equation:

$$\rho(xyz) = \frac{1}{V} \sum_{h} \sum_{k} \sum_{l} F_{hkl} e^{i\emptyset_{hkl}} e^{-2\pi i(hx+ky+lz)} \quad (11)$$

Where, V is the volume of the unit cell, and $F_{hkl}e^{i\emptyset_{hkl}}$ is the structure factor for the reflection whose Miller indices are hkl. The phase of the structure factor is $\emptyset_{hkl}$ and the summation is performed over all structure factors of different Miller indices. (RHODES, 2006; RUPP, 2010). It is important therefore to note that all structure factors contribute to the calculation of the electron density at all points (xyz) of the unit cell.

The common methods to solve the phase problem are: isomorphous replacement, anomalous diffraction or molecular replacement. In this work, both hCCS and hSOD1 have known structures so all the structures were solved using phase information taken from the native protein structure by molecular replacement in conjunction with experimentally measured intensities from the complex, using the program PHASER (MCCOY *et al.*, 2007).

From the molecular replacement, an approximate model for the structure of the asymmetric unit is obtained. Structure factors calculated on the basis of this model often disagree with observed structure factors. The index of agreement between calculated and observed structural factor amplitudes is commonly represented by a parameter called R_{factor}, defined as:

$$R = \frac{\Sigma||F_{obs}|-|F_{calc}||}{\Sigma|F_{obs}|} \quad (12)$$

Similarly R_{free} is a quantitative parameter that also indicates how good the generated model is. It is calculated in the same way as R_{factor}, but with 5% of the reflections that are intentionally separated during the scaling process. These reflections are not used in refinement and therefore have higher values when

compared to the values of R_{factor} but have the advantage of being unbiased by the refinement protocol.

In the current work all refinement was performed in reciprocal space by structure factor amplitude back calculations in order that the model becomes increasingly closer to the real molecule with calculated amplitudes $|Fc|$ approaching observed amplitudes $|Fo|$ (WLODAWER *et al.*, 2008). Reciprocal space refinement with Phenix (ADAMS *et al.*, 2010) or Refmac (MURSHUDOV *et al.*, 2011) was intercalated with successive rounds of manual model building in COOT (EMSLEY *et al.*, 2010) to inspect the fit of the model to the electronic density.

The quality of the model during refinement was checked using Molprobity (CHEN *et al.*, 2010). Parameters such as: bonds lengths, angles, the Ramachandran diagram and atom clashes values were taken into consideration. The refinement was carried out until the Rfactor had its value stabilized between the cycles, the difference between Rfree and Rfactor do not exceeds (7%) and after verifying the model stereochemistry (WLODAWER *et al.*, 2008). The generated figures of three-dimensional structures and electron density representations were made using Chimera (PETTERSEN *et al.*, 2004).

3.11 Analysis and structural comparisons

Human hSOD1 and hCCS sequences were compared to the BLAST Model Organisms Database. Prokaryotic sequences were removed before alignment with Clustal Omega (WATERHOUSE *et al.*, 2009) and visualization with WebLogo 3.0. A few eukaryotic sequences with atypical insertions in the regions of interest were also removed to aid visualization.

The predictions of physicochemical properties of sequences obtained were carried out in ExPasy server (ProtParam tool). Positional rsmd calculations from structural superposition, columbic surface charge as well as the electrostatic potential (using the APBS tool) were calculated within Chimera (PETTERSEN *et al.*, 2004). Finally, buried surface area, solvation free energy of interaction (ΔGint) and the interface contacts of the proteins were analysed with PISA (KRISSINEL; HENRICK, 2007).

3.12 Lipossome Binding assays

To establish if the distribution of copper to hCCS and cytosolic hSOD1 may involve the formation of a transient binary (hCCS - hCTR1 (human copper transporter 1)) or ternary (hSOD1 – hCCS - hCTR1) complexes in the context of a membrane scaffold we performed a liposome binding assay using: wt hCCS and hSOD1 C57,146A homodimers, the heterodimer (wt hCCS – hSOD1 C57,146A) and hCCS mutants (e.g., hCCS domain I, hCCS domain II, hCCS domain I,II, hCCS A231G and hCCS R30A, K31A).

For this experiment, lipid membranes were prepared from cholesterol (CHOL), 1-palmitoyl-2-oleoyl-sn-glycero-3-phospho-L-serine (POPS) and 1,2-Dipalmitoyl-sn-glycero-3-phosphocholine (PC) at a ratio of 1:7:2, respectively. CHOL, POPS and PC powder were dissolved in chloroform and dried under nitrogen gas. To generate the liposome, 500 nmol of lipids were hydrated with 50 µl of 20 mM Tris-HCl pH 7.4, 150 mM NaCl and incubated with agitation at room temperature for 45 min.

Thereafter, the lipid was sonicated in a warm water bath. Liposomes were incubated with 2 nmol of protein at 37 °C for 60 minutes whilst stirring. After that, the solutions were centrifuged at 16,000 xg for 30 min at 20 °C and the supernatant placed in a new eppendorf tube for further analysis.

The lipid pellet was resuspended in 200 µl buffer, pelleted again and the supernatant also collected. The liposome pellet was resuspended in 24 µL of buffer and 6 µL of 4x SDS-PAGE sample buffer. Cytochrome bc1 complex, which is well known to be constitute by intrinsic membrane proteins, was used as a positive control in 25 mM Potassium phosphate, pH 7.5, 100 mM NaCl, 3 mM Sodium azide, 0.015 % DDM.

The supernatant, washing solutions and pelleted fractions were analysed by reducing, denaturing SDS-PAGE. The band quantification was performed with ImageJ software, which calculated the intensity corresponding to each band and then the area under the peak. All fractions corresponding to the same sample were always loaded onto the same gel, to avoid differences in staining. The areas corresponding to all fractions of a given sample were summed and the percentage of membrane binding calculated. The experiment was carried out in triplicate.

4 Results and discussion

4.1 Protein Purification, oligomeric state and complex formation

wt hSOD1, hSOD1 A4V, hSOD1 H46R, hSOD1 C57,146A, hSOD1 C57A, hSOD1 C146A and hSOD1 H46Q/H48R as well as recombinant wild-type human CCS and its mutants were expressed, cells harvested and purified as described in section 3.1. All the fractions were analysed by SDS-PAGE and those found to contain the proteins of interest were concentrated and applied to a Superdex 200 16/60 GL (GE healthcare) column pre-equilibrated with 20 mM Tri-HCl (pH 7.4), 150 mM NaCl and 5 mM DTT operated with an ÄKTA purifier (GE Healthcare) at 4°C (Figure 11).

Figure 11 - Size exclusion chromatograms using Superdex 200 16/60 GL (GE Healthcare) gel filtration column. (A) Profiles for wt hSOD1, hSOD1 H46R, hSOD1 C57,146A, hSOD1 H46R/H48Q, hSOD1 A4V, hSOD1 C146A, hSOD1 C57A. (B) Profiles for wt hCCS, hCCS C22A, hCCS C25A, hCCS C22,25S, hCCS C244,246A, hCCS C12,22,25,244,246A, hCCS DII,III and hCCS DII. (C) SDS-Page 15% for the proteins after elution from SEC. Lanes: 1) Protein Ladder. 2) wt hSOD1 3) hSOD1 H46R 4) hSOD1 H46R/H48Q 5) hSOD1 A4V 6) hSOD1 C57A 7) hSOD1 C146A 8) hSOD1 C57,146A. (D) SDS-Page 15% for the hCCS and mutants. Lanes: 1) Molecular mass markers 2) wt hCCS 3) hCCS C22,25S 4) hCCS C12,22,25,244,246A 5) hCCS A231G before TEV cleavage 6) hCCS A231G 7) hCCS C22A before TEV cleavage 8) hCCS C22A 9) hCCS C25A before TEV cleavage 10) hCCS C25A 11) hCCS C244,246A before TEV cleavage 12) hCCS C244,246A 13) hCCS DI,II 14) hCCS DII,III 15) hCCS DII 16) hCCS DII R232A.

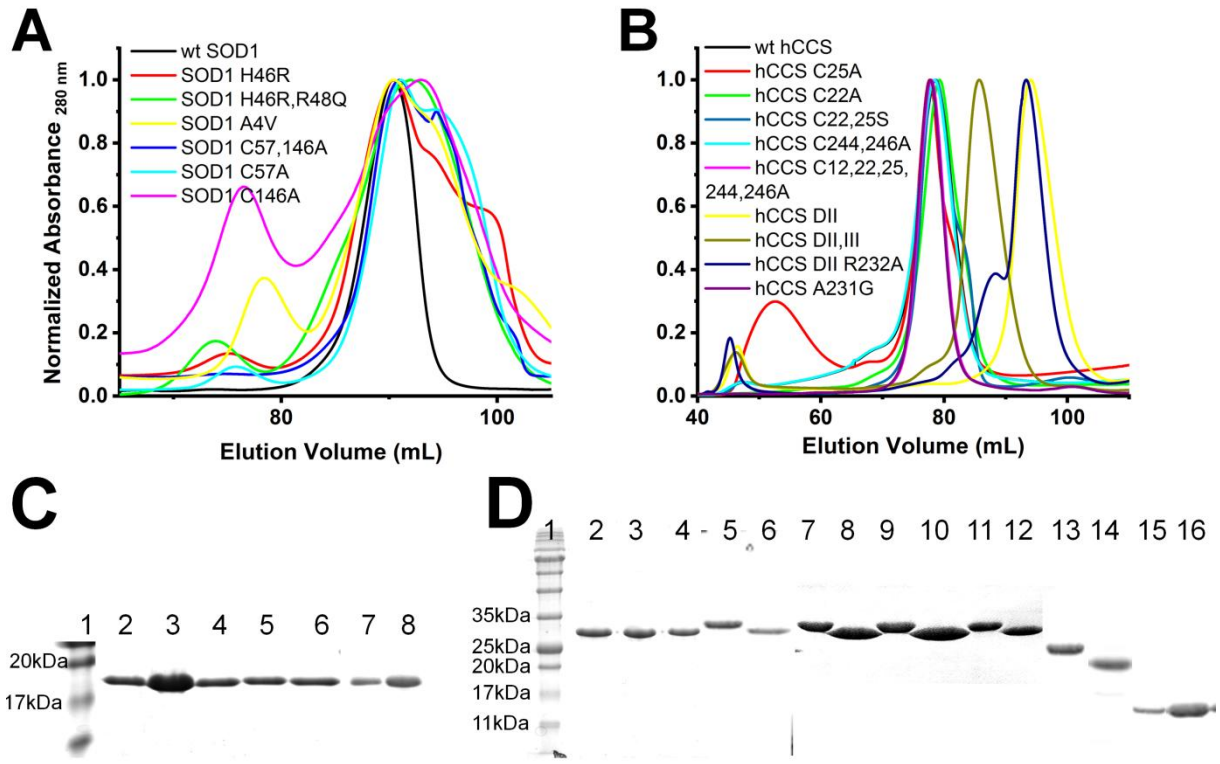

Source from: Own authorship.

Figure 11 A and B shows the size-exclusion chromatograms for some of the hSOD1s, hCCSs and their mutants, respectively. The wild type full length proteins have molecular mass of approximately 15 kDa and 29 kDa, respectively, as previously shown in Table 1. Examined by SEC a dominant peak at ~90 mL is observed for wt hSOD1 (Figure 11 A) and at ~80 mL for wt hCCS (full length) (Figure 11 B), as extensively studied, both proteins are described to be predominantly dimeric in solution (also further confirmed by SEC-LS in Figure 12 E and F)

(CAPPER *et al.*, 2018; WRIGHT; ANTONYUK; HASNAIN, 2016; WRIGHT; HASNAIN; GROSSMANN, 2011).

For the hSOD1s, the wild type is unique in showing a single peak in solution, with all of the mutants presenting more complexes profiles. The chromatograms for hSOD1 A4V, hSOD1 H46R and hSOD1 H46R/H48Q have a shoulder in their profiles, possibly due the already described propensity of the ALS-hSOD1 mutants to monomerize (HOUGH *et al.*, 2004).

Indeed, studies have shown that while the zinc-metalated and disulphide oxidized wt hSOD1 has been found to have a dimer dissociation constant (Kd) of 2.2 nM (BROOM *et al.*, 2015; WILCOX *et al.*, 2009), in the case of the A4V mutant this is weakened to a value of Kd = 957 ± 30 nM. Both hSOD1 H46R and hSOD1 H46R/H48Q display a strong tendency for the disulphide reduced state and have a low affinity for zinc, with a reduced dimer affinity of hSOD1 H46R/H48Q = 5.3 µM (CAPPER *et al.*, 2018). Moreover, the mutation of Cys57 and/or Cys146 decrease the affinity of the homodimeric hSOD1 to about 51.0 µM (CULIK *et al.*, 2018). Together, the weakened affinities may result in the partial monomerization observed in the chromatograms profile with a shoulder (Figure 11 A).

On the other hand, the full length hCCS mutants (e.g., hCCS C22A, hCCS C25A, hCCS C22,25S, hCCS C244,246A, hCCS C12,22,25,244,246A and hCCS A232G) displayed much less variation in the elution volume compared to the wild type (Figure 11 B), indicating they are all likely to be homodimers in solution. However, no information can be taken regarding the oligomeric state of the truncated hCCS domains. To further analyse them we have loaded the samples: hCCS DI, hCCS DII, hCCS DI,II and hCCS DII,III as well as the wt hCCS and wt hSOD1 onto the SEC-LS. Figure 12 displays the results and Table 3 compares the theoretical and predicted molecular mass and the most probable oligomeric state:

Figure 12 - SEC-LS analysis for wt hCCS, hCCS domains and wt hSOD1. Proteins were separated and analyzed by SEC and subsequently LS. (A) hCCS domain I (B) hCCS domain II (C) hCCS domain I,II (D) hCCS domain II,III (E) wt hCCS (F) E,Zn wtSOD1^{SS}. The column AdvanceBio 300 Å, 4.6 x 300 mm and particle size 2.7 µm (Agilent) was used for (A), (B) and (C) while Superdex 75 10/300 GL (GE Healthcare) for (D), (E) and (F). Chromatograms display the UV absorbance at 280 nm for all constructs except for hCCS DI which was monitored at 222 nm. Determinate values of average molar mass for the peaks are displayed in black.

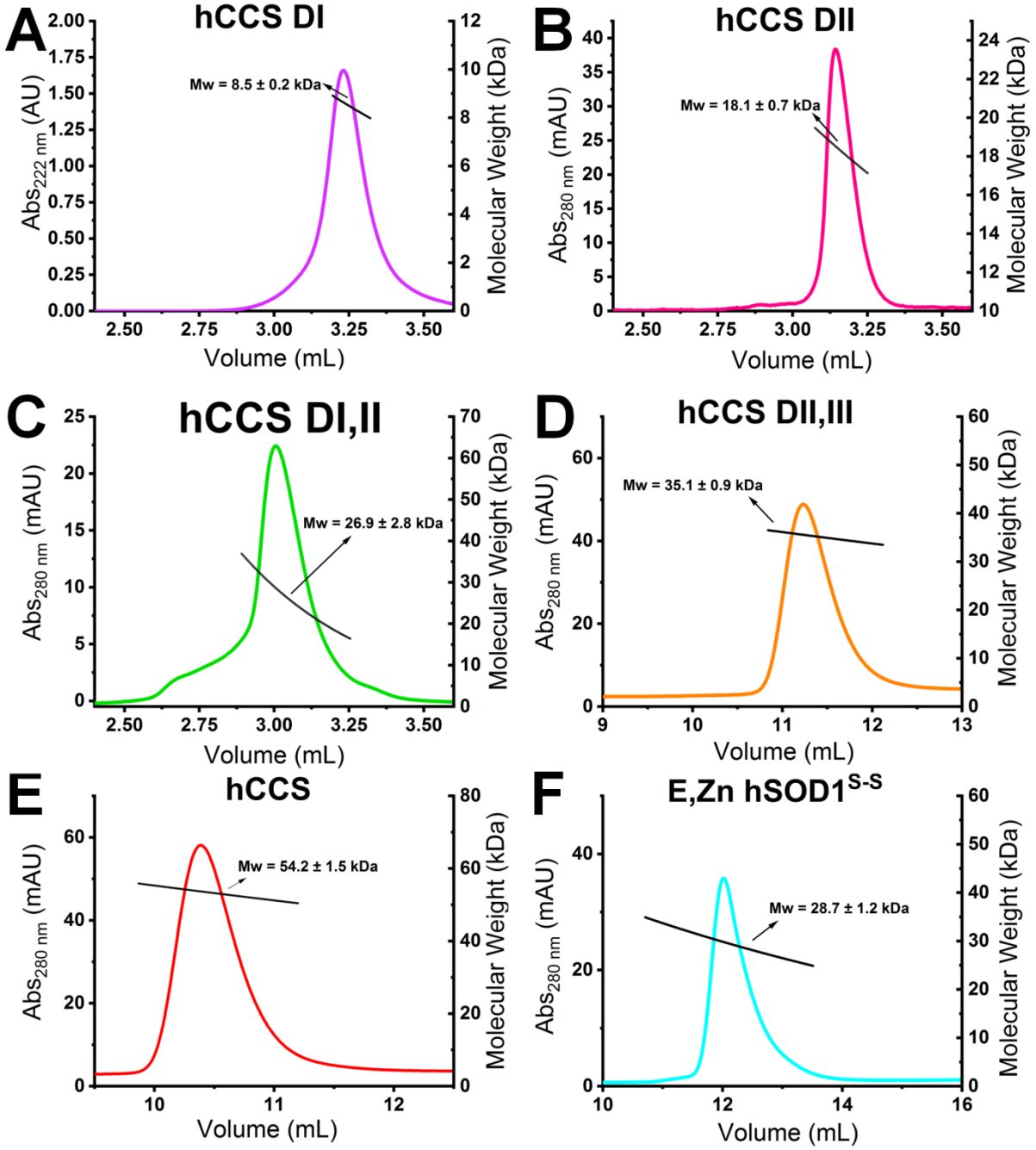

Sourc e from: Own authorship.

Table 3 – Theoretical and predicted molecular weight for wt hSOD1 and hCCS wild type and mutants.

Protein	Theoretical molecular weight (kDa)	Experimental molecular weight (kDa)	Oligomeric State
hCCS DI	9.1	8.5 ± 0.2	Monomeric
hCCS DII	15.7	18.1 ± 0.7	Monomeric
hCCS DI,II	24.6	26.9 ± 2.8	Monomeric
hCCS DII,III	20.2	35.1 ± 0.9	Dimeric
wt hCCS	29.1	54.2 ± 1.5	Dimeric
wt hSOD1	15.8	28.7 ± 1.2	Dimeric

Source from: Own authorship.

In all cases, the concentration of each species was 60 µM, with the exception of hCCS DI which was analyzed at 5 mg/mL. The copper apo zinc metalated wt hSOD1 and wt hCCS were also investigated and, as previously reported confirmed to be a homodimer in solution (CAPPER *et al.*, 2018; WRIGHT; ANTONYUK; HASNAIN, 2016).

On the other hand, the SEC-LS results for: hCCS DI, hCCS DII and hCCS DI,II revealed that the proteins were monomers in solution, while hCCS DII,III probably present an equilibrium between monomers and dimers, more probable shifted towards dimeric form. The theoretical molecular weights of all constructions are listed in Table 1 and Table 3. The increased dimer affinity of hCCS DII,III over the other truncated mutants, suggests a role of domain III in hCCS homodimerization. To define the effect of concentration on its oligomeric state the hCCS: DII, DI,II and DII,III were tested at higher concentrations (Figure 13):

Figure 13 – Protein oligomerization analysis as a function of concentration. Chromatograms display the UV absorption at 280 nm for all constructs except for hCCS which was monitored at 222 nm because of the low concentrations used. (A) hCCS Domain II at 60 µM and 300 µM. (B) hCCS Domain I,II at 60 µM and 200 µM. (C) hCCS Domain II,III at 60 µM and 200 µM. (D) hCCS concentration was diluted from 750 µM to 21 µM and (E) further to 0.7 µM. The SEC column used was the AdvanceBio 300 Å, 4.6 x 300 mm and particle size 2.7 µm (Agilent), except for hCCS DII,III which the Superdex 75 10/300 GL (GE Healthcare) was employed.

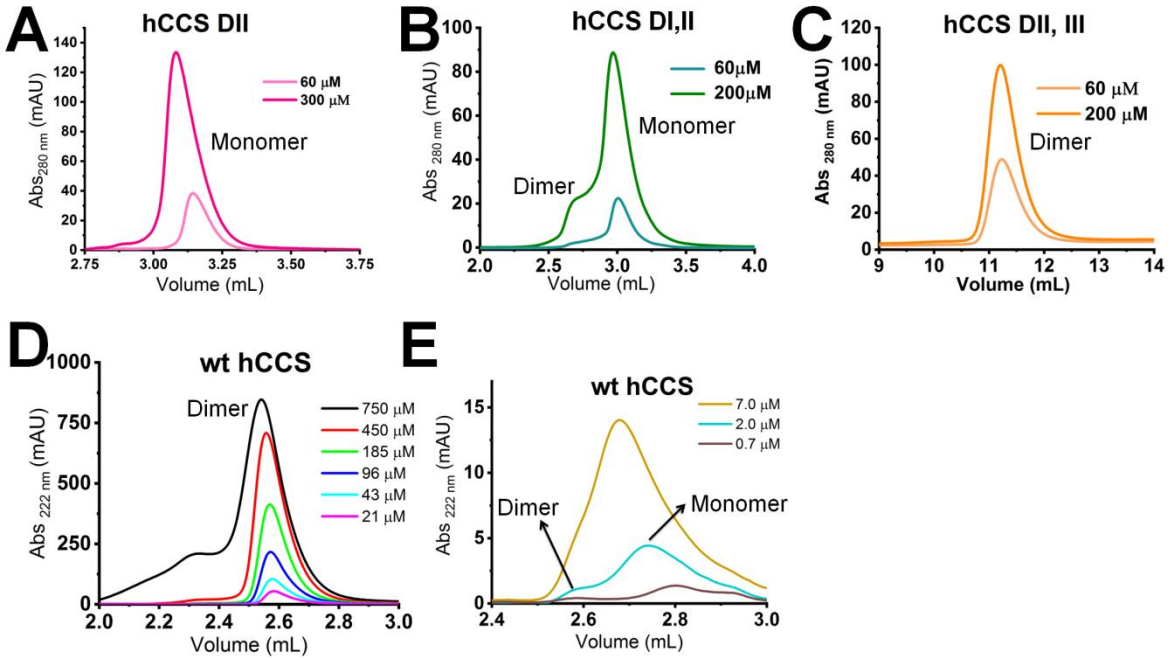

Source from: Own authorship.

hCCS DII showed slightly increase in elution volume (Ve) value as a function of concentration, which suggests a dynamic equilibrium between a monomer and a higher molecular weight species, presumably a dimer. The construct including domains I and II on the other hand, clearly displays the formation of dimeric species which probably has a dissociation constant in the mid-low micromolar range (Figure 13 B). Finally, there were no clear transitions in the Ve values for hCCS DII,III in the concentration range analyzed, which reinforces its higher dimeric affinity.

While the affinity constants for the holo, apo, disulphide reduced and disulphide-oxidized hSOD1 as well as the hSOD1-ALS mutants have been extensively studied, the hCCS homodimer affinity is completely unknown. Albeit the yeast ortholog has a dimer dissociation constant close to 3.0 µM (HALL *et al.*, 2000), the two proteins do not share high sequence similarity as already discussed in 1.2.2. In an attempt to quantify the dimer dissociation constant of the full length wt hCCS the protein was studied in a wide range of concentrations, from 750 µM to 0.7 µM in a

SEC column (Figure 13 D and E). At the maximum concentration, significantly higher molecular mass aggregates (larger than dimers) are observed (Figure 13 D) but as the concentration is decreased, this oligomerization disappears. A main peak compatible with a dimeric species is observed in all curves over the range of 750 µM to 21 µM where basically no variance is observed in the elution volume.

The likely monomer/dimer equilibrium can be seen only at concentrations lower than 7 µM. For instance, at 2 µM two distinct species are clearly observed in solution (Figure 13 D E). Using the SEC results a dimer affinity constant could be calculated if lower protein concentrations were allowed, but the signal at 222 nm was already excessively low, limiting the precise of the determined value of Kd. However, the transition observed suggests that hCCS homodimeric dissociation constant is within the low micromolar range, close to that previously described for yeast CCS (HALL *et al.*, 2000).

After protein purification the complexation between hCCSs and human SOD1s was performed by mixing the proteins stoichiometric protein ratios, as all proteins are dimers in solution and have different molecular weight we were able to isolate the heterocomplex using size exclusion chromatography. Figure 14 depicts the identification of a heterodimer (45 kDa) as a peak observed in an intermediate position from those for homodimeric hCCS (60 kDa) and hSOD1 (30 kDa) when loaded individually. Most of the hCCS and hSOD1 mutants were single point mutations and it did not cause variation in the elution volume.

Figure 14 - Size exclusion chromatographic analysis of heterodimers and their constituents. Proteins were loaded singly onto Agilent 1260 series HPLC using Bio SEC-3 4.6 x 300 mm column with 3 µm bead size and 300 Å pore size at flow rate of 0.3 ml/min and 20 °C. (A) E,Zn wt hSOD1 - hCCS. (B) E,Zn hSOD1 A4V - hCCS. (C) E,Zn hSOD1 H46R - hCCS. (D) E,Zn wt hSOD1 - hCCS C22A. (E) E,Zn wt hSOD1 - hCCS C25A. (F) E,Zn wt hSOD1 - hCCS C22,25S. (G) E,Zn wt hSOD1 -hCCS C244,246A. (H) E,Zn hSOD1 H46R/H48Q - hCCS. (I) E,Zn hSOD1 C57,146A - hCCS C22,25S. (J) E,Zn hSOD1 C57,146A - hCCS. (K) E,Zn hSOD1 C57,146A - hCCS C12,22,25,244,246A. (L) E,Zn wt hSOD1 - hCCS DII. (M) E,Zn wt hSOD1 - hCCS DII,III.

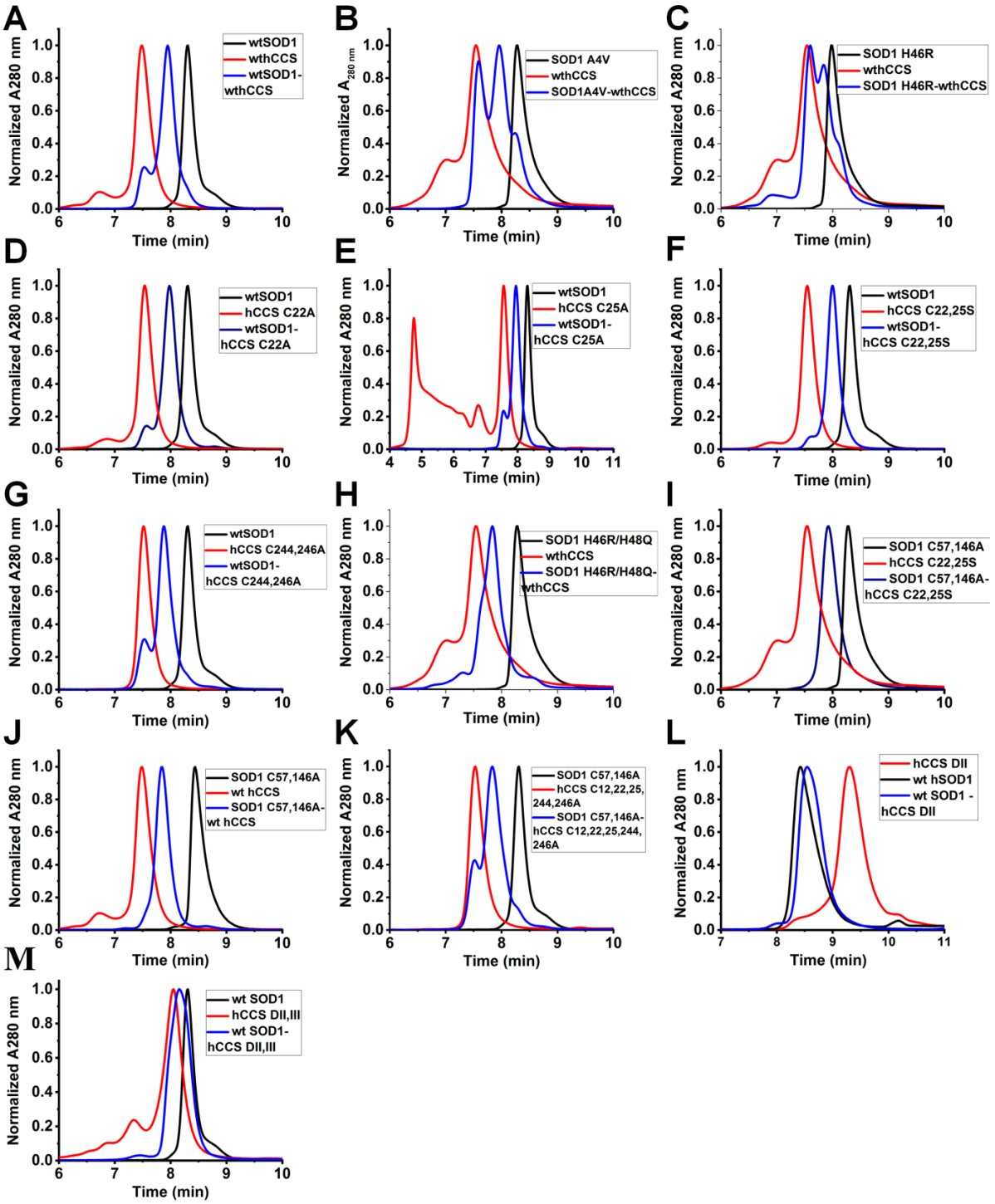

Source from: Own authorship.

Interestingly, the ALS-mutant hSOD1 heterocomplexes (i. e., Figure 14 B, Figure 14 C and Figure 14 H) show two shoulders on gel filtration of the mixture at the positions where the maxima for hCCS and hSOD1 are found when loaded alone. The results therefore reveal the lower efficiency of these mutants to form heterocomplexes when compared to the wild type. The interaction between the two components is crucial during the maturation process which hSOD1 undergoes in order to increases its stability. A defective interaction in the case of the fALS mutants may lead to deficient hSOD1 maturation and may be a possible mechanism by which these mutants present enhanced toxicity (CAPPER *et al.*, 2018; WRIGHT; ANTONYUK; HASNAIN, 2016). Indeed, the disulphide-reduced and metal-free hSOD1 has been hipothesized to be an intermediate in the aggregation process suggesting that proper maturation of hSOD1 is essential to avoid the formation of toxic species (FURUKAWA; O'HALLORAN, 2005; GERTSMAN *et al.*, 2019; MCALARY *et al.*, 2019; RAKHIT; CHAKRABARTTY, 2006).

Additionally, the unexpected behaviour of hCCS C25A, (Figure 14 E) is worthy of note. When loaded individually onto the column the protein presented a peak corresponding to considerably aggregated species or higher order oligomers, different to that observed for wt hCCS and hCCS C22A (Figure 14 A and D, respectively). This result suggests that the mutation of Cys25 facilitates aggregation possibly by leaving Cys22 exposed. Interestingly, the introduction of hSOD1 to the hCCS C25A in equimolar proportions eliminates all the oligomeric species and resulted basically in a single heterodimeric species. Thus, hSOD1 succeed in rescuing the hCCS C25A mutant from aggregation.

Moreover since the hSOD1 and hCCS DII have almost the same molecular weight (15.8 kDa and 15.7 kDa, respectively) distinguishing between homodimers of hSOD1 and heterodimers was expected to be difficult. As already discussed, the hCCS DII is a monomer (Figure 12 B) while the wt hSOD1 (Figure 12 F) and the hCCS DII – wt SOD1 are dimers with basically the same elution volumes (Figure 14 L). Since the elution volume for the copper chaperone domain II was the most altered between the three species, the strategy for this heterodimer was the use of a slight excess of hCCS DII over hSOD1 in order to guarantee the entire absence of hSOD1 in the form of homodimers.

The heterodimers were further analysed over time in order to study the formation of an intermolecular disulphide bond and the resulting stability of the complex as will be described below.

4.2 hCCS-hSOD1 disulphide bond transfer and copper acquisition

The involvement of hCCS in SOD1 maturation has been shown in vitro as well as in vivo (BANCI *et al.*, 2010a, 2012a, 2013a; WONG *et al.*, 2000) as have the need for aerobic conditions (BANCI *et al.*, 2013a). hCCS dependent hSOD1 disulphide oxidation was investigated by monitoring the dissociation of heterodimeric complexes over a time course using Agilent 1260 series HPLC (Agilent) coupled with a Bio SEC-3 4.6 x 300 mm column with 3 µm bead size and 300 Å pore size (Agilent). Combinations of hCCS and hSOD1 mutants including those affecting copper site amino acids and disulphide exchange cysteines were employed to elucidate the role of different protein moieties on complex stability (Figure 15). In our experiments we used disulphide reduced E,Zn hSOD1.

Figure 15 - hSOD1-hCCS heterodimers stability over time using SEC. We monitored the complexes at 0 hours and after: 2, 5 and 10 days. The flow rate used was 0.25 mL/min and temperature of 20 °C. (A) E,Zn wt hSOD1 – wt hCCS. (B) E,Zn wt hSOD1 - hCCS C22A. (C) E,Zn wt hSOD1 - hCCS C25A. (D) E,Zn wt hSOD1 - hCCS C22,25S. (E) E,Zn wt hSOD1 - hCCS C244,246A. (F) The fraction of heterodimer remaining in solution was determined over time and plotted as a function of the area under the relevant SEC elution peak height monitored at 280 nm.

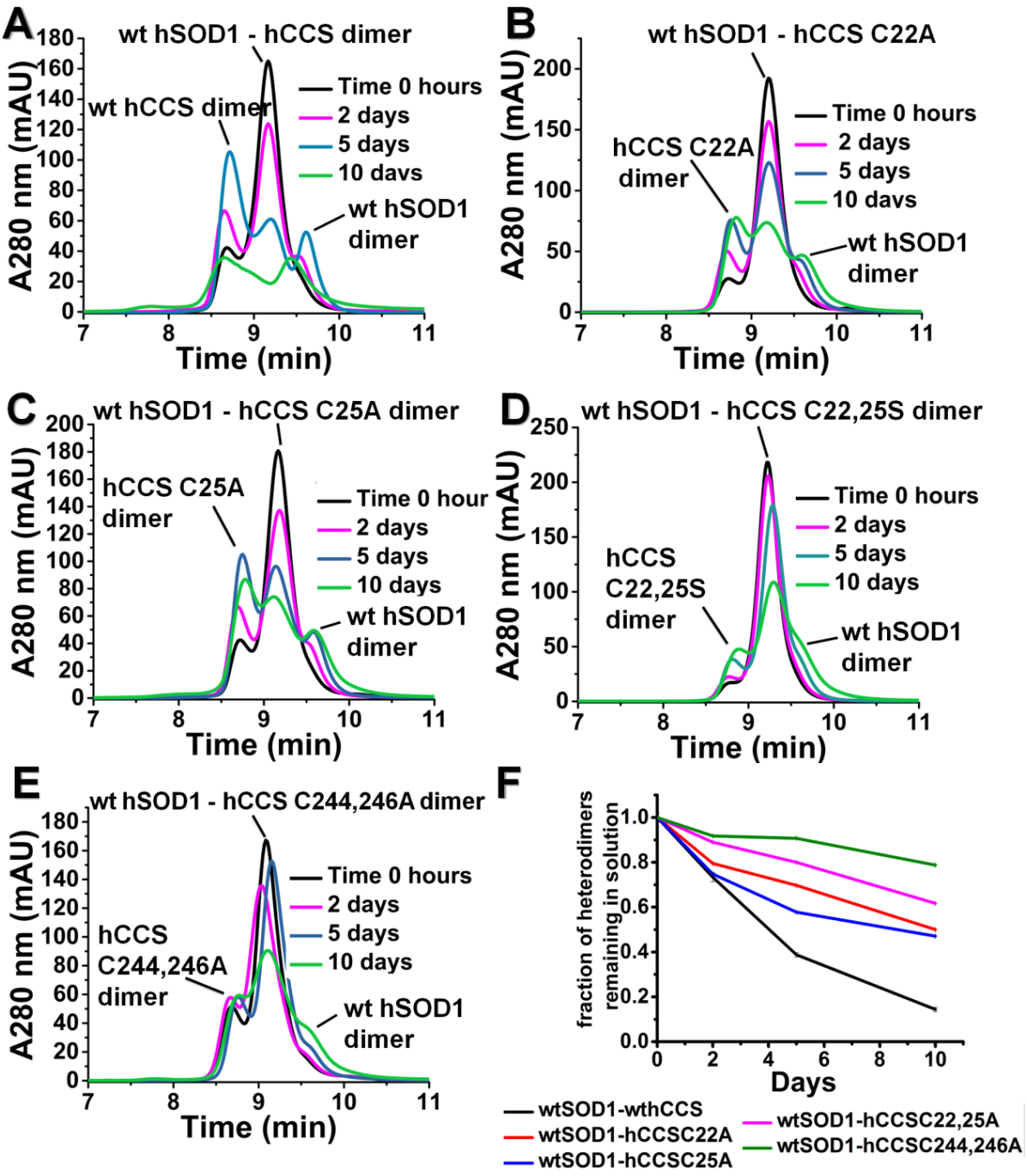

Source from: Own authorship.

We can observe that the wild-type hSOD1-hCCS complex readily dissociates into its components after 5-10 days of incubation even in the absence of copper

(Figure 15 A). This is in agreement with previous work (BANCI *et al.*, 2012b; WRIGHT; ANTONYUK; HASNAIN, 2016). The hCCS C-terminal CXC motif (involving residues 244 and 246) is known to transfer a disulphide bond to hSOD1 and knocking out this functionality almost completely inhibits complex dissociation. The hCCS Atx1-like domain (DI) binds copper and is responsible for its transfer to hSOD1 (BANCI *et al.*, 2012b).

However, when one cysteine in hCCS DI was mutated (hCCS C22A or hCCS C25A) the heterodimers exhibit decreased dissociation rates (Figure 15 B and C). This was most notable for hCCS C25A - wtSOD1 which shows faster dissociation between 2-5 days, but then remained fairly stable in solution until the end of the experiment (Figure 15 F). Moreover, the combination of C22S and C25S mutations had an additive effect and was more stable than the single DI cysteine mutants with approximately half of the complex remaining after 10 days (Figure 15 D and F), but still less stable than hSOD1 - hCCS C244,246A, which had more than 80% heterodimers remaining in solution (Figure 15 E and F).

To ascertain if the hCCS-hSOD1 complex dissociation results directly from the formation of the hSOD1 intra-subunit disulphide bond (Cys57-Cys146), the disulphide status was evaluated with addition of AMS followed by SDS-PAGE under non-reducing conditions at day 0 and day 10 (Figure 16). AMS adds 0.5 kDa per reactive thiol shifting the mobility of the protein in non-denaturing gels. SOD1 has 4 cysteine residues (Cys6, Cys57, Cys111 and Cys146), and as the AMS reactivity generally goes to completion a shift of roughly 2 kDa was expected for reduced wt hSOD1.

Typically, the 15.8 kDa wt hSOD1 migrates anomalously on SDS gels at a higher molecular weight than expected (17 to 20 kDa) as shown in Figure 16 B, lane 7. Similarly, the exact same molecular mass was observed for the oxidized wt hSOD1 after reaction with AMS (Figure 16 B, lane 6) suggesting that none of the four Cys residues were able to react. This can be rationalized based on the stability of the oxidized protein. Clearly Cys47 and Cys146 are unavailable since the disulphide bridge is present in the oxidized form and presumably Cys6 and Cys111 are inaccessible to the reactant due dimerization. When hSOD1 is oxidized the protein forms a homodimer, in which both Cys6 and Cys111 are located at the interaction interface between the monomers.

The fully reduced wt hSOD1 when treated with AMS (Figure 16 B, lane 9) displayed a major band close to 25 kDa, indicating a shift in mobility of approximately 6.0 kDa. Although a shift was anticipated, the value itself is much higher than expected (2 kDa) and is probably related to the fact that the native SOD1 already shows and anomalous migration on SDS-PAGE as mentioned above. Furthermore, the aberrantly large shift in mobility of hSOD1 after thiol alkylation has been previously reported and was described to be caused specially by Cys111 anomalous migration (CARROLL *et al.*, 2009).

We further examined the specific contribution of Cys57 and Cys146 (the focus of the experiment) to the shifts in apparent molecular mass. For this purpose we inserted as experimental control, the fully reduced hSOD1 C57,146A treated with AMS. The results displayed an intermediate band or bands (Figure 16 B, lane 8) between the reduced and oxidized forms of wt hSOD1 (Figure 16 B, lane 9 and 6, respectively). In the case of this mutant, at most two cysteines (6 and 111) could be modified. The fact that they apparent have undergone reaction (different from the oxidized native enzyme) is consistent with the fact that the mutant protein (as well as reduced SOD1 itself) is monomeric, less stable, and described as highly flexible (CULIK *et al.*, 2018; LINDBERG *et al.*, 2004), presumably leading to the exposure of Cys6, Cys111 or both.

Moreover, since the oxidation state of hCCS was not relevant for complex association or dissociation, we did not focus our analyzes on this protein. The band corresponding to the wt hCCS and mutants were indicated by a red arrow in Figure 16 B and C. In view of these considerations, we will now discuss how the disulfide bond formation is linked with heterocomplex dissociation.

Figure 16 - hSOD1 disulphide status was analyzed by AMS modification. (A) wt hSOD1 control: Lane 1: 0 days, lane 2: 10 days. (B) wt hSOD1 disulphide status at time 0. Lane 1: wt hCCS – wt hSOD1, lane 2: hCCS C22S - wt hSOD1, lane 3: hCCS C25A – wt hSOD1, lane 4: hCCS C22,25S – wt hSOD1, lane 5: hCCS C244,246A – wt hSOD1, lane 6: wt hSOD1 partially oxidized, lane 7: wt hSOD1 with no AMS modification, lane 8: hSOD1 C57,146A, lane 9: reduced wild-type hSOD1. (C) hSOD1 disulphide status after 10 days: Lane 1: wt hCCS – wt hSOD1, lane 2: hCCS C22A – wt hSOD1, lane 3 hCCS C25A – wt hSOD1, lane 4 hCCS C22,25S – wt hSOD1, lane 5: hCCS C244,246A – wt hSOD1, lane 6: wtSOD1 not completely reduced. M – Molecular mass markers.

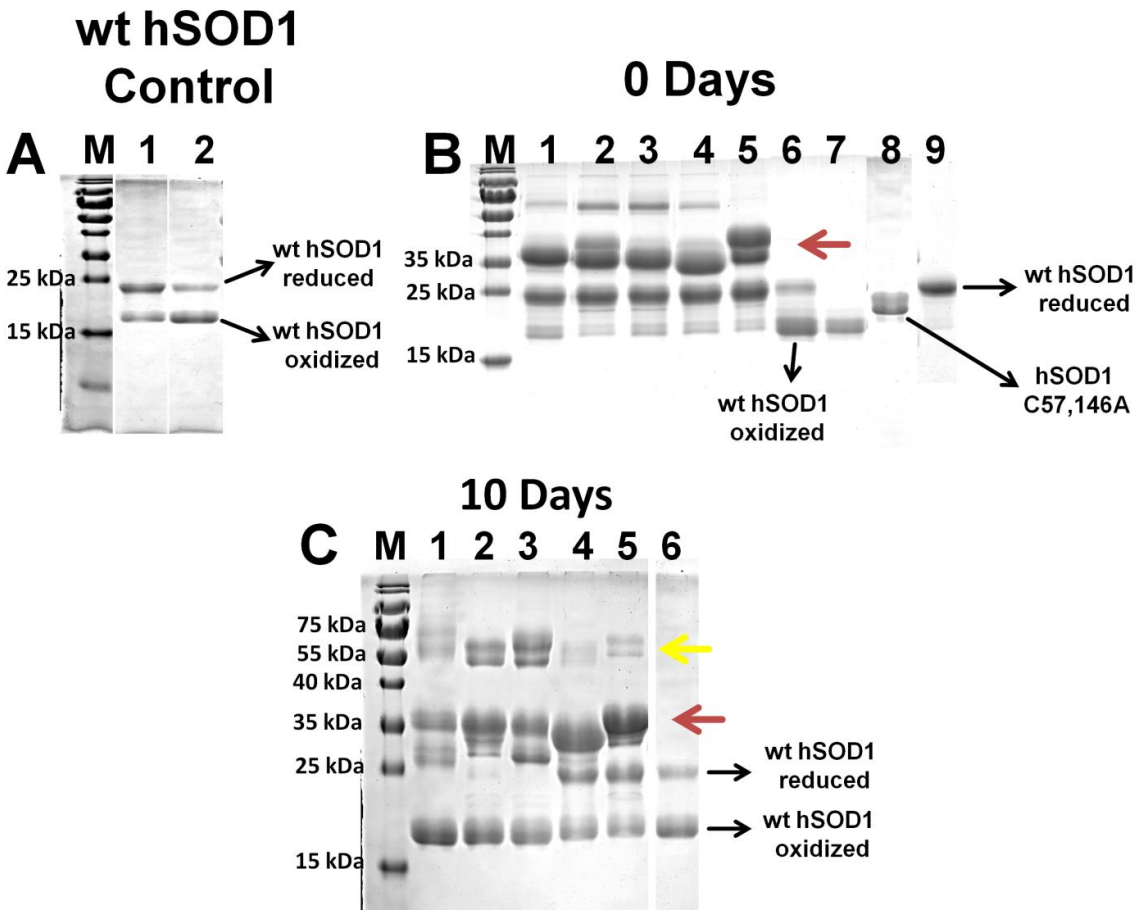

Source from: Own authorship.

Figure 16 A depicts no significant change in wild-type hSOD1 oxidation when exposed to air for 10 days without access to hCCS. After complex formation between wt hSOD1 and hCCS little oxidized hSOD1 was detected irrespective of the hCCS mutant provided, emphasizing the need for the disulphide reduced state during heterodimer formation (CULIK *et al.*, 2018; LAMB *et al.*, 2001; LINDBERG *et al.*, 2004).

After 10 days, the samples were also reacted with AMS, the results showed that wt hSOD1 was completely oxidized to some degree in each case (Figure 16 C). Moreover, high molecular weight bands appeared over 10 days (Figure 16 C, yellow

arrow) indicating oligomer formation. In fact, the oxidation of Cys6 and Cys111 have been described to be related to aggregation and possibly to act as a trigger for the development of amyloid-like structures (BANCI *et al.*, 2007, 2008).

Taken together, these results demonstrated that the extent of hSOD1 disulphide formation parallels complex dissociation in Figure 15; the hSOD1 Cys57 and 146 thiol are completely oxidized when wild-type hCCS is present whereas disulphide reduced hSOD1 is found in roughly equal proportion to disulphide intact species when C22,25S or C244,246A hCCS acts in thiol exchangers (lanes 4 and 5, Figure 16 C).

While hSOD1 can acquire copper from a source other than hCCS, there is no secondary route for disulphide formation. Our findings reinforce the crucial role of DIII in oxidation of the hSOD1 disulphide bond. However, different from the previous literature, our results also suggest that hCCS residues Cys22 and Cys25 in hCCS DI may have a cooperative action with domain III increasing its ability to oxidize transfer the hSOD1 disulphide bond (BANCI *et al.*, 2012b; FURUKAWA; TORRES; O'HALLORAN, 2004).

Furthermore, we wanted to address which cysteines in hSOD1 (i. e., Cys57 or Cys146) and the hCCS domains (Domain I or Domain III) may be involved in thiol oxidation. In the ySOD1-yCCS crystal structure a disulphide exchange between ySOD1Cys57 - yCCSCys229 (yCCSCys229 is equivalent to hCCSCys244) was trapped (LAMB *et al.*, 2001). Since we have shown that disulphide bond oxidation is the fulcrum of the complex dissociation, all samples used here display Cys57, Cys146 or both mutated to alanine. Thus, no complex dissociation should be seen. Moreover, reducing and non reducing SDS-PAGE was used to detect disulphide formation.

The following complexes were analysed: 1) hSOD1 C57,146A – hCCS C22,25S and hSOD1 C57,146A – hCCS C244,246A used as negative controls since both hSOD1 cysteines potentially able to form a disulphide bond were eliminated 2) hSOD1 C57A – hCCS C22,25S and hSOD1 C57A – hCCS C244,246A having just the cysteine at residue 146 and 3) hSOD1 C146A – hCCS C22,25S and hSOD1 C146A – hCCS C244,246A in which only the cysteine at position 57 is retained.

Initially, the copper chaperone and hSOD1 were mixed in equimolar proportions. Afterwards, only the peak corresponding to the complex eluted from the

Superdex 75 10/300 GL (GE Healthcare) was loaded onto the SDS-PAGE under non-reducing conditions to avoid formation of oligomers of the same species that could impair further analysis. The complexes were analyzed after different incubation times at 20 °C (Figure 17).

Figure 17 - hSOD1 disulphide transfer. Complexes were resolved by SDS-PAGE 15%. (A) Day 0 under reducing conditions. (B) Day 0 under non reducing conditions. (C) Day 3 under reducing conditions. (D) Day 3 under non reducing conditions. (E) Day 7 under reducing conditions. (F) Day 7 under non reducing conditions. For all SDS PAGE the lanes are as follow: Lane 1: hCCS C22,25S - hSOD1 C57,146A, lane 2: hCCS C244,246A - hSOD1 C57,146A, lane 3 hCCS C22,25S - hSOD1 C57A, lane 4 hCCS C244,246A - hSOD1 C57A, lane 5: hCCS C22,25S - hSOD1 C146A, lane 6: hCCS C244,246A - hSOD1 C146A.

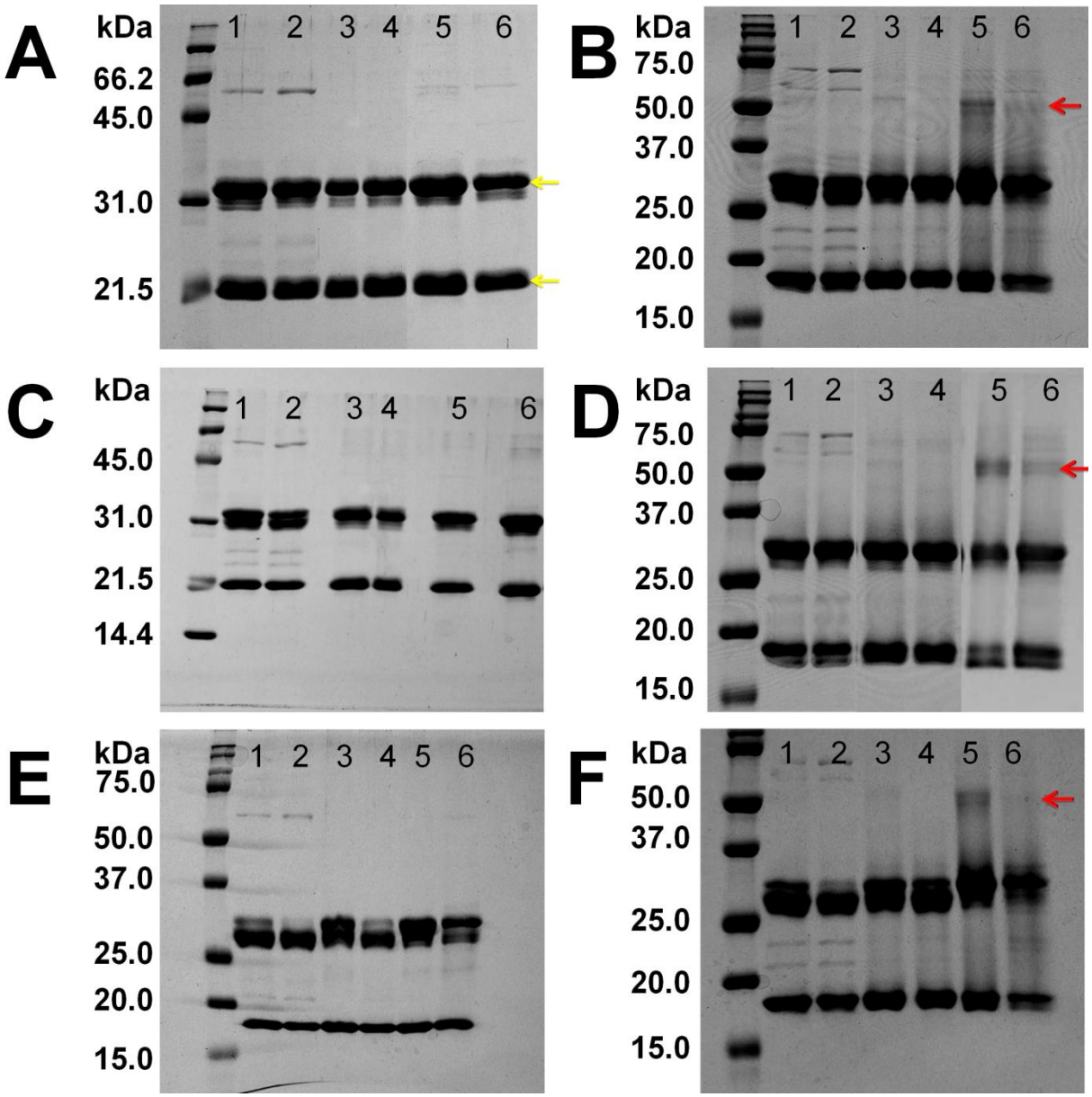

Source from: Own authorship.

In the case of disulphide interaction through hCCS Cys22,25,244 or 246 with SOD1 Cys57 or Cys146 we would expect a band around 45 kDa, characteristic of the heterodimer. In the SDS-PAGE corresponding to day 0 under reducing conditions we can only see bands equivalent to hCCS and to hSOD1, close to 31 kDa and 20 kDa, respectively (Figure 17 A, yellow arrows), demonstrating the purity of the samples.

Under non-reducing conditions the sample containing hCCS C22,25S - hSOD1 C146A (lane 5) displayed a band around 50 kDa (Figure 17 B), indicated by a red arrow. The band in the same region was also present, but at a significantly reduced intensity, in: hCCS C22,25S - hSOD1 C57A and hCCS C244,246A - hSOD1 C146A (Figure 17 B - lanes 3 and 6, respectively). No sign of these bands was present in the negative controls (Figure 17 A - lane 3, 5 and 6 and Figure 17 B - lane 1 and 2). The bands were within the molecular weight range which approximately matches the heterodimeric species. The slightly increase in the experimental molecular mass may be explained by the SOD1 apparent molecular weight which is systematically observed in SDS-PAGE to present an overestimate of its true molecular mass (15.8 KDa), as already discussed.

At day 3, the band indicated by the red arrow increased in intensity in lane 5 and 6 (Figure 17 D) and remained the same in lane 3 (Figure 17 D) and no signs of these bands were present in the negative controls (Figure 17 D - lanes 1 and 2 and Figure 17 C - lanes: 3, 5 and 6). Interestingly, after 7 days, in the hCCS C22,25S - hSOD1 C146A complex (Figure 17 F, lane 5) the band corresponding to the heterodimer was clearly evident, whilst it has disappeared in the case of the other complexes mentioned above, as can be seen in Figure 17 F lanes 3 and 6.

It is worthy of note that over time the band corresponding to the hCCS mutants seems to fade (Figure 17 E and F) and many new bands of molecular weights close to that of the copper chaperone have appeared. This is an indication of degradation, and a similar phenomenon has been reported previously for hCCS (LAMB *et al.*, 2000).

Taken together, our results suggest that disulphide transfer is most likely to occur via hCCS C244 or C246 and hSOD1 C57 interactions, in accordance with the yeast CCS-hSOD1 structure (LAMB *et al.*, 2001). However, in the absence of these specific cysteines (in hCCS DIII), it seems possible at least that thiol transfer could occur by employing other alternative cysteines depending on which are present, as is

also described by our experiments shown in Figure 15 and Figure 16, indicating a possible role for DI during the disulphide transfer. This would explain the observations presented in Figure 17 B and D were a possible disulphide interaction occurs between hCCS Cys22 or Cys25 with hSOD1 Cys57A (lane 6).

When the experiment was designed we expected to observe weak bands corresponding to the monomeric hSOD1 and hCCS proteins and strong bands matching the heterodimeric species, due to interaction between the cysteine residues in hCCS DI and/or DIII and SOD1 Cys57 or 146. However, the results obtained displayed the contrary. The bands corresponding to heterodimeric species showed relatively low intensities, indicating that only a small portion of the heterodimers formed the disulphide interaction. These results suggest that the exchange of the disulfide bond between hCCS and SOD1 might not be as trivially trapped as previously anticipated (BANCI *et al.*, 2012b; LAMB *et al.*, 2001). The flexibility concerning hCCS domain III may play a role decreasing the chances of a stable disulphide bond formation. Although, a lot remains to be understood regarding the mechanism of disulphide transfer, our in vitro results suggest more promiscuous thiol exchange specificity than has been described to date.

To gauge whether hCCS is able to form a complex with copper metalated hSOD1 and deduce the sequence of post-translational modifications, Cu,Zn hSOD1 C57,146A and E,Zn hSOD1 C57,146A were mixed at equimolar proportions with hCCS and analysed by SEC. In vitro addition of copper(II) to wt hSOD1 has a tendency to form the hSOD1 disulphide so we performed these experiments using the C57,146A hSOD1 double mutant. Figure 18 A and shows that copper and zinc metalated but disulphide reduced hSOD1 competently forms a complex with the wild type hCCS.

Figure 18 - Heterodimerization in presence and absence of copper. SEC using the Bio SEC-3 4.6 x 300 mm column (Agilent) at flow rate of 0.25 ml/min and 20 °C. (A) Zn hSOD1 C57,146A propensity towards heterodimer formation with wt hCCS with and without copper. (B) Cu,Zn hSOD1 C57,146A – wt hCCS and (C) E,Zn hSOD1 C57,146A – wt hCCS stability over the time.

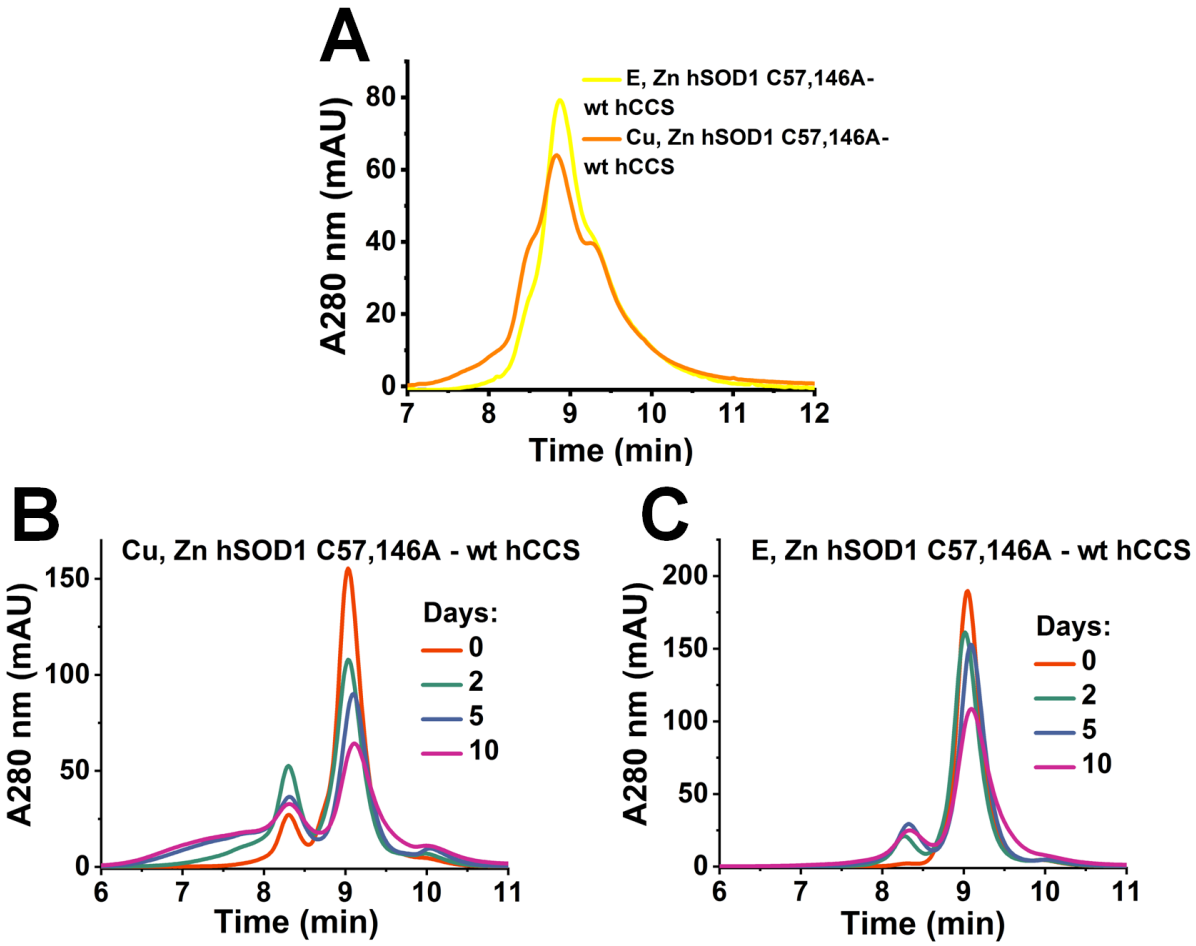

Source from: Own authorship.

In addition, we analysed heterodimer stability over time. Figure 18 B indicates that, while the copper-containing complex is more prone to tetramerization and aggregation in comparison with the copper-apo form (Figure 18 C), the heterodimer does not disassociate when there is no means to form the hSOD1 disulphide. This confirms that hSOD1 disulphide formation is the final step in hCCS catalysed maturation and is the prompt for complex disassociation.

Overall, these data confirmed the hypothesis that copper incorporation should be an early step in the hCCS-hSOD1 maturation process and does not have a key role in complex formation and stability. Moreover, along with others, we have shown that hSOD1 must be disulphide reduced to form a complex with hCCS and here we have verified the hypothesis that disulphide formation actuates complex dissociation.

Finally, we have shown that hCCS domain I can speed up hSOD1 disulphide oxidation which preferentially occur through and interaction between hCCS DIII and hSOD1 Cys57 (BANCI *et al.*, 2012b; FURUKAWA; TORRES; O'HALLORAN, 2004). However, in the absence of these specific partners, promiscuous interaction is observed.

Thus disulphide formation is both the last step in the hSOD1 maturation, pathway and the regulator of complexation with hCCS (Figure 16 and Figure 18). It seems that hCCS is able to distinguish between disulphide reduced and oxidized hSOD1 but the question that remains is: how the chaperone recognizes these states? To address this, sequence analysis and crystallographic studies were performed.

4.3 Crystallization

4.3.1 Heterodimer stability, crystal conditions and data statistics

In order to test the most promising candidates for crystallography experiments, heterodimer stability was studied by monitoring dissociation over a time course using SEC. Wt hSOD1, ALS related mutants (hSOD1 A4V and hSOD1 H46R) as well as artificial ones (hSOD1 C57,146A, hSOD1 H46Q/H48R) were tested together with wt hCCS, hCCS C22,25S and hCCS DII,III in an attempt to trap a monodisperse species in an unproductive dead-end complex with restricted conformational dynamics (Figure 19).

Figure 19 - Heterodimer stability over the time analysed using size exclusion chromatography with a flow rate of 0.3 ml/min. The column used was the Bio SEC-3 4.6 x 300 mm (Agilent). 5 mM DTT was used in all complexes. (A) wt hSOD1 - wt hCCS. (B) hSOD1 A4V – wt hCCS. (C) h hSOD1 H46R – wt hCCS. (D) hSOD1H46R/H48Q – wt hCCS. (E) hSOD1 C57,146A – wt hCCS. (F) wt hSOD1 - hCCS DII,III. (G) hSOD1 C57,146A – wt hCCS. (H) wt hSOD1 - hCCS C22,25S. (I) SDS-PAGE with the fractions of SEC from (E) fractions.

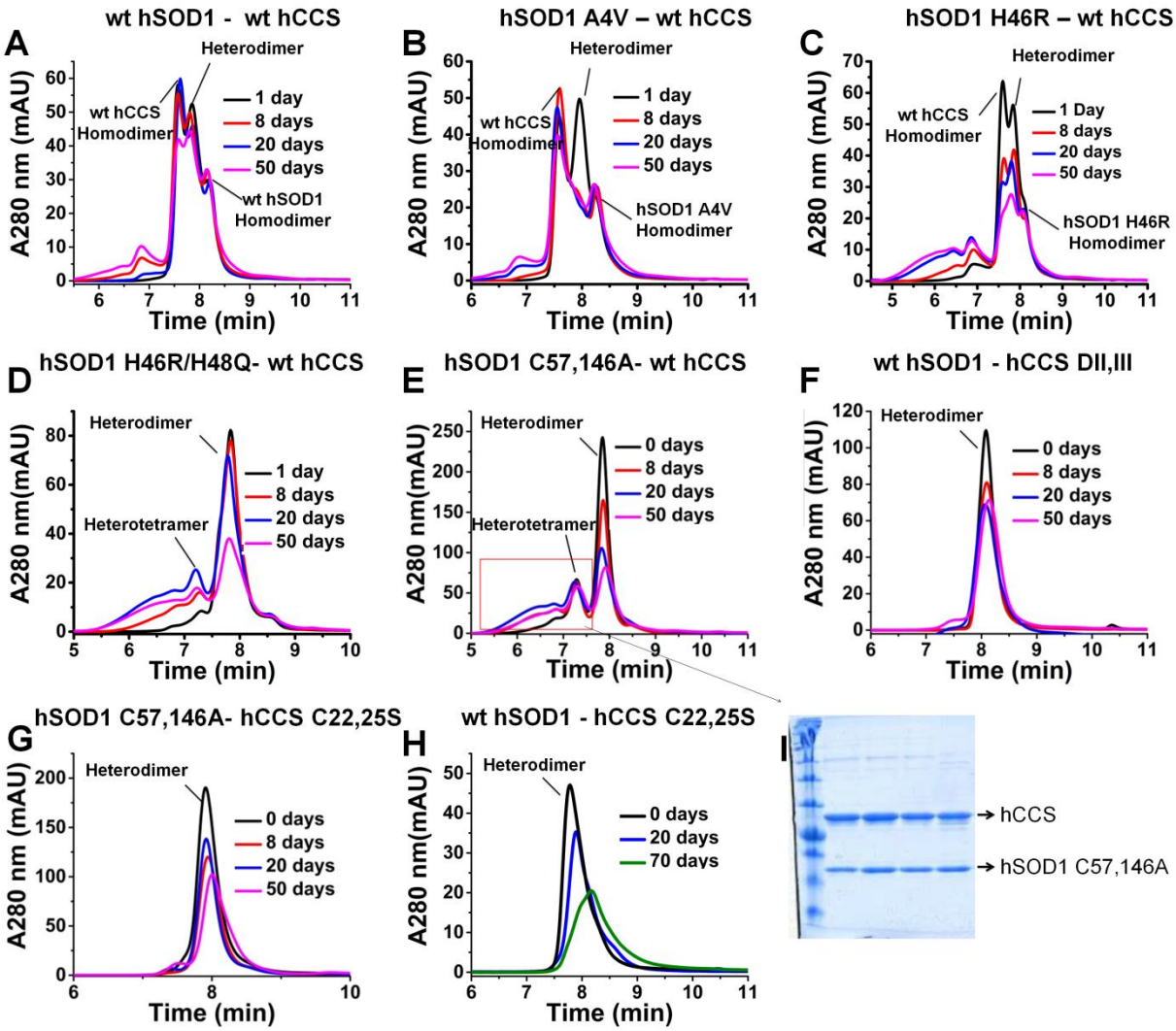

Source from: Own authorship.

As already discussed in Figure 14, the homodimers (i.e., hCCS and hSOD1) and the heterocomplex have different elution times allowing a full characterization of heterodimer formation and dissociation using size exclusion chromatography. In Figure 19 A, B and C, corresponding to: wt hCCS – wt hSOD1, wt hCCS - hSOD1 A4V and wt hCCS - hSOD1 H46R, respectively, the presence of three peaks in the chromatographic profile on the first day shows already partial dissociation or faulty interaction between the species. Over the course of the days, the characteristic

peaks of the heterodimeric species (at ~8mL) continue to decrease rapidly. This was faster for the latter two, consistent with previous studies that suggested a defective interaction between the chaperone and hSOD1 mutant in ALS related disease (CAPPER *et al.*, 2018; WRIGHT; ANTONYUK; HASNAIN, 2016).

On the other hand, wt hCCS - hSOD1 H46R/H48Q (Figure 19 D), wt hCCS-hSOD1 C57,146A (Figure 19 E) look stable over the time course of the experiment, with a major peak characteristic of the dimeric species. Nevertheless, some aggregation can also be seen. SDS-PAGE (Figure 19 I) showed that the aggregated species contain hCCS and hSOD1 in an equimolar ratio, indicating that this process does not involve complex dissociation.

The complexes: hCCS DII,III – wt hSOD1, hCCS C22,25S - hSOD1 C57,146A, hCCS C22,25S - wt hSOD1 (Figure 19 F, G and H, respectively) exhibited a single peak in solution and were therefore prioritized for crystallization trials. Moreover, based on their stability over time and results of the biophysical studies described in 4.2, diverse heterodimer combinations were rationalized.

The mutations were thought to reduce flexibility (e.g., hCCS DII and hCCS DII,III), and to avoid aggregation and disulphide transfer via cysteines residues in the copper chaperone (e.g., hCCS C22,25S, hCCS C244,246A, hCCS C12,22,25,244,246A) hSOD1 C57 and C146 oxidation was prevented by the use of mutants of these residues (e.g., hSOD1 C57A, hSOD1 C146A and hSOD1 C57,146A). Reductants such as DTT, TCEP (tris(2-carboxyethyl)phosphine) and β-mercaptoethanol were used whenever needed.

Sitting drop vapor diffusion crystallization trials were set up and crystals grew at 20 °C in 96-well plates with commercial screens. Optimization screens were carried out in 24-well plates using the hanging-drop vapour-diffusion method and microseeding methods as described in section 3.8. Crystals were obtained for the: hCCS DII,III – wt hSOD1 with and without reductants (Figure 20 A, B and C), hCCS C12,22,25,244,246A - wt hSOD1 (Figure 20 E), hCCS C22,25S – wt hSOD1 (Figure 20 F), hCCS C244,246A (Figure 20 H), hCCS C22,25S (Figure 20 I), and E,Zn hSOD1 C57,146A (Figure 20 J).

Figure 20 - Crystals, SDS GEL analysis and crystallization conditions. (A) (B) and (C) hCCS DII,III - E,Zn wtSOD1 crystals obtained without any reductant, with 10 mM DTT and 20 mM TCEP, respectively. (D) SDS-PAGE for the crystals hCCS DII,III- E,Zn wt hSOD1 (lane 2 and 3), Molecular mass markers is shown in lane 1. Crystals for: (E) hCCS C12,22,25,244,246A - E,Zn wtSOD1. (F) hCCS C22,25S - E,Zn wtSOD1. (G) SDS-PAGE for the crystals hCCS C12,22,25,244,246A - E,Zn wtSOD1 and hCCS C22,25S - E,Zn wtSOD1, lanes 2 and 3 respectively. Molecular mass markers is displayed in lane 1. (H) hCCS C244,246A. (I) hCCS C22,25S. (J) E,Zn hSOD1 C57,146A.

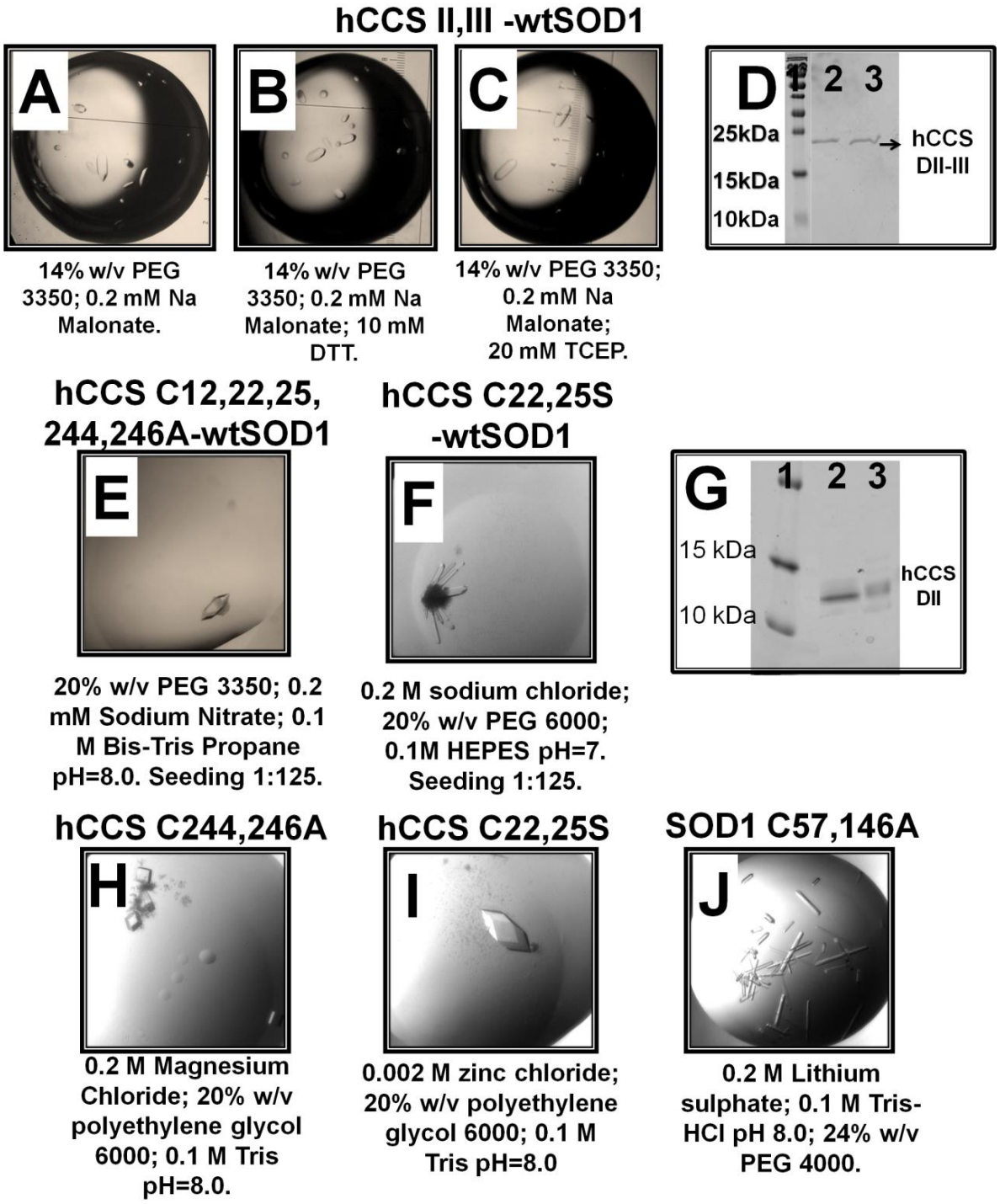

Source from: Own authorship.

All crystals were exposed to X-ray beams and the diffraction limit estimated. Crystals that diffracted to a resolution better than 3.5 Å were collected, data were processed and the structure solved by molecular replacement. Only promising data, which in this case means good resolution or proteins of interest in the asymmetric unit, were refined, validated and deposited.

Interestingly, crystals in Figure 20 A, B and C were crystallized under the same conditions with or without the addition of reductants, (DTT and TCEP). In all cases the space group was $P4_32_12$, and the crystals diffracted to a resolutions varying from 2.5 to 3.0 Å. However, rather than a heterodimer, the asymmetric units contained only hCCS. Even though both domains II and III were present in the crystallization solution and revealed by the SDS-PAGE (fig. 20 D) interpretable density was only observed for domain II. It is likely that the few amino acid residues at the termini were disordered and therefore no electron density could be observed.

The crystals for hCCS C22,25S – wt hSOD1 (Figure 20 F) and hCCS C12,22,25,244,246A – wtSOD1 (Figure 20 E) in turn when loaded onto SDS-PAGE also had only a single band corresponding to the copper chaperone domain II only, consistent with heterodimer dissociation and degradation in the crystallization drop (Figure 20 G), as previously described (LAMB *et al.*, 2000). So, although we have used a disulphide knock-out mutant to avoid dissociation (hCCS C12,22,25,244,246A in the case of fig 20E), the heterodimer still dissociates into its component parts.

While hCCS C12,22,25,244,246A – wt hSOD1 showed no improvement in the diffraction resolution, the crystal of hCCS C22,25S – wtSOD1 diffracted to resolutions of 1.55 Å. The structure was determined by molecular replacement using the hCCS DII structure (PDB code: 1DO5). The asymmetric unit displayed two hCCS domain II monomers which form a homodimer. The result was an improvement in resolution compared to the previously available hCCS DII crystallographic structure, (PDB code: 1DO5) which was reported at 2.75 Å. In our structure, the monomers A and B consists of residues 85-236 and 85-234, respectively with one Zn(II) ion per monomer as shown in Figure 21:

Figure 21 - The hCCS DII homodimer structure. The zinc ions are shown as gray spheres. PDB code: 6FN8.

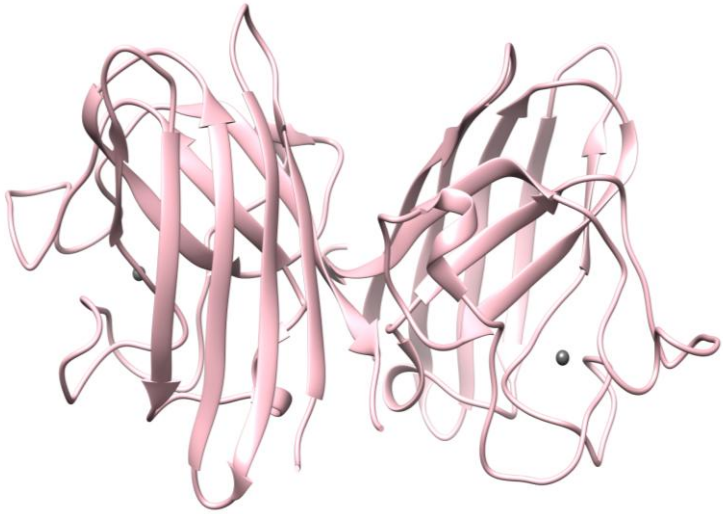

Source from: Own authorship.

As expected, the high resolution hCCS DII structure is very similar to that formerly described (1DO5) with which it presents mean RMSDs of 0.41 Å. However, the improvement in resolution allowed us to correctly model a significant number of residues involved in the interface between monomers, which plays an important role in the hCCS homodimer affinity, as will be described later (section 4.4.1).

Based on the success in crystallizing hCCS, trays for hCCS on its own were also set, aiming to determine the still unresolved full length human copper chaperone structure. To avoid degradation, 0.2 mM PMSF and/or EDTA were added during the purification of all proteins. The crystals for hCCS C244,246A (Figure 20 H) and hCCS C22,25S (Figure 20 I) grew after about one year and diffraction data were collected at SOLEIL Proxima 1, processed and used for molecular replacement. The crystals contained just hCCS DII due protein truncation, and diffracted at resolutions of 2.4 Å and 2.5 Å, respectively, lower than that already available.

Finally, we also crystallized and solved at 2.0 Å the previously unreported structure of E,Zn hSOD1 C57,146A (Figure 20 J). We aimed to potentially identify structural differences with the hSOD1 wild type structure. The molecular replacement was performed using as a model Cu,Zn wt hSOD1 (PDB code: 2C9V) and the results revealed six homodimers in the asymmetric unit, in which each monomer was coordinated to one Zinc ion (Figure 22).

Figure 22 - The E,Zn hSOD1 C57,146A homodimer. The zinc ions are shown as gray spheres. PDB code: 6FOI.

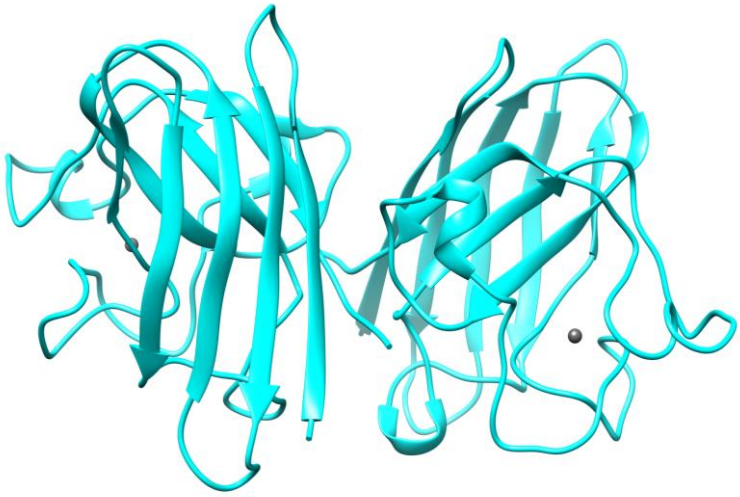

Source from: Own authorship.

The structural difference observed between the E,Zn hSOD1 C57,146A and the mature version of the enzyme, the Cu,Zn hSOD1^{SS} will be described in details in section 4.4.1. This structure provided insight into the hSOD1 preference for heterodimer formation when the cysteines are in the reduced state.

Overall, the results point out that despite our best efforts the heterodimer dissociates into its components over the time necessary for crystallization. As discussed in section 4.2 and shown in Figure 15 and Figure 16, the disulphide bond formation seems to be the last step prior to heterodimer dissociation, and so the use of hSOD1 C57,146A instead of wt hSOD1 seemed likely to increase heterodimer stability, since the knockout of the cysteines removes any way in which the heterodimer would dissociate.

The most promising mutants were carefully rationalized (based on the results from Figure 19) and the trays were set and optimized exactly as previously described in section 3.8. The crystals were obtained for the following heterocomplexes: 1) hCCS C22,25S - E,Zn hSOD1 C57,146A (Figure 23 A, B and C); 2) hCCS C12,22,25,244,246A - E,Zn hSOD1 C57,146A (Figure 23 E, F and G); 3) hCCS C12,22,25,244,246A - Cu,Zn hSOD1 C57,146A (Figure 23 H); 4) hCCS DII - E,Zn hSOD1 C57,146A (Figure 23 I); 5) hCCS C244,246A - E,Zn hSOD1 C57,146A (Figure 23 K); 6) wt hCCS - E,Zn hSOD1 C57,146A (Figure 23 I).

Figure 23 - Crystals, SDS gel analysis and crystals conditions. (A) Show the initial crystals for the hCCS C22,25S - E,Zn hSOD1 C57,146A requiring optimization. (B) and (C) show the improvement on crystals using classical optimization techniques, microseeding and microseeding matrix screening. (D) SDS-PAGE for the crystals hCCS C22,25S - E,Zn hSOD1 C57,146A in lane 2 and hCCS C12,22,25,244,246A - E,Zn hSOD1 C57,146A in lane 3. The molecular mass marker is displayed in the first lane. (E), (F) and (G) Show the initial and the improvement in hCCS C12,22,25,244,246A - E,Zn hSOD1 C57,146A crystals morphology by use and adjustment of seed stock concentration and microseeding matrix screening, respectively. (H) hCCS C12,22,25,244,246A - Cu,Zn hSOD1 C57,146A crystals (I) hCCS DII – E,Zn hSOD1 C57,146A. (J) SDS-PAGE for the crystals hCCS DII – E,Zn hSOD1 C57,146A in the second lane and the molecular mass markers in the first lane. (K) hCCS C244,246A - E,Zn hSOD1 C57,146A. (L) wt hCCS - E,Zn hSOD1 C57,146A.

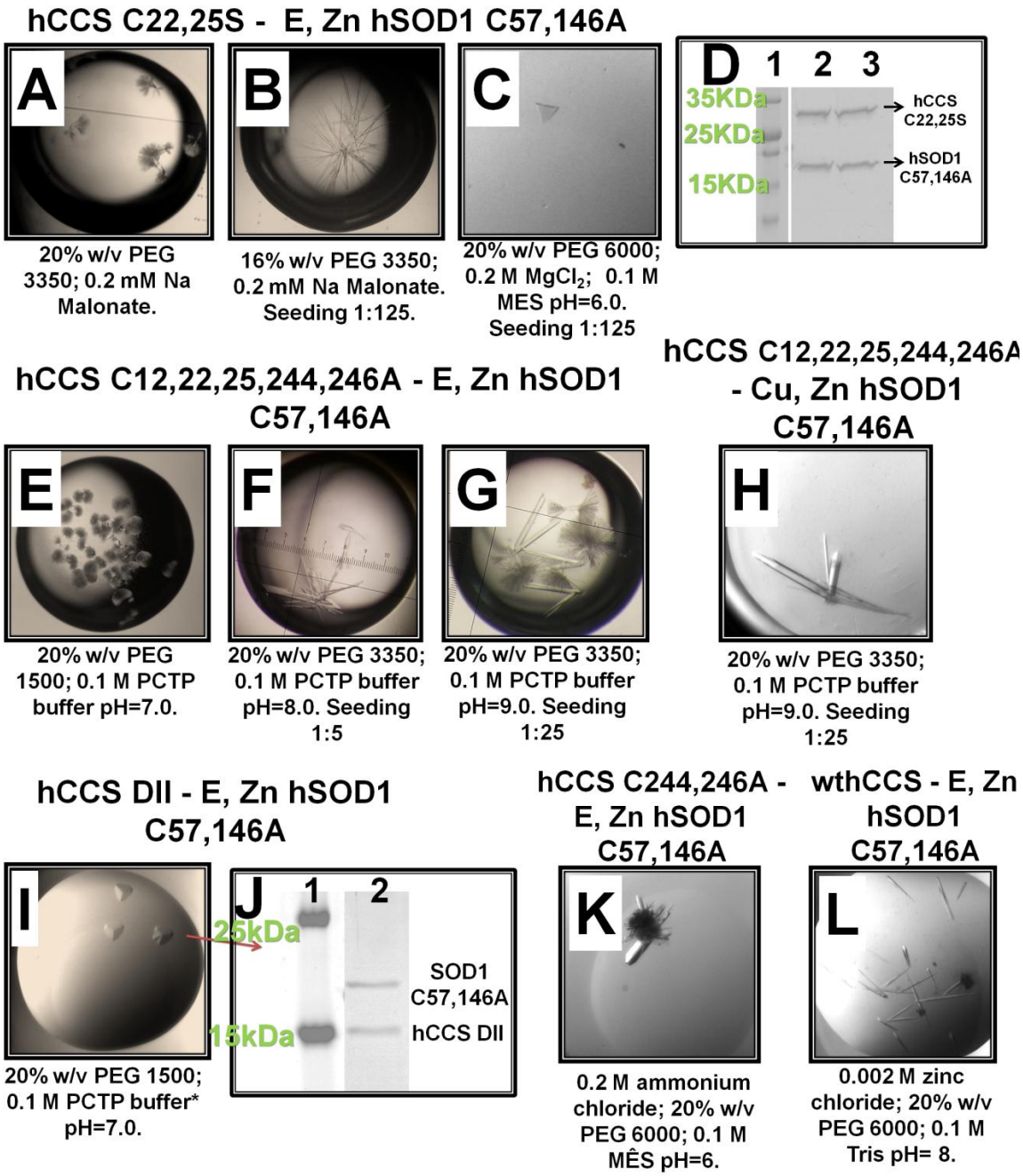

Source from: Own authorship.

The heterodimers in complex with hSOD1 C57,146A seemed to be more difficult to crystallize than with the wild type version of hSOD1. Various optimization techniques for hCCS C12,22,25,244,246A and hCCS C22,25S complexed with hSOD1 C57,146A were tested, including varying the temperature and protein: precipitant ratio and employing hanging drops, sitting drops and microbatch crystallization methods. However, improvement in crystal diffraction was only obtained using microseeding, as described in section 3.8. Moreover, due to the flexibility of the copper chaperone, domain truncations were tested to increase the chances of success in crystallization.

The hCCS DII - E,Zn hSOD1 C57,146A (Figure 23 I), henceforth referred to as the truncated heterodimer, crystallized in just 15 days and the SDS-PAGE (Figure 23 J) confirmed the present of a heterocomplex. The structure was solved at 2.55 Å, and contains 3 heterodimers in the asymmetric unit plus one hCCS DII (amino acid residues Gly83-Arg232) and one hSOD1 monomer (amino acids residues Ala1-Gln154) that interact respectively with hSOD1 and hCCS DII from other asymmetric units. Each heterodimer consists of a single hSOD1 monomer and a single hCCS DII monomer, as shown in Figure 24.

Figure 24 - The truncated heterodimer. The hSOD1 monomer is shown in cyan, hCCS DII in pink and zinc ions are shown as gray spheres. PDB ID 6FOL.

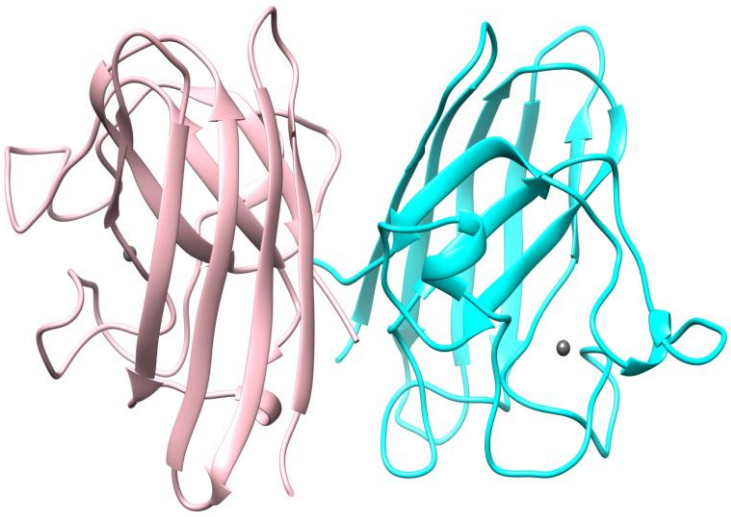

Source from: Own authorship.

As suggested previously for the yeast heterodimer (LAMB *et al.*, 2001) and also observed when comparing Figure 21, Figure 22 and Figure 24, the hSOD1, hCCS DII homodimer and hCCS DII - hSOD1 C57,146A heterodimer all interact

using the same interface, which includes the channel residues that leads to the hSOD1 active site (LAMB *et al.*, 2001). Furthermore, all the structures strongly resemble each other. However, superposition of either the hCCS DII or the hSOD1 homodimeric structures with the truncated heterodimer showed that a slightly rotation is needed upon hetero-complexation (Figure 25).

Figure 25 – Comparison of the truncated heterodimer with hCCS DII and E,Zn hSOD1 C57,146A homodimers. (A) A single chain in the E,Zn hSOD1 C57,146A homodimer, represented on dark gray, was superposed in the hSOD1 chain from the heterodimer (show in cyan). (B) A single chain from the hCCS DII homodimer, in light gray, was aligned to the truncated hCCS in the heterodimer. In both figures, the zinc ions are displayed as gray spheres. There are rotations concerning the heterodimerization, which can be observed by the second monomers that do not perfectly align structurally.

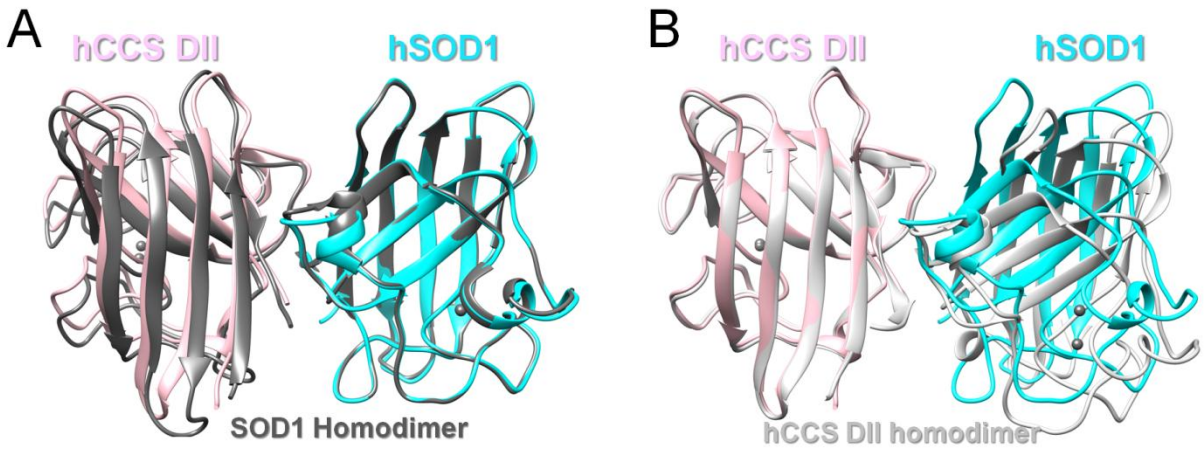

Source from: Own authorship.

Crystallization was also successful for hCCS C244,246A – E,Zn hSOD1 C57,146A (Figure 23 K) and wt hCCS – E,Zn hSOD1 C57,146A (Figure 23 L). However these crystals only diffracted to resolutions around 6-10 Å, reflecting the challenges encountered in crystallizing the heterocomplex.

Crystals for hCCS C22,25S – E,Zn hSOD1 C57,146A were optimized, as displayed in Figure 23 from A to C, using classical optimization techniques as well as microseeding and microseeding matrix screening. The improvement in crystals morphology paralleled its diffraction, which increased from around 10 Å (in Figure 23 A) to 3.05 Å (crystal shown in Figure 23 C). The analysis of the crystals by SDS-PAGE (Figure 23 D) revealed bands corresponding to the hSOD1 and hCCS present in equal proportions and indicated no degradation and/or heterodimer dissociation occurred.

The diffraction data were phased by using our truncated hCCS heterodimer. The new heterocomplex crystallized in space group $H3_2$, and displayed four heteroodimers in the asymmetric unit, which consist of two hSOD1 monomers interacting with their copper chaperone. The copper chaperone displayed a tripartite structure with Domain I, the AtxI like domain (residues Gln8-Asn85, represented in green in Figure 26 A), Domain II (residues Leu86-Ala234, in pink) and part of domain III structurally ordered (residues Gly235-Ile259, in yellow).

Figure 26 - The Elongated heterodimer. (A) The hSOD1 monomer is shown in cyan, hCCS DI in green, hCCS DII in pink and hCCS DIII in yellow. Zinc ions are shown in gray. PDB ID 6FON. The zoom displays the hydrogen bond formed between Asn85 and Gln238 (B) The hCCS assembly *in crystallo* is an octameric complex formed with the other complex present in the asymmetric unit and symmetry related molecules (in gray). The heterodimer is stabilized through contacts between the two hCCS DIII present into the asymmetric unit and via anti-parallel β-sheet interactions made by symmetrically related hCCS Domains III.

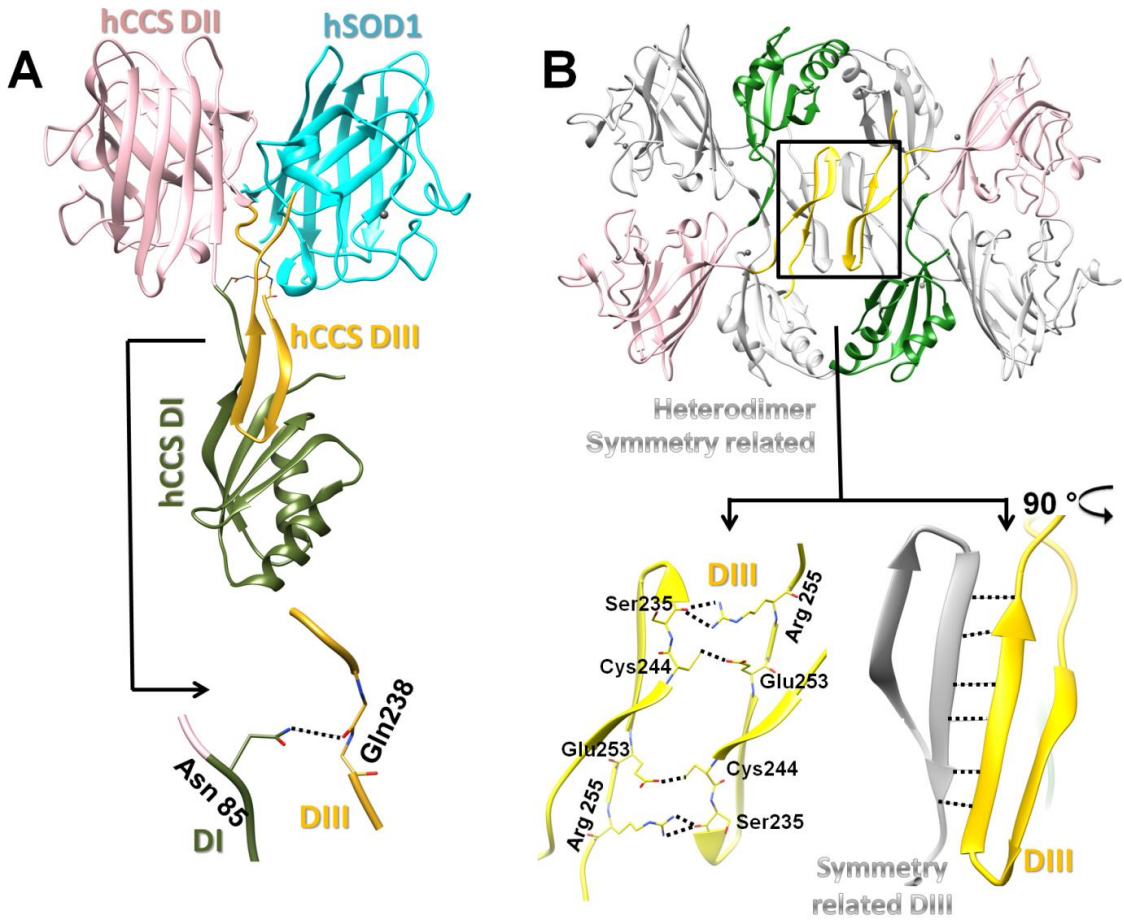

Source from: Own authorship.

We will refer to this structure as the elongated heterodimer due the copper chaperone domain I position, which swing away from domain II through movement of

a hinge region which connects them. The conformational dynamics of hCCS DIII is stabilized via an interaction between Asn85 from hCCS DI and Gln 238, as displayed in the zoom in Figure 26 A.

Notwithstanding the above, the elongated conformation of DIII is also stabilized via hydrogen bonds between the two hCCS DIII existent in the asymmetric unit and through lattices contacts with its symmetry related molecules, creating an anti-parallel β-sheet interface, as shown in Figure 26 B. The same β-sheet conformation for the hCCS DIII is also conserved in the yCCS-hSOD1 chimera structure (FETHEROLF *et al.*, 2017a).

Although the elongated heterodimer forms an octameric supramolecular assembly *in crystallo*, we do not expect this oligomeric form in solution. Rather, we hypothesize that this was an *in crystallo* artefact which stabilizes domain III, which is expected to be highly flexible based on its role during hSOD1 maturation. In fact, the high degree of conformation freedom is observed over the two heterodimers described so far, the yeast and chimera, in which domain III presents totally different conformations and structures, which will be described in details in section 4.4 (FETHEROLF *et al.*, 2017b; LAMB *et al.*, 2001).

The crystals for hCCS C12,22,25,244,246A – E,Zn hSOD1 C57,146A were also extensively optimized as show in Figure 23 E to G. The adjustment of seed stock concentration and microseeding matrix screening were fundamental to obtain the final resolution of 2.95 Å (crystals shown in Figure 23 G). Moreover, crystals for the same construction but with copper loaded were also obtained, using the same optimization strategy for the holo complex (Figure 23 H) and diffracted to a resolution of 3.3 Å. The incorporation of copper II to hSOD1 C57,146A was done prior to heterodimer formation as described in section 3.2.

Both crystals grew in the same conditions and revealed the same packing. The apo copper structure was phased with our truncated heterodimer, and thereafter used for the molecular replacement in the copper holo one. Both structures contain in the asymmetric unit 24 molecules divided equally between hSOD1 and hCCS, forming 12 heterodimers.

The hCCS display electron density map for domain I from residues Gln8 or Gly9 (depend on the chain) up to Asn85 (green in Figure 27), domain II from residue Leu86 to Ala234 (pink) and part of domain III, from residues Gly235 to Pro240,

Lys241, Gln242 or Ile243 (yellow) in all heterodimers in the asymmetric unit, with the exception of chain V in which only the hCCS DII (Ans85 to Ala234) was observable. In these structures, different from the elongated complex, domain I assumes a position spatially close to domain II, and for this reason will be referred to as the compact heterodimer, as shown in Figure 27:

Figure 27 – The Compact heterodimers. (A) The E,Zn compact heterodimer. hSOD1 monomer is shown in cyan, hCCS DI in green, hCCS DII in pink and hCCS DIII in yellow. Zinc ions are shown as gray spheres. PDB ID 6FP6. The orientation of hCCS DII is the same as showed in figure 26. (B) The compact heterodimer rotated by 90 °. (C) The Cu,Zn compact heterodimer was oriented and the colour pattern was the same as shown in (B) and copper shown as an orange sphere. (D) hCCS DIII stabilization via contacts with hCCS DI and hSOD1 Thr58.

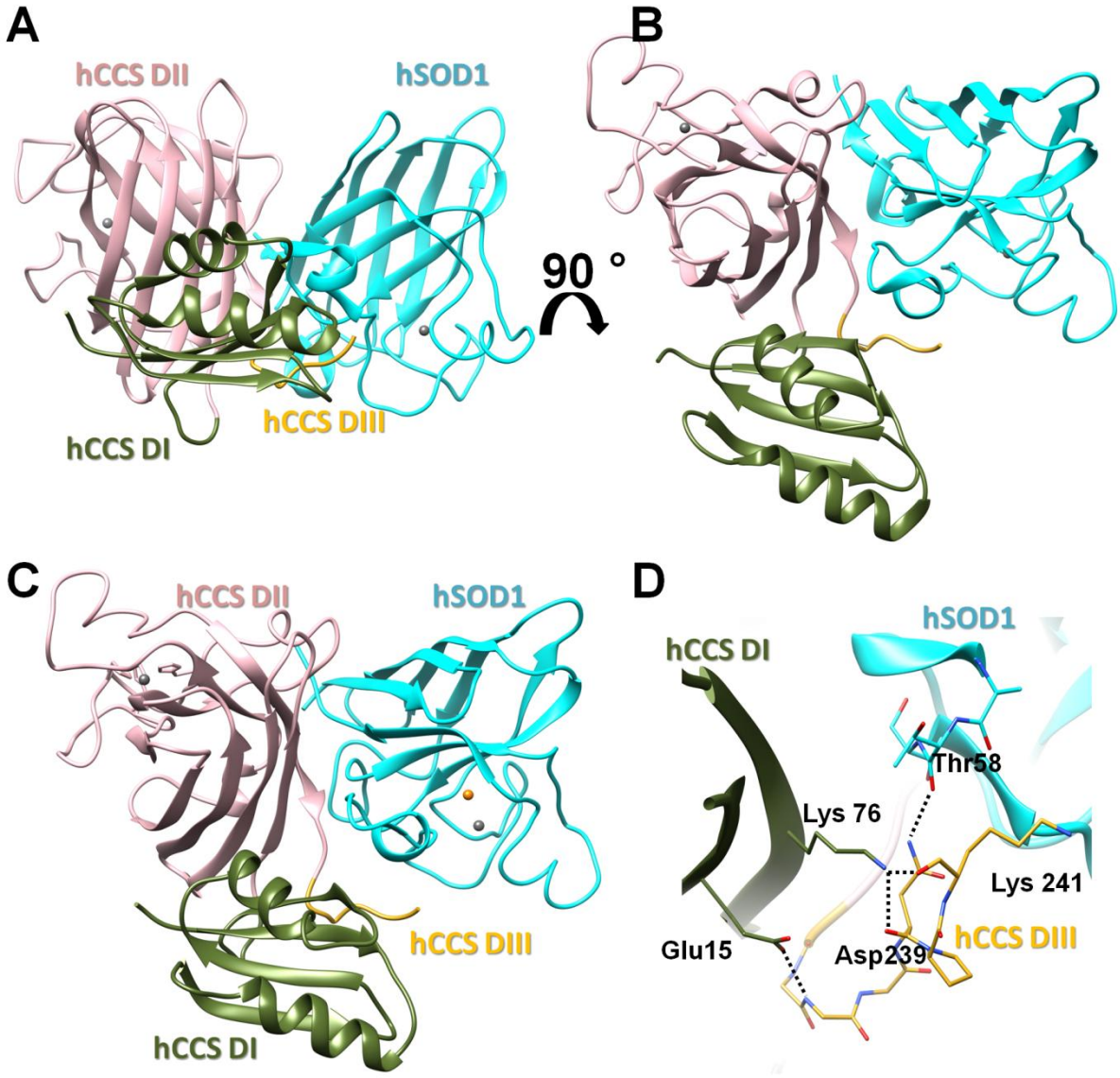

Source from: Own authorship.

All the twelve heterodimers present in the asymmetric unit showed the same relative orientations for domains I, II and III conformation. The different orientations for hCCS DI between the compact and elongated heterodimer (Figure 27 and Figure 26, respectively) underscore the plasticity of the linker between DI and DIII which may be related to its physiological role. Moreover, also different from the elongated form, the compact heterodimer shows only a few residues for hCCS DIII which is stabilized via contacts with DI and residue Thr58 within the disulphide sub-loop as shown in Figure 27 D. We will discuss the structures in more details in section 4.4.

In summary, all crystals were tested for X-ray diffraction at the Soleil Synchrotron (beam-line Proxima 1) and/or at the Diamond Light Source. The vast majority of the crystals in Figure 20 and Figure 23 had poor or no diffraction or did not correspond to the protein of interest. The successfully cases are summarized in Table 4 and the parameters for data collection and refinement of each crystal are summarized in Table 5.

Table 4 - Crystals, best resolution, content of the asymmetric unit and X-ray source.

Crystal	Resolution	Proteins in asymmetric unit	Synchrotron
hCCS C22,25S- E,Zn wt hSOD1 (Figure 20 F)	1.55Å	hCCS DII homodimer	Soleil
E,Zn hSOD1 C57,146A (Figure 20 J)	2.00 Å	E,Zn hSOD1 C57,146A homodimer	Diamond Light Source
hCCS DII – E,Zn hSOD1 C57,146A (Figure 23 I)	2.55 Å	Truncated Heterodimer	Soleil
hCCS C22,25S – E,Zn hSOD1 C57,146A (Figure 23 C)	3.05 Å	Elongated Heterodimer	Soleil
hCCS C12, 22,25,244,246A - E,Zn hSOD1 C57,146A (Figure 23 G)	2.95 Å	Compact Heterodimer	Soleil
hCCS C12, 22,25,244,246A - Cu,Zn hSOD1 C57,146A (Figure 23 H)	3.30 Å	Compact holo Heterodimer	Diamond Light Source

Source from: Own authorship.

continue

Table 5 - Data Collection and Refinement Statistics.

	E,Zn hSOD1 C57/146A homodimer#	**hCCS domain II homodimer#**	**hCCS domain II – E,Zn hSOD1 C57/146A heterodimer#**	**hCCS C22,25S - E,Zn hSOD1 C57/146A heterodimer#**	**hCCS C12,22,25,244, 246A - E,Zn hSOD1 C57/146A heterodimer#**	**hCCS C12,22,25,244, 246A - Cu,Zn hSOD1 C57/146A heterodimer#**
Data collection						
Space group	$P2_1\ 2_1\ 2_1$	$P\ 4_3\ 2_1\ 2$	$H3_2$	$H3_2$	$P3_2$	$P3_2$
Cell dimensions						
a, *b*, *c* (Å)	74.7, 163.0, 174.6	68.4, 68.4, 136.2	244.7, 244.7, 182.3	172.5, 172.5, 219.2	181.1, 181.1, 141.1	180.9 180.9 141.2
α, β, γ (°)	90, 90, 90	90, 90, 90	90, 90, 120	90, 90, 120	90, 90, 120	90, 90, 120
Resolution (Å)*	81.48-2.00 (2.03-2.00)	68.36-1.55 (1.63-1.55)	49.40-2.55 (2.69-2.55)	44.19-3.05 (3.21-3.05)	49.01-2.94 (3.10-2.94)	156.62-3.30 (3.48-3.30)
No. reflections	144348	47679	67927	24104	110021	77737
R_{merge}*	8.4 (83.2)	11.1 (83.2)	13.0 (80.6)	13.0 (142.9)	16.5 (94.4)	20.9 (103.3)
$I / \sigma I$*	12.3 (1.9)	18.8 (1.5)	9.5 (2.0)	18.7 (1.9)	8.5 (1.9)	6.8 (1.7)
CC1/2	0.998 (0.783)	0.998 (0.33)	0.995 (0.409)	0.999 (0.693)	0.989 (0.717)	0.987 (0.604)
Completeness (%)*	100 (100)	100.0 (99.9)	95.7 (97.2)	100 (100)	100 (100)	100 (100)
Redundancy*	6.1 (5.7)	105 (4.5)	6.8 (6.7)	14.1 (14.5)	5.9 (5.8)	5.1 (5.2)
Wilson B-factor ($Å^{-2}$)	27.7	11.7	39.2	82.0	54.0	67.2
Refinement						
ASU content	6 hSOD1 homodimers	1 hCCS DII homodimer	4 hSOD1-hCCS DII heterodimers	2 hSOD1-hCCS heterodimers	12 hSOD1-hCCS heterodimers	12 hSOD1-hCCS heterodimers
Resolution (Å)	81.48-2.00	61.1-1.55	49.40-2.55	42.07-3.05	49.01-3.0	54.59-3.30
No. reflections	136979	45353	64691	22855	98527	77627
R_{work} / R_{free} (%)	22.1 / 26.0	18.6 / 21.7	20.8 / 24.8	19.9 / 24.6	19.2 / 22.9	20.5 / 24.0

No. of atoms						*conclusion*
Protein	13294	2362	8925	5967	33112	33081
Water	1064	393	270	2	75	10
No. of residues	1835	303	1206	808	4549	5334
Average *B*-factors ($Å^2$)						
Protein	46.0	17.8	55.0	95.3	74.6	73.4
Water	43.8	33.7	41.4	78.3	41.9	40.5
R.M.S. deviations						
Bond lengths (Å)	0.007	0.005	0.003	0.010	0.007	0.002
Bond angles (°)	1.15	0.94	1.67	1.46	1.15	0.396
PDB ID	**6FOI**	**6FN8**	**6FOL**	**6FON**	**6FP6**	**-**

[#] Each data set is taken from a single crystal.
* Values in parenthesis refer to the highest resolution shell.
Source from: Own authorship

In common, all these structures of the hSOD1 activating complex were crystallized by inhibiting complex dissociation and aggregation through discerning mutagenesis of cysteines involved in normal and unusual disulphide bond formation and by hCCS truncations. They represent snapshots of the hSOD1 maturation process and the first visualization of a protein complex involved in human copper trafficking. They are also the first visualization of the ubiquitously expressed and abundant human hSOD1 with a physiologically relevant macromolecule. In the next section, structural investigation will be performed to understand the reason why the hCCS homodimer has a high affinity for disulphide reduced E,Zn hSOD1 and why it is lost upon its maturation.

4.4 hSOD1 maturation catalyzed by hCCS

4.4.1 Homodimers dissociation and Heterodimer formation

Previous studies have reported that disulphide reduced E,Zn hSOD1 has a dimer dissociation constant (Kd) of 51 μM (CULIK *et al.*, 2018) while the mature form (Cu,Zn hSOD1^{SS}) is 2.2 nM (BROOM *et al.*, 2015; WILCOX *et al.*, 2009). Although the Kd for hCCS is not available, we have addressed in section 4.1 that it is likely to be in the low-micromolar range, close to value for the yeast orthologous CCS which is 3.0 μM (HALL *et al.*, 2000). Furthermore, to better understand the affinity between the intermediates involved in hCCS catalyzed SOD1 maturation, recent work quantified the interaction of hCCS with hSOD1 in different redox status and metallation states (BOYD *et al.*, 2018). The data are summarized in Table 6:

Table 6 – The dissociation constant for hCCS and hSOD1 on different redox and metallation states.

Protein	Dissociation constant (Kd)
hCCS - Cu,Zn hSOD1^{SS}	Do not interact
hCCS - E,E hSOD1^{SH}	36 ± 0.7 nM
hCCS - E,Zn hSOD1^{SH}	114 ± 16 nM
hCCS - Cu,Zn hSOD1^{SH}	371 ± 74 nM

Source from: (BOYD *et al.*, 2018)

The results obtained clearly show that upon increasing post-translational modifications (i.e., hSOD1 zinc and copper incorporation and disulphide oxidation) there is a decreasing affinity of hCCS for hSOD1 (BOYD *et al.*, 2018), which is reasonable as hCCS is supposed to bind to the immature form of hSOD1 and then dissociate from the mature. Comparing the results, we can also observe that E,Zn hSOD1 C57,146A binds to hCCS 500-fold tighter than to itself. On the other hand, hCCS has its affinity for E,Zn hSOD1 C57,146A increased by about 30-fold when compared to another hCCS.

Therefore, clearly both proteins are likely to interact. To shed light on the molecular basis underlying the preference of E,Zn hSOD1 C57,146A for a hetero over homodimeric species, the interfaces of: Cu,Zn wt hSOD1 (already available as PDB ID 2C9V), E,Zn hSOD1 C57,146A, the hCCS DII homodimer as well as the truncated, compact and elongated heterodimer were first analyzed by Pisa to calculate the buried surface area and solvation free energy of interaction (ΔGint) upon dimerization. Table 7 summarize the results:

Table 7 – Pisa Assembly list.

Molecule composition	**Name**	**Surface Area (Å^2)**	**Buried Area (Å^2)**	**ΔG_{int} (kcal/mol)**
hCCS DII - hCCS DII	hCCS DII homodimer	13463*	1513*	-6.3*
hCCS DII - E,Zn hSOD1 C57,146A	Truncated heterodimer	13950*	1346*	-8.8*
Cu,Zn hSOD1 - Cu,Zn hSOD1	Mature hSOD1	14046	1392	-10.8
hCCS C22,25S - E,Zn hSOD1 C57,146A	Elongated heterodimer	20465*	1510*	-9.2*
hCCS C12,22,25,244,26A - E,Zn hSOD1 C57,146A	Compact heterodimer	16656*	1869*	-10.8*

*Values are the average between the complex present in the asymmetric unit

Source from: Own authorship

The ΔGint value, which is the solvation free energy upon dimerization and does not include interactions across the interface such as salt bridges and hydrogen bonds, shows a progressive decrease in the order: hCCS homodimer<hCCS-hSOD1

truncated<mature hSOD1 following the dimer affinities of each species. However, for the full length heterodimers the ΔGint value increased noticeably, presumably a consequence of the presence of the hCCS extra domains.

Therefore, due to this unexpected behaviour of ΔGint, a more detailed analysis of the dimerization interfaces is necessary in order to better understand the mechanisms of association and dissociation. Thereby, specific interactions (hydrogen bonds, salt bridges) across the interfaces were calculated using Pisa in an attempt to examine the reasons for the binding preference.

We analyzed all the homodimers as well as the heterodimers (e.g. truncated, compact and elongated) structures obtained in this work. For the heterodimers, the results revealed that only the residues present in the hCCS hSOD1 like domain were responsible for the heterocomplexation and the interactions were conserved between the complexes. No interaction was observed between hCCS DI or DIII and hSOD1 despite the presence of these domains. Thus, the average hydrogen bonding found in the truncated heterodimer interface was considered due the higher resolution of the structure. The exception was the unique interaction found between Asn239 in hCCS DIII and Thr58 in the hSOD1 disulphide loop in the compact heterodimer structure which was therefore accounted. Table 8 summarized the average of distances considering all molecules contained in the asymmetric unit.

Table 8 - Interface hydrogen bonding interactions.

Amino Acid	Group	Distance	Group	Amino Acid
hSOD1 PDB code: 2C9V				
Gly51	Amine (N)	2.75 Å*	Carbonyl (O)	Ile151
Ile151	Amine (N)	2.81 Å*	Carbonyl (O)	Gly114
E,Zn hSOD1 C57,146A homodimer				
Gly51	Amine (N)	2.78 Å*	Carbonyl (O)	Ile151
Ile151	Amine (N)	2.79 Å*	Carbonyl (O)	Gly114
hCCS DII homodimer				
Conserved from hSOD1‡				
Arg232	Carbonyl (O)	3.06 Å*	Amine (N)	Gly135
Arg232	Amine (N)	2.86 Å*	Carbonyl (O)	Gly195
Specific to hCCS				
Arg232	Side chain amine (NE)	3.13 Å*	Carbonyl (O)	Ile194
Arg104	Guanidinium (NH2)	3.54 Å*	Carboxylate (OD2)	Asp136
Arg104	Guanidinium (NH2)	3.21 Å*	Carboxylate (OD2)	Thr138
Asp136	Carboxylate (OD2)	2.99 Å*	Side chain OH (OG)	Ser233
Truncated heterodimer				
Conserved from hSOD1				
hSOD1 Gly51	Amine (N)	2.92 Å	Carbonyl (O)	hCCS Arg232
hSOD1 Gly114	Carbonyl (O)	2.83 Å	Amine (N)	hCCS Arg232
Conserved from hCCS				
hSOD1 Asp52	Amine (N)	2.92 Å	Carbonyl (O)	hCCS Arg232
hSOD1 Asp52	Carboxylate (OD2)	3.46 Å	Guanidinium (NH1)	hCCS Arg104
hSOD1 Thr54	Side-chain OH (OG1)	3.40 Å	Guanidinium (NH2)	hCCS Arg104
hSOD1 Ile113	Carbonyl (O)	2.47 Å	Guanidinium (NE)	hCCS Arg232
Specific heterodimer				
hSOD1 Ile151	Amine (N)	2.82 Å	Carbonyl (O)	hCCS Gly195
hSOD1 Ile151	Carbonyl (O)	2.74 Å	Amine (N)	hCCS Gly135
Compact heterodimer				
Specific for this heterodimer				
hSOD1 Thr58	Carbonyl (O)	2.82 Å	Guanidinium (ND2)	hCCS Asn239

* Symmetrical hydrogen bond distances are averaged

‡ The main interactions involve the protein main chain and therefore are conserved on hCCS despite residues modifications, e. g. hSOD1 Ile151 and hCCS Arg232.

Source from: Own authorship.

The distances displayed in Table 8 will be analyzed throughout this section. Firstly we will underline the structural basis that weakens the immature hSOD1 and hCCS homodimeric interfaces and then describe why the heterodimer formation is facilitated. To begin with, it has been already discussed here the importance of hSOD1 being in the disulphide reduced state to complex with hCCS and its propensity to be monomeric when fully cysteine depleted. However, Table 8 points out that the main-four hydrogen bonds found at the interface of mature hSOD1 are also conserved in the disulphide knock-out form, and they also display very similar distances. In fact, the analysis of the crystal structures showed no significant differences between the E,Zn hSOD1 C57,146A and the mature version of the enzyme, the Cu,Zn hSOD1SS (Figure 28 A). The RMSD for Cα atoms between the structures was 0.3 Å.

Figure 28 - hSOD1 disulphide sub-loop conformational freedom. (A) Alignment of Cu,Zn $SOD1^{S-S}$ in gray (PDB code 2C9V) with E,Zn Cys57,146Ala hSOD1 in cyan. The conformation of the disulphide sub-loop (residues 51-60) in the Cu,Zn $SOD1^{S-S}$ conformation (gray) is compared with alternative conformations (cyan): (B) The E,Zn Cys57,146Ala hSOD1 (C) The Structure of monomeric E,Zn hSOD1 (solution NMR, PDB:1KMG), RMSD 0.97. (D) The disulphide reduced E,Zn hSOD1 (solution NMR, PDB: 2AF2), RMSD 1.12 Å.

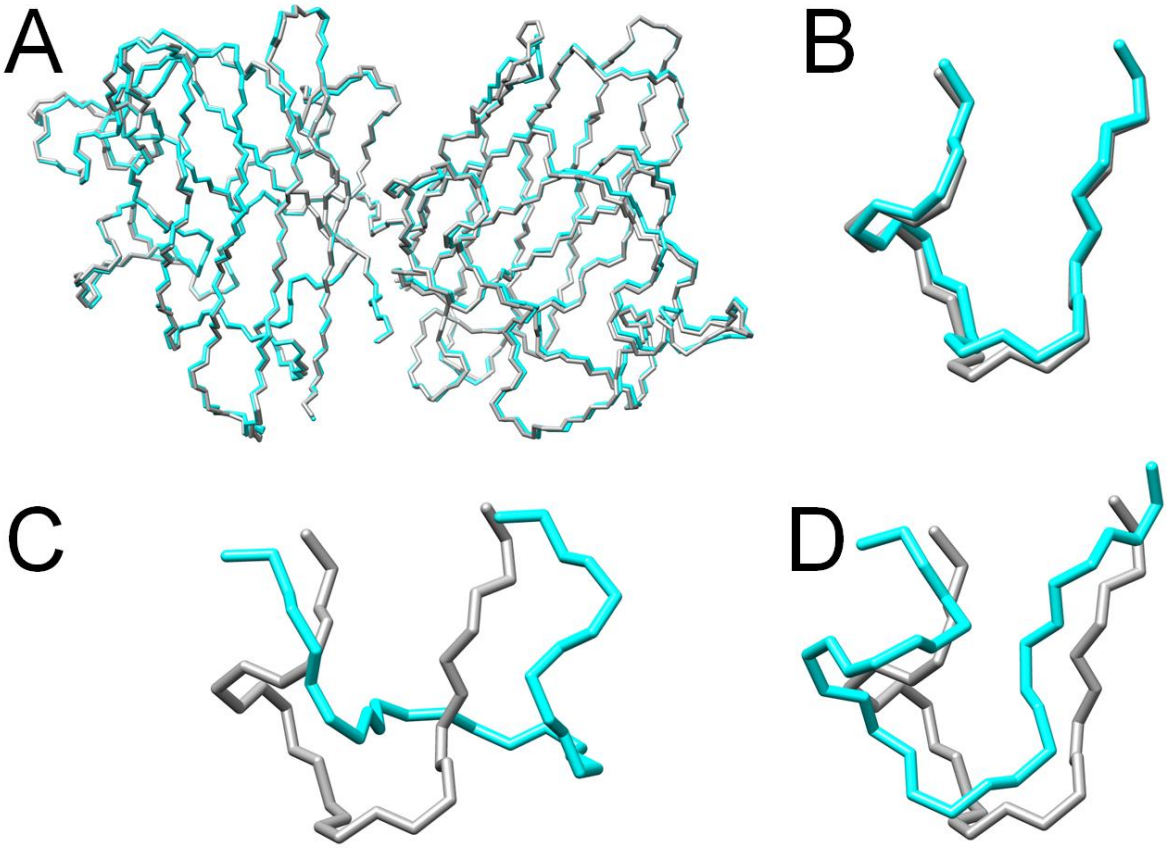

Source from: Own authorship.

Nevertheless, we propose that the E,Zn hSOD1 C57,146A conformation obtained was an artefact of crystallization. Studies have shown that once loop IV (which comprises the disulphide sub-loop) loses its covalent anchor to the central β-sandwich, it undergoes a pronounced reorientation in the region of residues 50–61 (CULIK *et al.*, 2018; LINDBERG *et al.*, 2004), different from that observe in our structure (Figure 28 B). In fact, NMR studies have reported the high mobility of loop IV in the E,Zn hSOD1 disulphide-depleted protein (Figure 28 C and D) (BANCI et al., 2002, 2006). Due the extended conformational space of loop IV, it plays a role in the interface region favouring hSOD1 monomerization for entropic reasons (HÖRNBERG et al., 2007).

We speculate that the disulphide reduced hSOD1 (E,Zn hSOD1 C57,146A) is forced to dimerize as a consequence of crystal packing, and thereby loop IV is forced to occupy the native-like position. The fact that we trapped the loop IV in the exact same conformation as observed in the mature hSOD1 structure, demonstrates that although a large number of conformational states are allowable for the loop, the native state is one of these which is energetically accessible (and maybe favourable) even in the absence of the disulphide bridge. This accessibility may be important for facilitating the oxidation of the bridge.

On the other hand, the analysis of hydrogen bonds in the hCCS Domain II homodimer (Table 8) also showed conservation of the four hydrogen bonds involved in the hSOD1 dimer interface, but with slightly longer averaged distances. Intriguingly, extra hydrogen bonds and a salt bridge were also found in the copper chaperone homodimeric interface, despite the fact that hCCS DII is a monomer in solution at the same concentrations and conditions as hSOD1 (section 4.1). To gain insight into the residues causing this destabilization, the structure was further scrutinized.

Briefly, as previously published (LAMB *et al.*, 2000), the structure has an intact intradisulphide bond (Figure 6) and a zinc ion which are both absent in the homologous yCCS structure. The Cys141-Cys227 intradisulphide bond in hCCS is analogous to the Cys57-Cys146 bridge in hSOD1. Firstly we investigated if the oxidation and reduction of the disulphide bond in hCCS DII, as occurs in hSOD1, would affect its oligomeric state and ability to form hetero complexes (Figure 29).

Figure 29 - Reappraisal of the hCCS DII structure. (A) The disulphide bond between Cys227 and Cys241 is conserved (2Fo-Fc electron density map contoured at 1σ). (B) Size exclusion chromatograms of disulphide reduced and oxidized hCCS DII. (C) SEC of hCCS DII disulphide reduced and oxidized complexed with hSOD1 C57,146A show that both species is able to heterodimerize. The column used in (B) and (C) was the AdvanceBio 300Å, 2.7 µm, 4.6x300 mm.

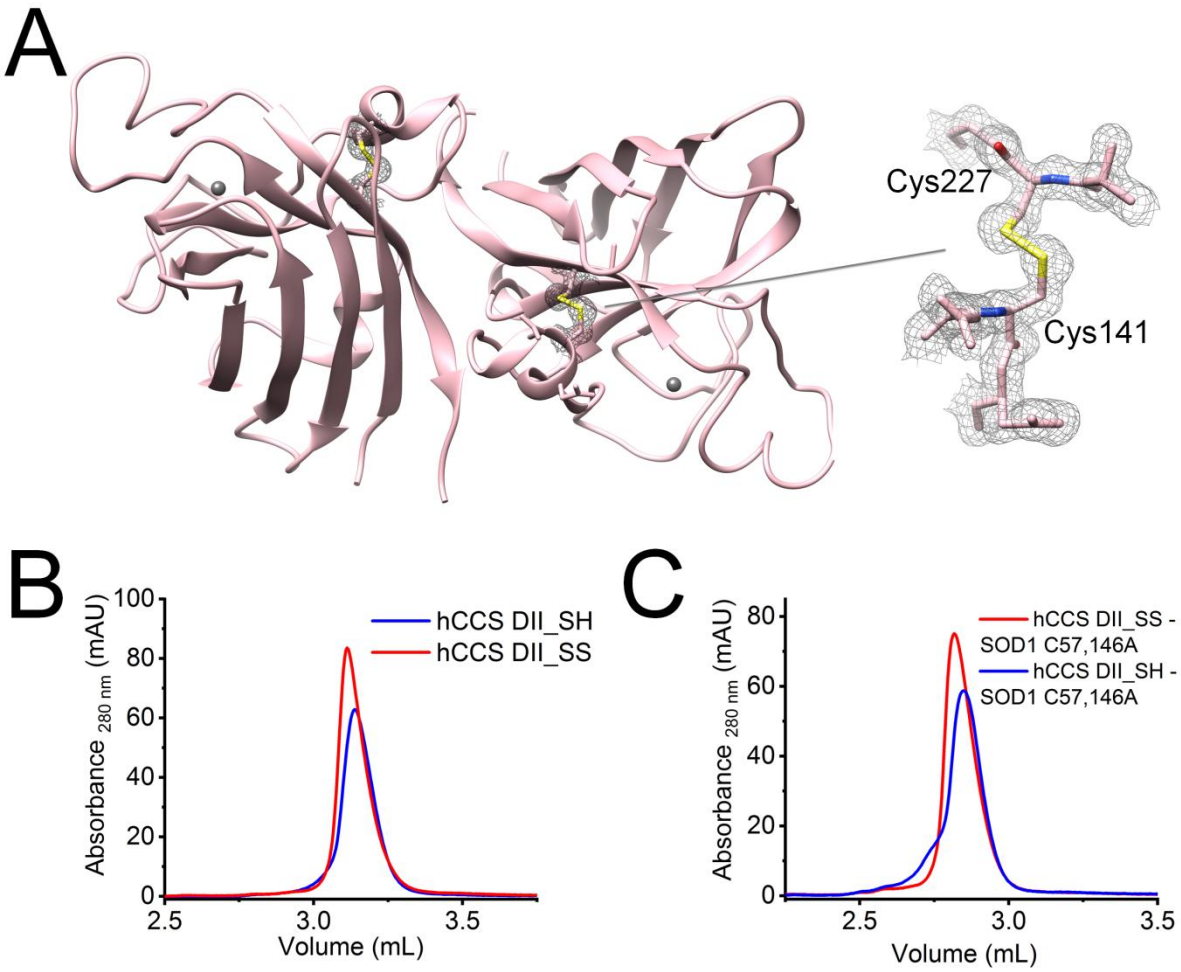

Source from: Own authorship.

The results show that regardless of the oxidation state, hCCS DII is a monomer in solution (Figure 29 B and Figure 12) and is able to complex with E,Zn hSOD1 C57,146A (Figure 29 C). The copper chaperone's lower affinity for itself and capacity for heterodimerization may be favoured, as suggested previously, due to a decrease in electrostatic repulsion upon complexation with hSOD1 (LAMB *et al.*, 2000). For example, Arg196 in hCCS has as a counterpart a second arginine residue (Arg232), whose side-chain guanidinium is found 4.0 Å from the similarly charged Arg196 guanidinium, causing electrostatic repulsion at the interface (Figure 6). The corresponding residue in hSOD1 is an isoleucine (Ile151), which would be expected

to favour hetero over homodimerization. To test this hypothesis, we assessed if the hCCS DII R232A mutation could increase the hCCS DII homodimer affinity (Figure 30).

Figure 30 - hCCS Domain II R232A oligomeric state analysis. (A) After affinity chromatography the protein was loaded onto the Superdex 200 16/60 GL (GE Healthcare) and eluted in three peaks. They were collected separately as fraction 7, 8 and 9. (B) Fraction 9 was analysed using SEC-static light scattering. (C) Fraction 7 analysed using SEC-static light scattering. Each species had polydispersity index of 1.0. (D) The fraction 8 was monitored at day 0 and after two days in the SEC column and clearly show shift of the equilibrium favouring monomeric species.

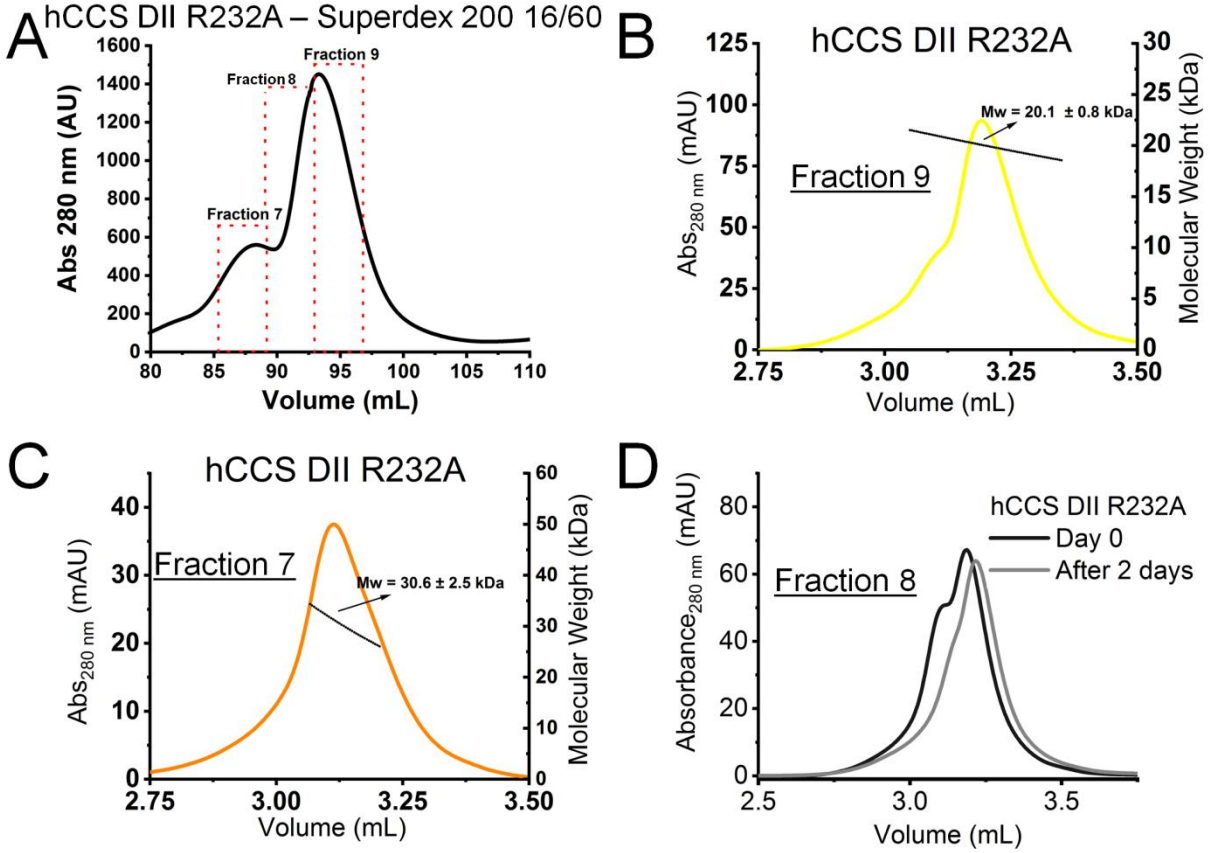

Source from: Own authorship.

In fact, the substitution decreased the charge in the interface and unlike hCCS DII, which is predominantly monomeric, the hCCS DII R232A can be found in solution as a monomer or a dimer (Figure 30 B and C). However, over time the monomer-dimer equilibrium in the hCCS DII R232A sample favoured the monomeric species (Figure 30 D). This information raises the question of what else may disfavour the hCCS DII homodimer interface.

Interestingly, even though the canonical hydrogen bonds in the interface of both the hCCS DII and the hSOD1 homodimers are conserved (Figure 31 A and B), as previously discussed (Table 8), the carbonyl-amine hydrogen bond lengthens from 2.75 Å to 3.06 Å in hSOD1 and hCCS homodimers, respectively (Figure 31 C). The hCCS inter-subunit affinity is possibly weakened by the methyl group on the hCCS Ala231 side-chain, which in order to be accommodated suffers a shift of 13° and 49° in the phi and psi angles respectively, for residue Gly135 compared to the equivalent angles for Gly51 in hSOD1. As a consequence the Gly135 is pushed away from Arg232.

Figure 31 - Structure and dimer affinity of the hCCS domain II. (A) The two canonical hSOD1 inter-subunit hydrogen bonds. (B) The hydrogen bonds were conserved at the hCCS domain II dimer interface despite substitution of hSOD1 Ile151 for the larger and charged hCCS Arg232, which comes in close proximity to the Arg196, causing electrostatic repulsion at the interface. (C) The hCCS (pink) dimer interface Arg232-Gly135 hydrogen bond was weakened by the steric effect of Ala231 side chain and Arg232. The Gly135 was pushed away from Arg232 lengthening the distance of the interaction. (D) Mutation of Ala231Gly hCCS vastly slowed complexation. (E) Eukaryotic CCS sequence alignment showed Arg 232 Ala231 was very highly conserved. (F) as was hSOD1 Gly150.

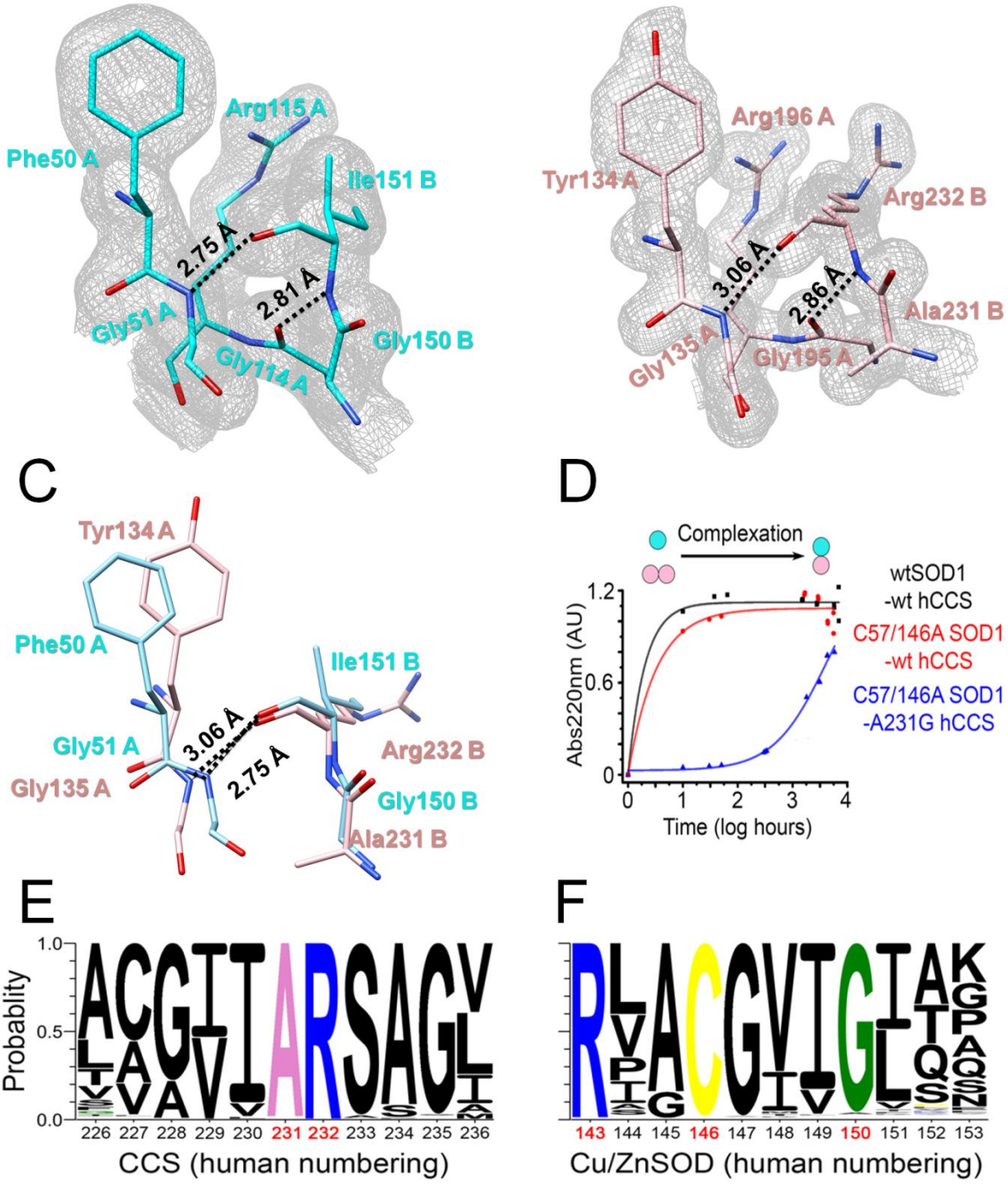

Source from: Own authorship.

In fact, a mutant of the hCCS to mimic the counterpart residue found in hSOD1 dimer interface (Gly150) was performed. The hCCS Ala231Gly mutant results in an increase in the hCCS homodimer affinity and consequently slowed complexation with hSOD1 more than 300-fold (Figure 31 D). Both Gly150 and Ala231 are highly conserved in eukaryotic Cu/ZnSODs and their cognate chaperones respectively as well as the hCCS Arg232 (Figure 31 F and E, respectively). Together, these results indicated that the arginine and alanine appeared to have been acquired and maintained specifically to weaken the hCCS interface. In contrast to the low nanomolar dissociation constant of mature hSOD1, hCCS has a low micro-molar affinity (Figure 12 and Figure 13) and hSOD1 activation can occur within a physiologically relevant time scale as a result.

So far, we have uncovered the atomic details by which hCCS and the immature hSOD1 have low homodimeric affinities. In the next step, we will discuss why the disulphide depleted hSOD1 facilitate its complexation with hCCS. For this purpose, the heterodimeric crystallographic structure between hCCS DII and hSOD1 C57,146A will be analysed Figure 32.

Figure 32 - hSOD1 induced fit upon complexation with hCCS. (A) Superposition of hSOD1 in the heterodimer (dark gray) with hSOD1 in the homodimer (cyan) and superposition of hCCS DII in the heterodimer (pink) with hCCS in the homodimer (light gray). The zinc ion is shown as a gray sphere and the copper ion as an orange sphere. (B) Complexation with hCCS forced the hSOD1 disulphide sub-loop to adopt an open conformation separating the amino acids involved in disulphide formation. The distance from the Cβ carbons of residues 57 and 146 increases from 3.8 (disulphide intact) to 8.0 Å (disulphide reduced).

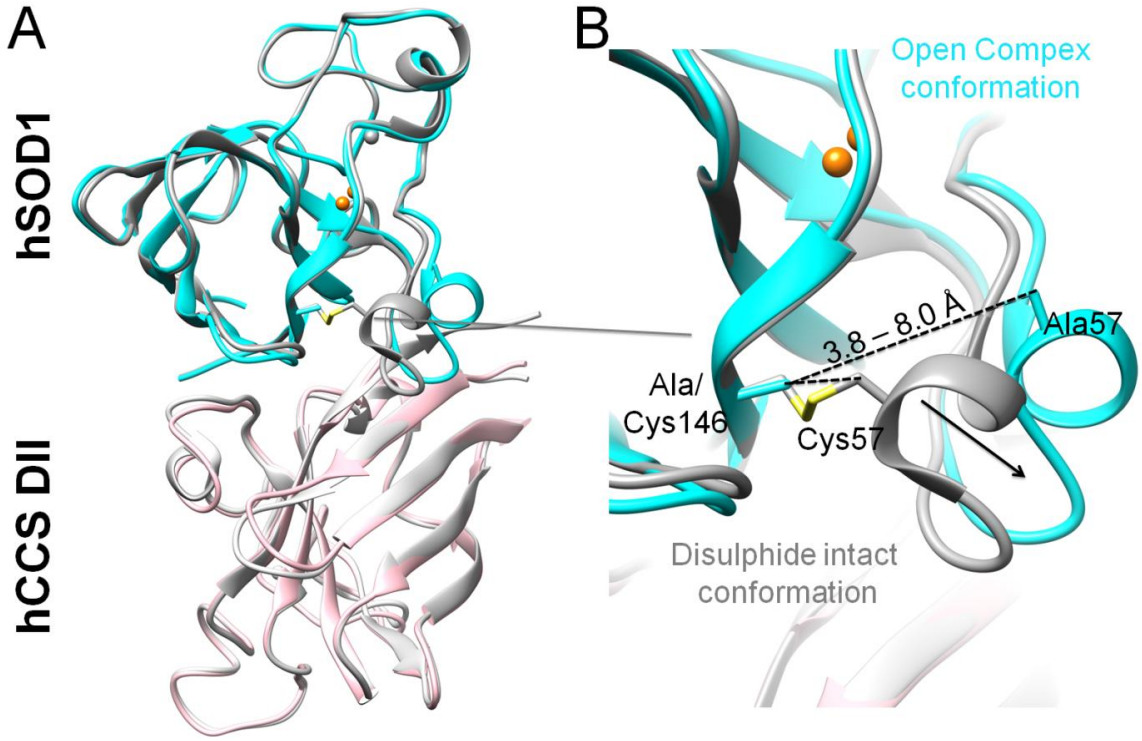

Source from: Own authorship.

When comparing the hCCS DII structure in the homo or heterodimeric structures (Figure 32 A) no significant conformational modification can be seen. In fact, the copper chaperone seems to behave as a rigid body both able to complex with its metallo enzyme or on its own. On the other hand, a comparison of the hSOD1 disulphide-reduced structure in the homo and heterodimer revealed more significant differences (Figure 32 A and B). The superposition showed that in the disulphide-reduced heterodimer the triad of residues Asp52-Asn53-Thr54 (DXT) projects further into the interface when compared with the conformation observed in the oxidized homodimer. The sub-loop opened up and the distance from the Cβ carbons of residues 57 and 146 increased from 3.8 to 8.0 Å.

Upon heterodimerization loop IV adopted a conformation that could not be accommodated if the hSOD1 disulphide were present (Figure 32 B), and is also observed when hSOD1 is complexed with yeast CCS (i.e., yCCS – hSOD1 and

yCCS – ySOD1) (FETHEROLF *et al.*, 2017b; LAMB *et al.*, 2001), as shown in Figure 33:

Figure 33 - The structural rearrangement in loop IV accompanying disulphide reduction. The structure of the mature form of hSOD1 (PDB ID 2C9V) in gray was superposed with: hSOD1 C57,146A from the truncated heterodimer, obtained in this work (6FOL, in cyan), the yeast hSOD1 H48F from the yeast heterodimeric structure (1JK9, purple) and with hSOD1 H46R,H48Q from the chimera structure (5U9M, blue).

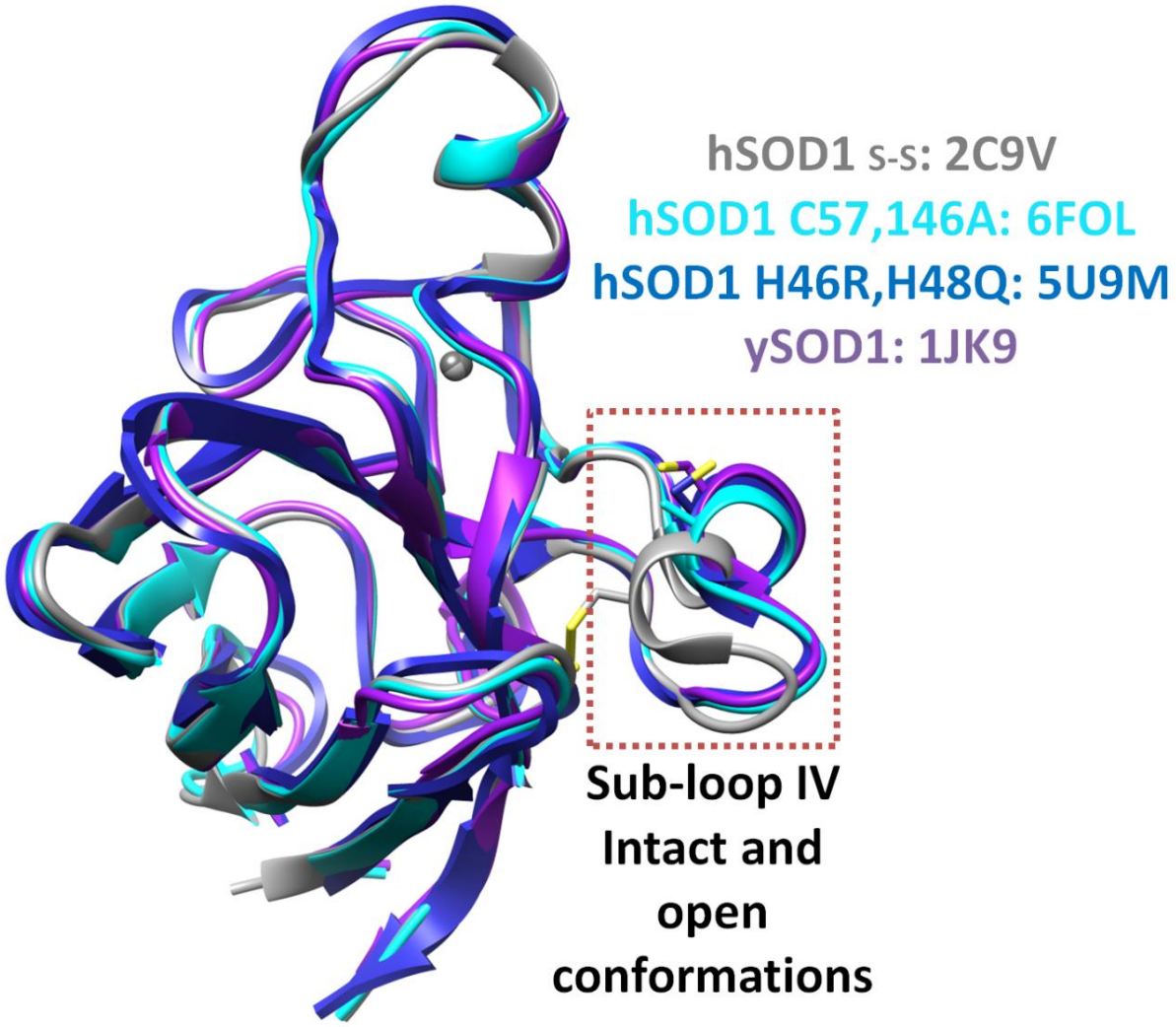

Source from: Own authorship.

Even though the shift in the disulphide sub-loop was also observed in all hSOD1 heterodimers solved previously, both authors described it to be mainly caused by yCCS DIII intercalation between the loop IV and the β-barrel (FETHEROLF *et al.*, 2017b; LAMB *et al.*, 2001). Nonetheless the truncated structure that we presented in this work does not contain the hCCS domains III and exhibited

the same conformation rearrangement which raises the possibility that the opening movement is driven by a different mechanism. Indeed, heterodimer formation seems to be favoured due to hCCS DII stabilization of loop IV via hydrogen bonds formed between: hCCS Arg104 and hSOD1 Asp52 from the DXT motif, hCCS Arg104 and hSOD1 Thr54 and hCCS Arg232 and hSOD1 Asp52, henceforth referred to as the R104,R232-DXT network (shown in stick representation in Figure 34).

Figure 34 – hSOD1 loop IV stabilization via hydrogen bond formation upon complexation with hCCS. (A) The truncated heterodimer (hSOD1 in cyan and hCCS DII in pink) and (B) the residues involved in R104,R232-DXT interaction have been highlighted. The distances shown are averages calculated over all the heterodimers present in the asymmetric unit. The 2Fo-Fc electron density maps were contoured at 1σ.

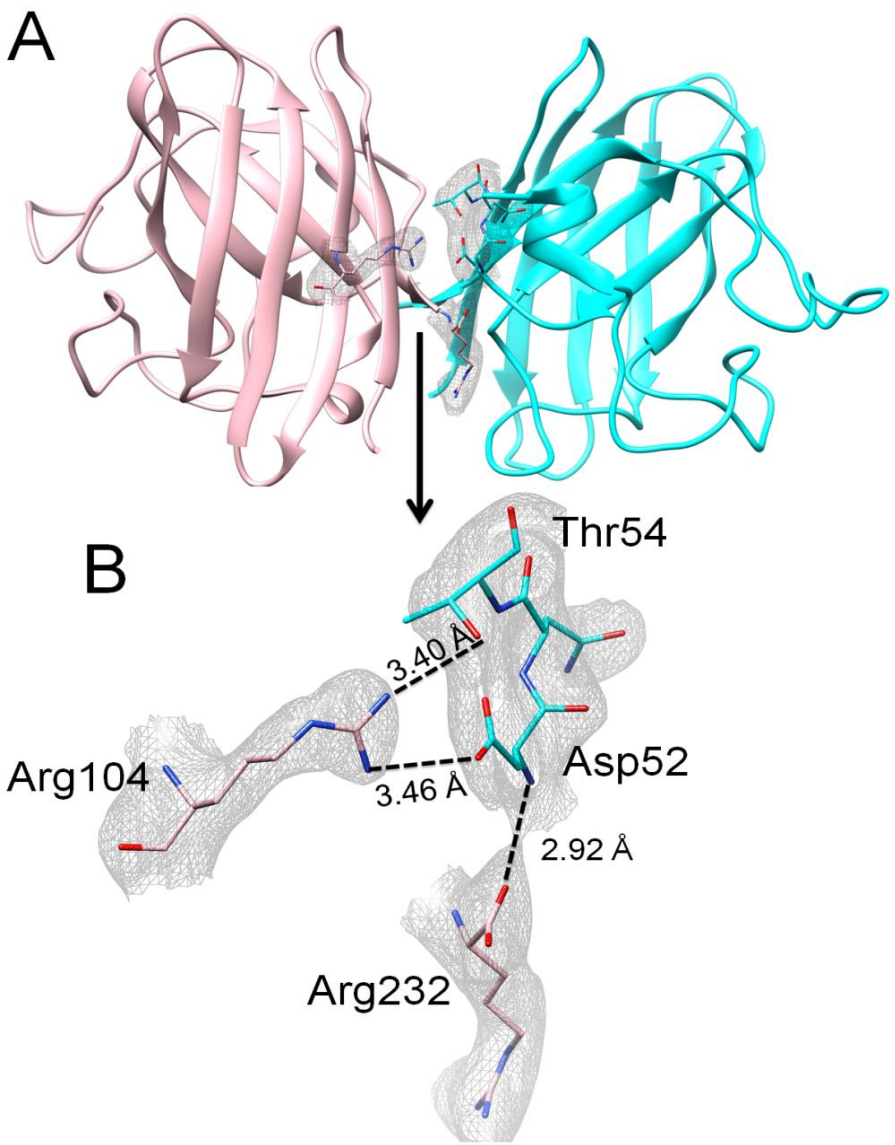

Source from: Own authorship.

Due to the low resolution, 2.55 Å, the electron density for the side chains involved in the salt bridge is not well defined and alternative conformations might be plausible. This leads to an uncertainty in the average distances and as a consequence, in the strength of the interactions. Nevertheless, we hypothesized that the enthalpic contribution of the R104,R232-DXT network interactions may be sufficient to compensate the loss in entropy caused by the stabilization of the hSOD1 loop IV. Consistent with our observations, this interaction can be also observed in yeast SOD1 - CCS crystal structure (Lamb et al 2001) (Figure 35).

Figure 35 - The DXT-Arg105 network in yeast complexe. (A) The heterodimer structure yCCS-ySOD1 (PDB ID 1JK9) in gray, and the amino acid residues: Arg105 and Thr54 and Asp52 are shown as solid sticks in magenta and blue, respectively. (B) The residues involved in the salt bridges were zoom in, the hydrogen bond between them is at 3.3 Å in length.

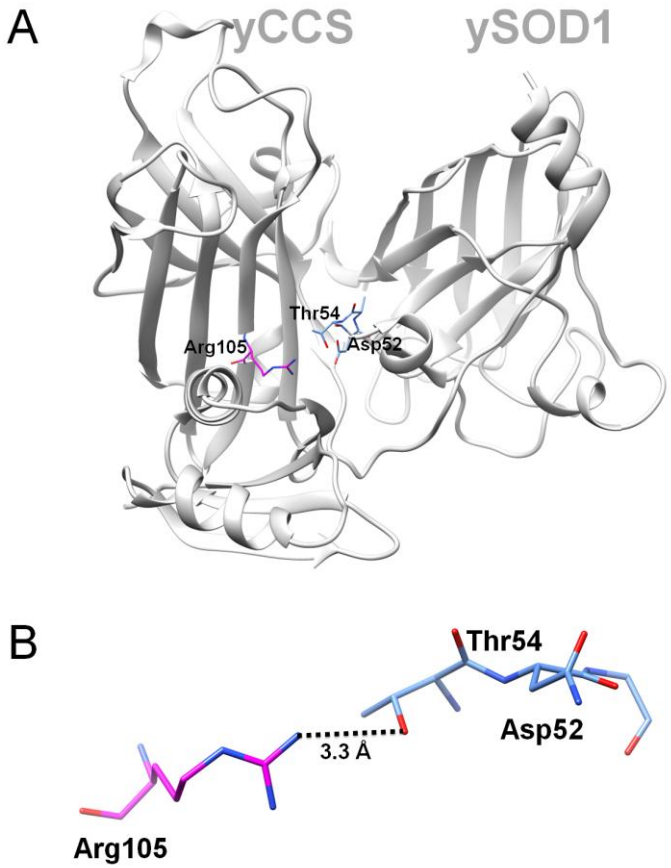

Source from: Own authorship.

The yeast SOD1 complexed with its metallochaperones (PDB ID 1JK9) also presents the Arg105 forming a hydrogen bond with Thr54 (from the DXT motif) at a distance of 3.3 Å (Figure 35 A and B). This result reinforces the notion that the

interaction between Arg104, Arg232 and the DXT motif is an important switch for favouring the heterodimer.

However, different from what was observed for the other heterodimers, in the yCCS complexed with human SOD1 (PDB ID 5U9M) the R105/DXT interaction was disrupted. Arg105 was shifted when compared to yeast and/or our human heterocomplexes and formed hydrogen bonds with residues Glu223 and Asn225 from the yCCS DIII (Figure 36 A and B).

Figure 36 – Loop IV stabilization in the chimeric complex. (A) Chimeric heterocomplex (PDB ID 5U9M) in gray, with hCCS domain III in green and Arg105, Cys229, Thr54 and Asp52 shown in sticks. (B) In the chimeric structure Arg105 makes contact with Asn225 and Glu223 (in green) from DIII. The loop IV is stabilized in the open conformation via interaction with Cys229 (in green) and Ser218 (in magenta) from hCCS DIII and DII, respectively.

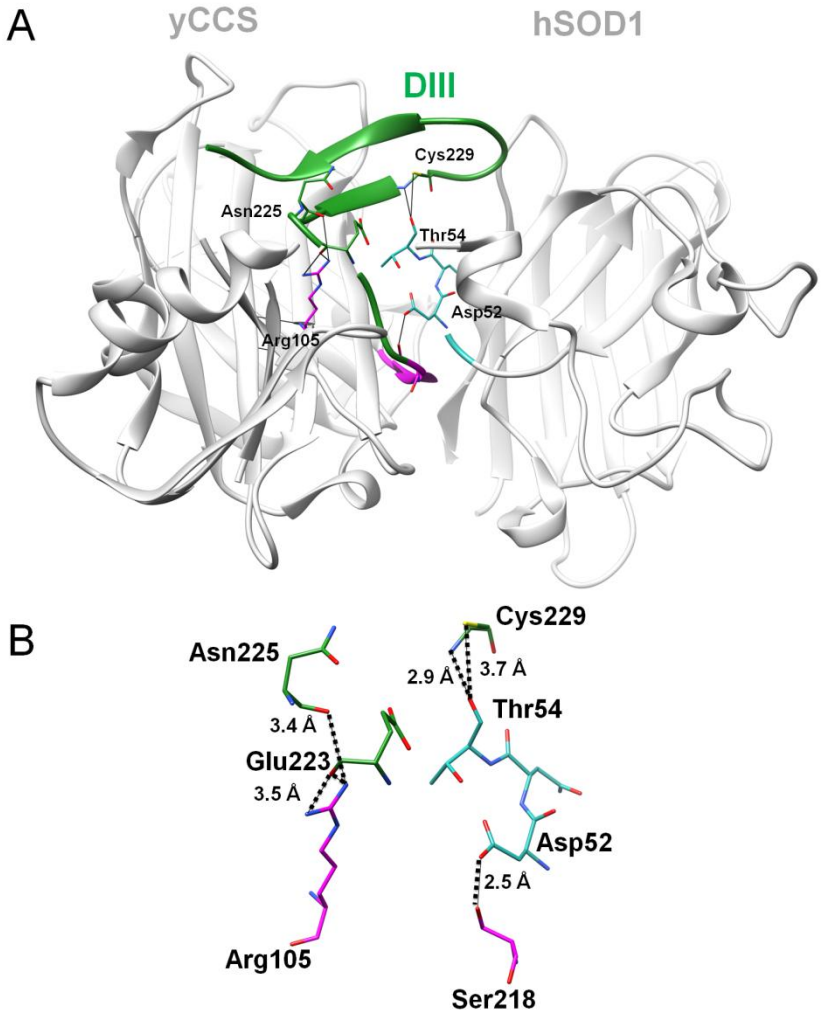

Source from: Own authorship.

Additionally, domain III presented an unusual conformation, lying at the interaction interface between yCCS and hSOD1 (Figure 36 A) and stabilizing the

disulphide sub-loop through hydrogen bonds between yCCS Cys229 and hSOD1 Thr54 (Figure 36 A and B). We speculate that the mutations carried on yCCS DIII (i.e., E238A/E239A/R240A) substantially decreased the charge in the C-terminal tail, facilitating the unexpected domain III conformation which together with Ser218 (which interacts with hSOD1 Asp52), stabilized the hSOD1 disulphide sub-loop in the same open conformation.

Similarly to the chimeric heterodimer, our compact heterodimer also displayed a hydrogen bond interaction involving the hCCS c-terminal Asn239, as already shown in Figure 27. Based on the fact that the physiological role of hCCS DIII is to transfer the disulfide bond to Cys57, the interaction with the loop IV may bring the functional hCCS CXC motif close to hSOD1 Cys57. However, when considering all of the structures solved to date, DIII of hCCS assumes a wide variety of different conformations, some of which interact with SOD1 and others do not. Thereby, although an increase in the heterodimer affinity is expected upon DIII interaction, it does not seem crucial for heterodimer formation. In fact, hCCS DII and hSOD1 were able to form a complex both in solution and in the crystallographic structure despite the absence of domains I and III, as shown in Figure 14 and Figure 29.

These observations bring our attention back to the interactions involving R104, R232 and the DXT motif, which are the only interactions that come from the hCCS domain II. In fact, the introduction of an Arg104 mutation (R104A) in full length hCCS has been shown to decrease the thermal stability of the heterodimer (SALA *et al.*, 2019). Moreover, mutation of Thr54 to Arg in hSOD1 is related with ALS (BANCI *et al.*, 2008). We speculate that the insertion of a positive charge into the SOD1 disulphide loop IV may significant decrease the hCCS-hSOD1 affinity due electrostatic repulsive forces caused by the close proximity of hCCS Arg104 and hSOD1 Arg54, disrupting the R104-DXT interaction. As a consequence, the heterocomplex might not be formed and SOD1 would not be able to acquire the necessary post-translational modifications, via interaction with hCCS, causing it to be more prone to monomerization and subsequently aggregation, triggering the ALS phenotype.

All these results indicate that the R104,R232-DXT interaction is presumably relevant during heterodimerization and perturbations brought about by disulphide formation would be expected to strain or break interactions across the dimer interface and facilitate complex dissociation. Therefore, apparently the same residues (loop IV)

responsible for favouring the monomeric form of reduced hSOD1 for entropic reasons (CULIK *et al.*, 2018; HÖRNBERG *et al.*, 2007; LINDBERG *et al.*, 2004), are also responsible for favouring heterodimerization through hydrogen bond formation when complexed with hCCS. Additionally, the R104,R232-DXT network cannot form in the SOD1 homodimer because the residue equivalent to Arg104 is an Asn.

On the other hand, the chaperone sequence contains an aspartate conserved at position 136 (the first position of the DXT motif). The investigation of the homodimeric human copper chaperone structure solved in this work also reveals the presence of this networking interaction with a distance between the H-bond acceptor and donor which is about the same as in the heterodimer (Figure 37).

Figure 37 - The 2Fo-Fc electron density map of the hCCS homodimer contoured at 1σ illustrating the hydrogen bonding distances between Arg104, Asp136 and Thr138.

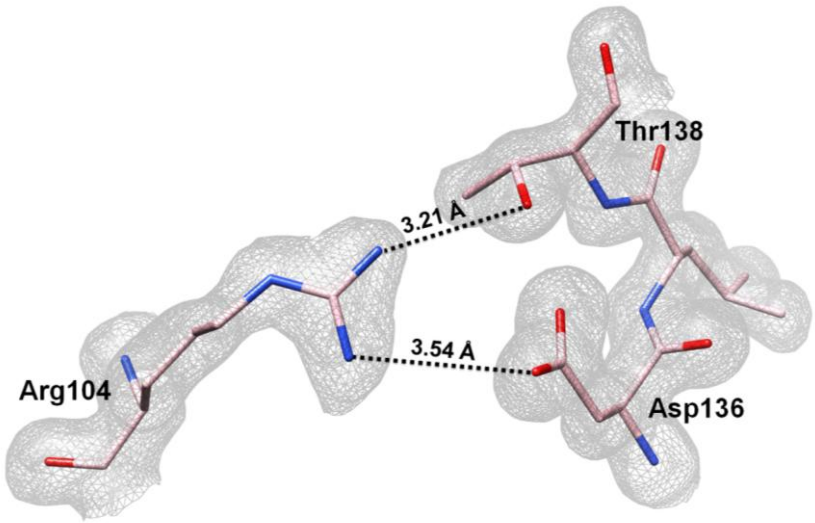

Source from: Own authorship.

The presence of the Arg104-DXT interaction in the hCCS homodimer is not surprising; monomer-dimer equilibrium in hCCS is not expected to be affected by (de)stabilization of the loop IV due to the redox state of cysteines 141 and 227 as occurs in hSOD1, which no longer recognized itself when the disulphide bond is reduced. In fact, we have shown that the oxidized or reduced hCCS DII is able to complex with the hSOD1^{SH} (Figure 29 B and C). The copper chaperone DII seems to be a monomer due the presence of repulsive forces or steric effects (Figure 12 and Figure 30), thus the dimeric form observed in the asymmetric unit may be forced by the high protein concentration in the crystallization condition.

In addition, the importance of the hSOD1 disulphide sub-loop and the Arg104-DNT interaction are also corroborated by the conservation of these residues in eukaryotic Cu/ZnSOD1 and hCCS and its orthologs respectively (Figure 38).

Figure 38 - Sequence alignment of hSOD1 and hCCS in eukaryotic species in the region of the hSOD1 disulphide sub-loop (DXT motif) and hCCS Arg104. The regions are highlighted in blue and residues in red.

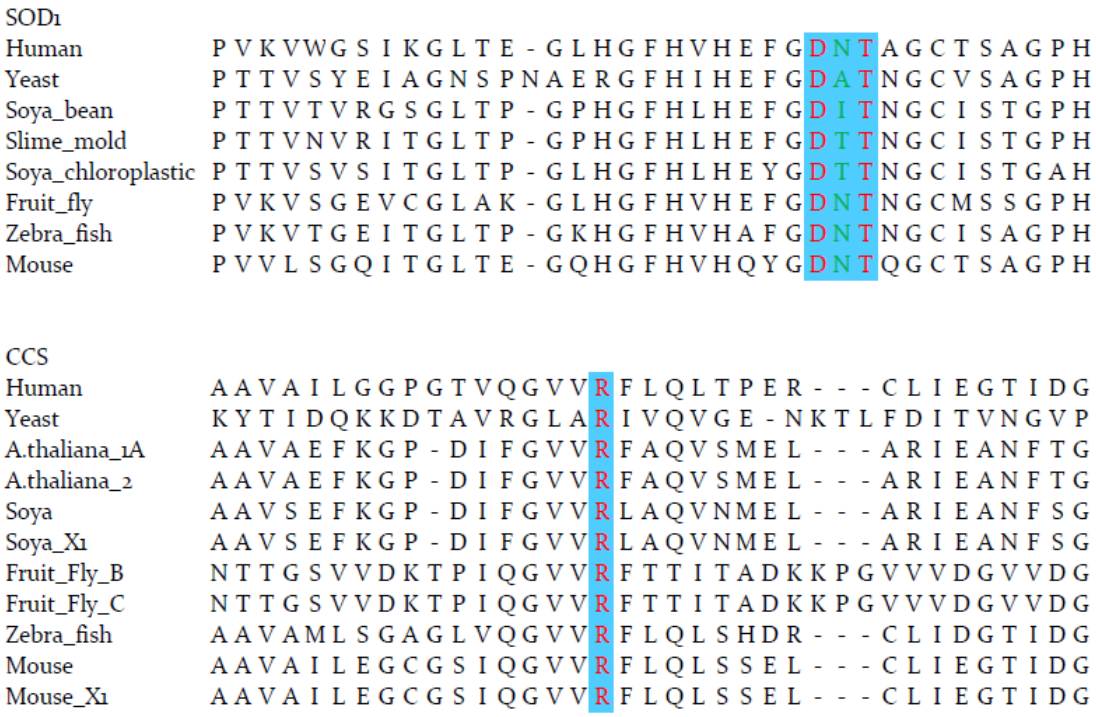

Source from: Own authorship.

So far, our analyzes have demonstrated the hSOD1 disulphide sub loop when reduced is responsible for weakening the E,Zn hSOD1 homodimer interface by entropic terms. While the hCCS homodimer is disfavoured by the presence of positive amino acids residues (e. g. Arg196 and Arg232) and the presence of the hCCS Ala231 methyl group which weakens the hydrogen bond in the homodimer interface, the heterodimerization is favoured because without the Cys57-Cys146 covalent tether the hSOD1 disulphide sub-loop (via its DXT motif) is stabilized by interacting with hCCS Arg104 and Arg R232. In this way, hCCS provides a surface of repulsive and attractive interactions which mould the plastic hSOD1 disulphide sub-loop into a stable and novel conformation.

4.4.2 Relationship between loop IV and enzymatic activity

It is well known the important role that an arginine residue (Arg143) plays in the catalytic cycle of hSOD1 (BEYER *et al.*, 1987; DUPEYRAT *et al.*, 2004). In the enzymatically active form of the protein Arg143 interacts via hydrogen bonding with Cys57 and Gly60. In fact, loop IV (to which the latter two residues belong) is also part of the charged channel that guides the superoxide radical towards the active site. The disulphide-reduced hSOD1 from the heterocomplex has been described to present an altered conformation of this loop (as described in 4.4.1 and showed in Figure 32) leading to a shift in the position of Arg143, which interposes between Cys57 and 146 in the space normally occupied by the disulphide sub-loop and interacts with Asn53, in the hSOD1 DNT motif (Figure 39).

Figure 39. Displacement of Arg143 of SOD1 in the apo copper disulphide-reduced truncated heterodimer. The hSOD1 Arg143 native conformation is showed in gray and the on assumed in the hetero-complex in cyan. The side chain interleaved between β-barrel and disulphide sub-loop, hydrogen bonded with Asn53 from the DNT motif. The 2Fo-Fc electron density maps were contoured at 1σ level.

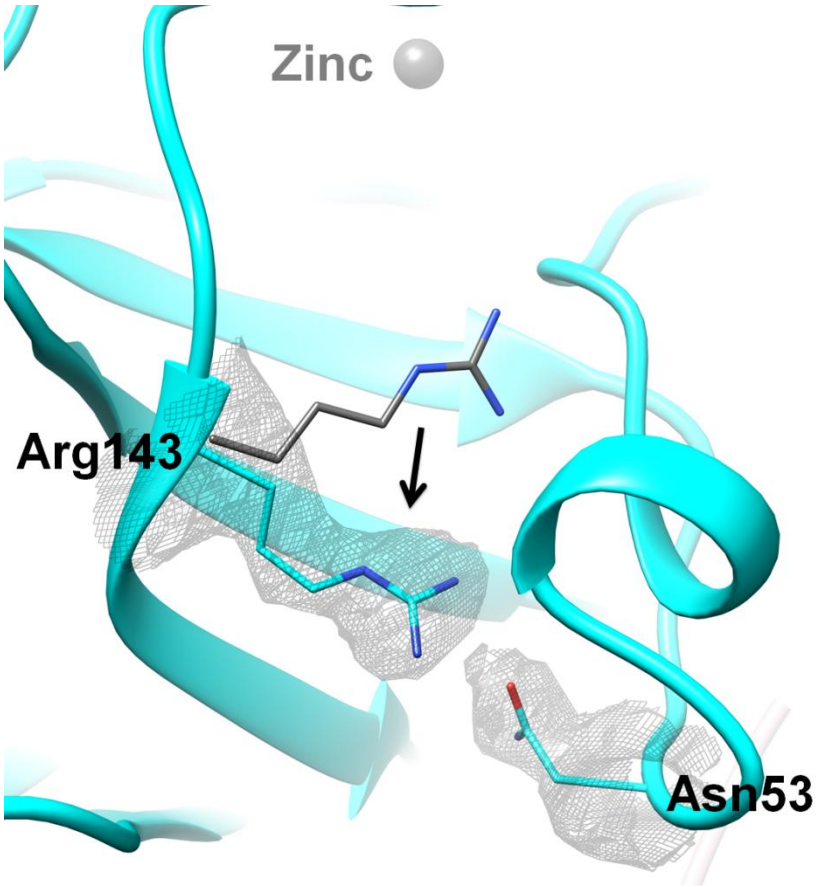

Source from: Own authorship.

As a result, the Arg143 no longer projects into the active site as it does in the mature hSOD1 homodimer, creating an inactive enzyme. We hypothesize this effect is part of the maturation mechanism. As a consequence of the complexation with hCCS and the shift in loop IV via the interaction of Arg104/Arg232 with the hSOD1 DNT motif and hCCS DIII, the Arg143 side chain ensures the amenability of the active site to receive copper while forming a physical barrier between residues Cys57 and Cys146, thereby inhibiting the formation of the hSOD1 disulphide.

Interestingly, once copper transfer to hSOD1 has been completed the Arg143 side-chain position is more uncertainty; it seems to switch between the active and inactive conformation, as displayed in Figure 40. In our structure of copper and zinc loaded compact heterodimer (Cu,Zn hSOD1 C57,146A), from the 12 heterodimers present in the asymmetric unit, the dual conformation of Arg143 is clearly present in at least 9 of the 12 chains. In Figure 40 we show that observed in chain E.

Figure 40 - Displacement of Arg143 in the Cu,Zn hSOD1 C57,146A. The hSOD1 Arg143 native conformation is showed in gray and the conformations in the heterocomplex in cyan. The 2Fo-Fc electron density map was contoured at 1σ.

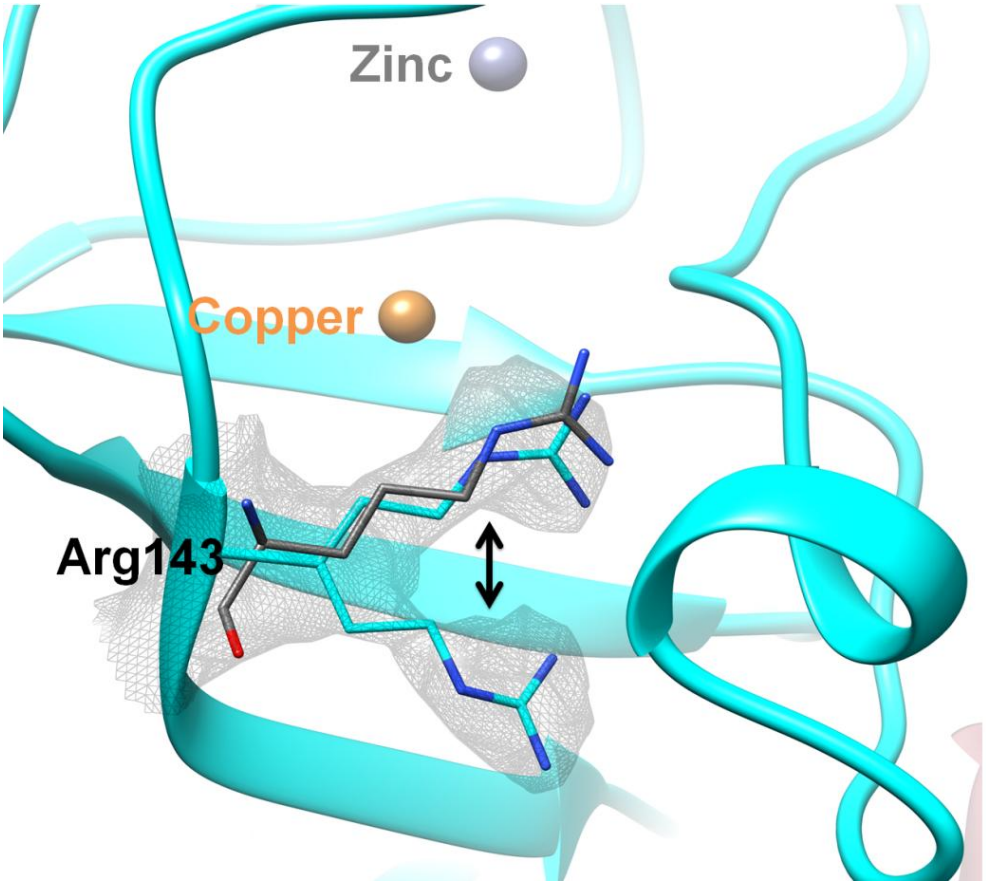

Source from: Own authorship.

This result indicates that upon copper and zinc ion binding the flexibility of loop IV is attenuated and favours that observed in the mature hSOD1 homodimer, even in the absence of the oxidation of the disulphide bond. As a consequence, the enzymatically active conformation for Arg143 is facilitated and the disulphide bond can be formed as the arginine no longer acts as a static physical barrier between the Cys57 and Cys146. The results emphasize that the copper transfer is prioritized over disulphide formation so that interactions which yield inactive or unstable hSOD1 products are minimized.

It is noteworthy on examining structures of complexes formed between SOD1 and CCS, Arg143 assumes different conformations, as shown in Figure 41. In the yeast complex, the residue is slightly raised relative to the arginine in the catalytic position; this effect is caused by an interaction with a sulphate ion and Ala230 in hCCS domain III (Figure 41 B). In the chimera structure, Arg143 assumes a conformation which strongly resembles the one seen in the mature form, stabilized via a salt bridge formed with Cys57 of hSOD1 (FETHEROLF *et al.*, 2017b; LAMB *et al.*, 2001).

Figure 41 – Comparison of the hSOD1 Arg143 conformational movement. (A) The structures compared were: The mature hSOD1 (PDB ID 2C9V, in gray), the hSOD1 C57,146A from the truncated heterodimer (6FOL, purple), the ySOD1 H48F (1JK9, orange) from the yeast complex and the hSOD1 H46R,H48Q from the chimeric structure (5U9M, cyan). (B) In the yeast complex Arg143 is stabilized via interactions with: yCCS Ala230 and a sulphate ion present in the crystallization condition. (C) In the chimeric structure, the stabilization of Arg143 occurs by interaction with hSOD1 Cys57.

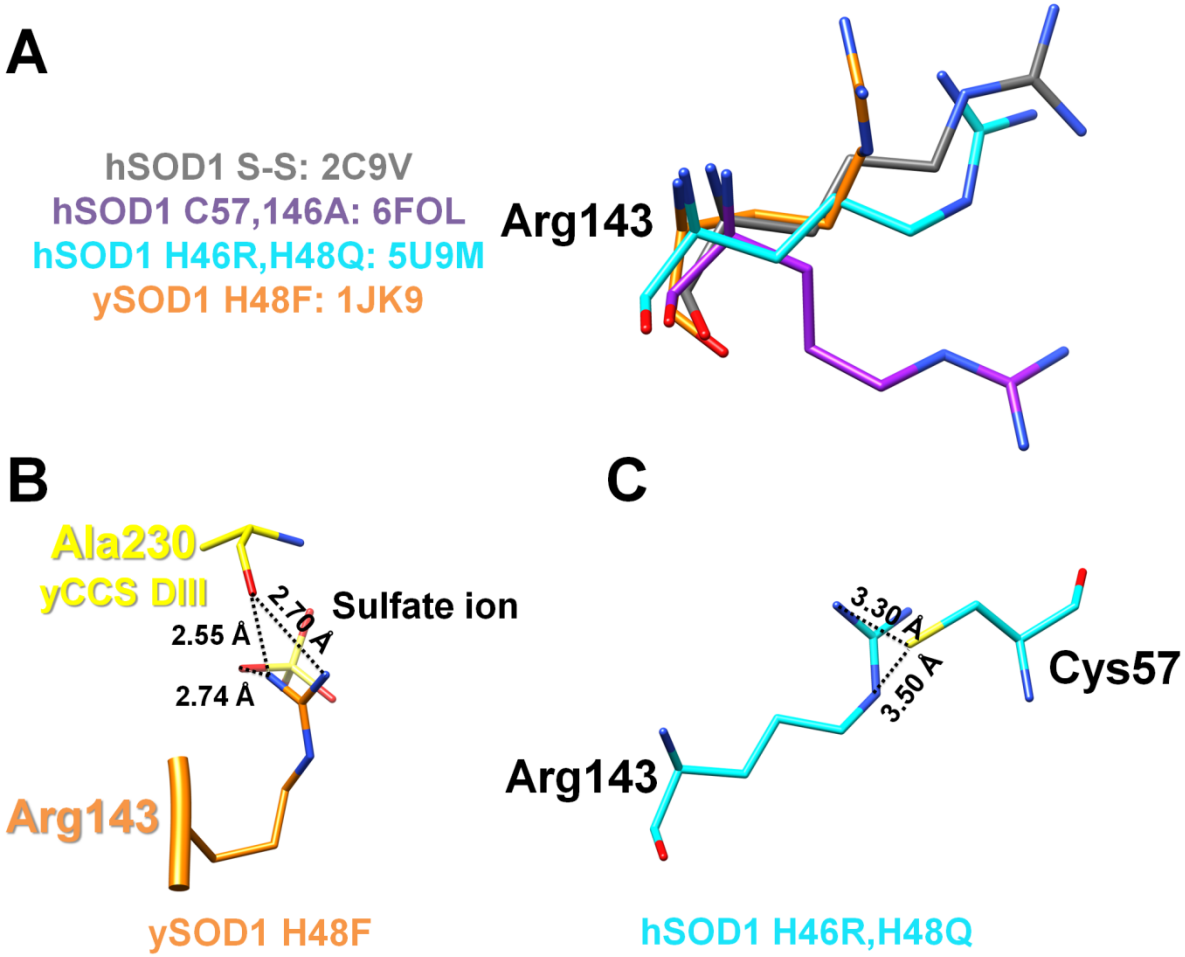

Source from: Own authorship.

We hypothesize that these varieties of conformations might occur because the reduced disulphide bond between Cys57 and Cys146 enables the displacement of loop IV and allows more degrees of freedom for Arg143. In each heterodimer it seems that the arginine is stabilized by a different mechanism depend on the hSOD1 and hCCS mutations used.

Taken together, our findings strongly reinforce the relationship between the oxidation state of the disulphide bridge, the movement of loop IV, the metal coordination and the conformation of Arg143 on dimerization and enzymatic activity. Since similar regions of the structure appear to be fundamental for both enzyme

activation and for the formation of the active homodimer, it would seem that these events must be coupled during hSOD1 maturation.

4.4.3 Copper transfer

A consensus has been established that effectively there is no free copper available in eukaryotic cells (RAE *et al.*, 1999). All the copper ions are coordinates to proteins. It is well described that the hSOD1 acquires its copper ion via transfer from hCCS albeit the biochemical basis of copper transfer is not completely understood.

Over the years groups have raised several different hypothesis on this subject (ALLEN; BADARAU; DENNISON, 2012; BANCI *et al.*, 2010b, 2012b; BOYD *et al.*, 2019; FETHEROLF *et al.*, 2017b; RAE *et al.*, 2001). In this work, although we have crystallized the compact heterocomplex with the copper present, the ion was incorporated *in vitro* prior to the complexation (see section 3.2). The study of copper transfer from hCCS to hSOD1 is a challenging endeavour as it involves the highly unstable copper(I), which can be handled only under non-reducing conditions.

Even though we have done some experiments focused on the copper transfer, no reliable results were obtained and the data are not shown. However, our results might shed some light on the mechanism of copper transfer thus we will discuss some aspects that we believe to be relevant.

The first role of CCS is to acquire its cargo from a direct interaction between hCCS domain I and the hCTR1. Subsequently the copper must be transferred to hSOD1 (ALLER; UNGER, 2006; KAHRA; KOVERMANN; WITTUNG-STAFSHEDE, 2016; SKOPP *et al.*, 2019). Previous studies suggested the capacity of both hCCS DI and DIII to coordinate the copper ion via the motifs MXCXXC and CXC, respectively (CARUANO-YZERMANS; BARTNIKAS; GITLIN, 2006; FURUKAWA; TORRES; O'HALLORAN, 2004; SCHMIDT *et al.*, 1999).

However, the copper dissociation constant for CCS domain I was calculated to be $1.1 \pm 0.6 \times 10^{-18}$ M while the affinity for domain III was two orders of magnitude lower, $2.7 \pm 1.4 \times 10^{-16}$ M (ALLEN; BADARAU; DENNISON, 2012). This result strongly points to a role of only CCS domain I in the copper trafficking. On hSOD1, the copper binds to the tetra-histidine site with a dissociation constant of 6.97 ± 2.26 10^{-21} M (BOYD *et al.*, 2018). Therefore, an affinity gradient seems to be responsible to thermodynamically drive the copper to the final destination.

As already discussed in section 4.3.1 we have crystallized the hSOD1 with its full length metallochaperone in the elongated and compact conformation. Comparing the two structures, there is a movement of around 47 Å in the hCCS copper-binding domain, as shown in Figure 42.

Figure 42 - Mobility of the hCCS domain I. Superposition of hCCS DII from the elongated and compact heterodimers show the displacement of 47 Å in domain I.

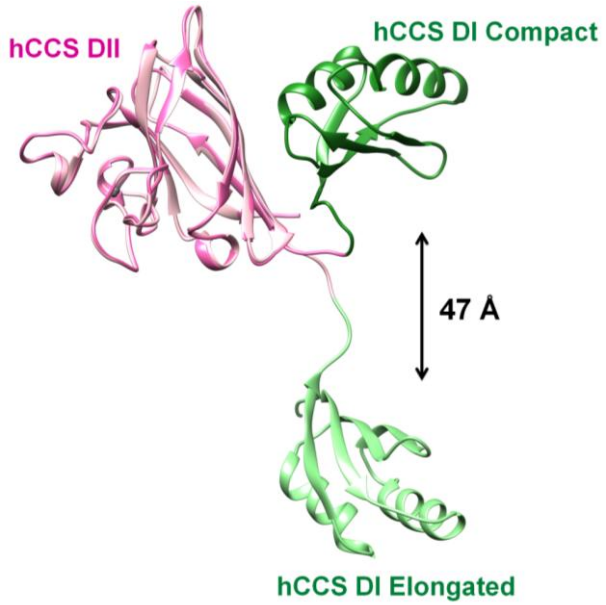

Source from: Own authorship.

The very high conformational plasticity of hCCS is reasonable since domain I is predicted to move from a conformation which facilitates copper acquisition from hCTR1 and subsequently to a position which enables its transfer to the hSOD1. Additionally, as already described in 4.4.2, when the hSOD1 is complexed with its metallochaperone there is an opening movement in loop IV and a reorientation of Arg143 to an enzymatically inactive position. We analyzed the electrostatic surface map of the oxidized Cu,Zn hSOD1, reduced E,Zn hSOD1 and E,Zn hSOD1 disulphide reduced when complexed with hCCS. Figure 43 depicts the results.

Figure 43 – The copper binding site in hSOD1. (A) Structure of hSOD1 is displayed as ribbon. Electrostatic surfaces, at ± 4kT, where positively and negatively coloured in blue and red, respectively. The asterisk in yellow indicates the copper binding site. The surfaces are shown with the same orientation as in (A) and represent: (B) Cu,Zn hSOD1$^{S\text{-}S}$. (C) E,Zn hSOD1$^{S\text{-}H}$. (D) E,Zn hSOD1$^{S\text{-}H}$ from the truncated heterodimer. The green arrow indicates the hole caused by the movement of Arg143.

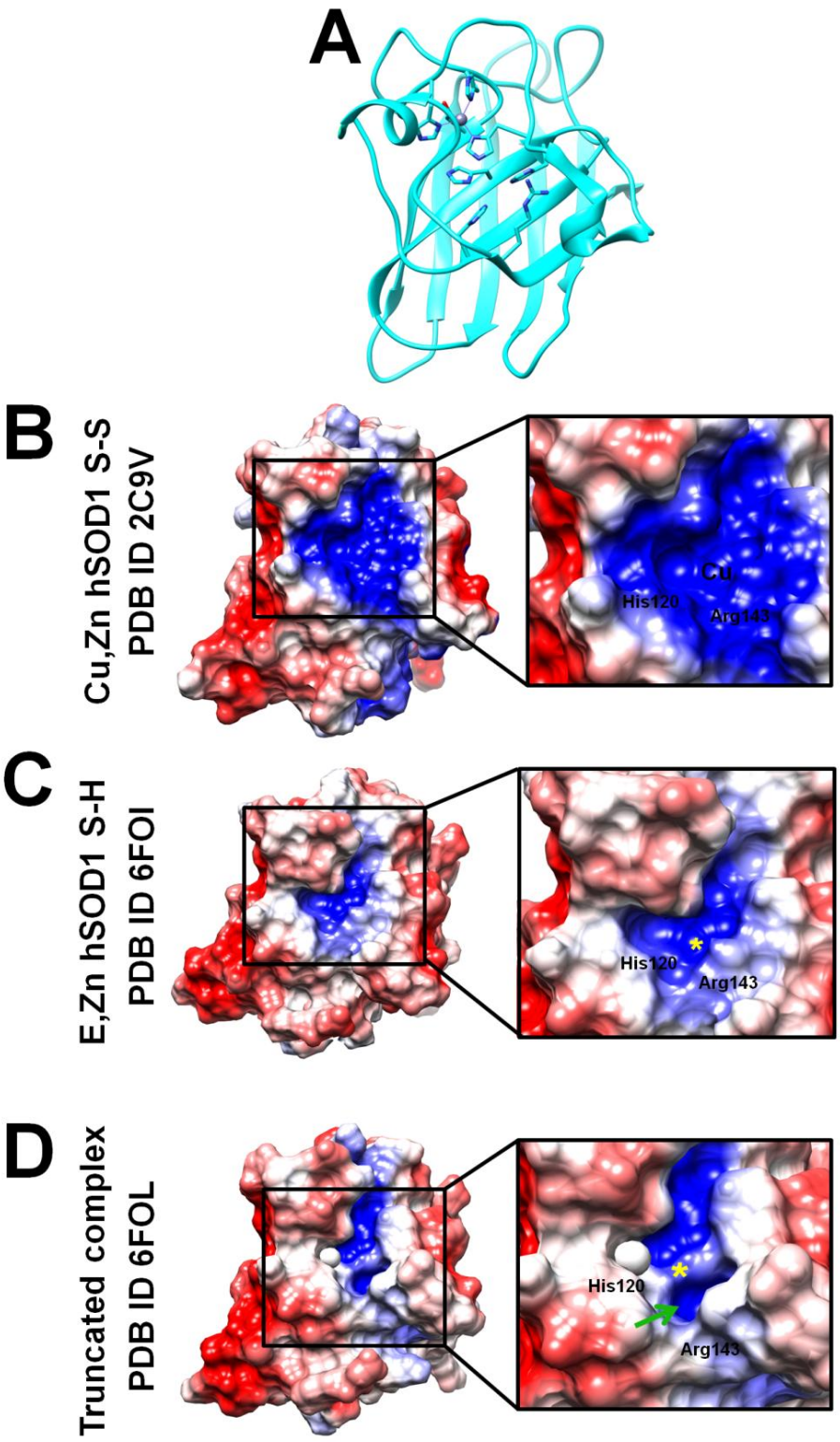

Source from: Own authorship.

Cu,Zn hSOD1disulphide oxidized has a significant positive electrostatic charge near the copper binding site, but the rest of the surface is negative charged. This effect has been suggested to direct the superoxide radical to the active site and therefore enhance the enzyme activity (GETZOFF *et al.*, 1983). Interestingly, when the copper is absent the extent of the positive charge is decreased in both E,Zn hSOD1 homodimer and E,Zn hSOD1 complexed with hCCS (Figure 43 C and D, respectively), moreover in hSOD1 heterocomplex there is a hole caused by the movement of arginine 143 to the idle position (indicated by the green arrow in Figure 43 D). Therefore, we hypothesize that slightly negative charge in the upper rim of the copper site added to the extra space facilitates the attraction and transferring of copper from hCCS domain I to the tetra histidine site in hSOD1.

4.4.4 Disulphide transfer and heterodimer dissociation

Once copper is incorporated and the Cys57-Cys146 disulphide bond is oxidized the heterocomplex disengages. The disulphide bond confers stability to hSOD1 and is critical for enzymatic activity (SEA *et al.*, 2015). Despite considerable effort, we do not have structures available or a detailed mechanism to explain this process.

In the literature several hypotheses are proposed, but up to now there is no consensus and the process is far from completely understood (BANCI *et al.*, 2012b; CARUANO-YZERMANS; BARTNIKAS; GITLIN, 2006; FETHEROLF *et al.*, 2017b; LAMB *et al.*, 2001; RAE *et al.*, 2001). A recent proposition was made by Fetherolf and collaborators which indicated a role for Cys57 or Cys146 as part of an initial copper coordination site holding it until the disulphide bond is oxidized (FETHEROLF *et al.*, 2017b).

On the other hand, Lamb and collaborators suggested that the CXC motif in yCCS domain III acts as a disulphide donor. In their work they solved the crystal structure of the ySOD1-yCCS heterocomplex (LAMB *et al.*, 2001). The structure displays the Cys229 in yCCS DIII forming an intermolecular disulphide bond with ySOD1 Cys57 (Figure 44 A). The sulphydryls of cysteines 57 and 146 would subsequently be oxidized via an exchange reaction involving yCCS Cys229 and ySOD1 Cys57.

Figure 44 – The disulphide exchange mechanism in the yeast heterocomplex (based on PDB ID 1JK9). (A) yCCS domain I, II and III are displayed in green, magenta and yellow, respectively. ySOD1 is in cyan and the zinc ions in gray. The disulphide bond exchange between yCCS cys229 and ySOD1 cys57 was trapped (both residues being shown as sticks). (B) The two non-crystallographically related heterodimers in the asymmetric unit viewed looking down the non-crystallographic two-fold axis. The yCCS domain III interacts with the domain II from the second heterodimer.

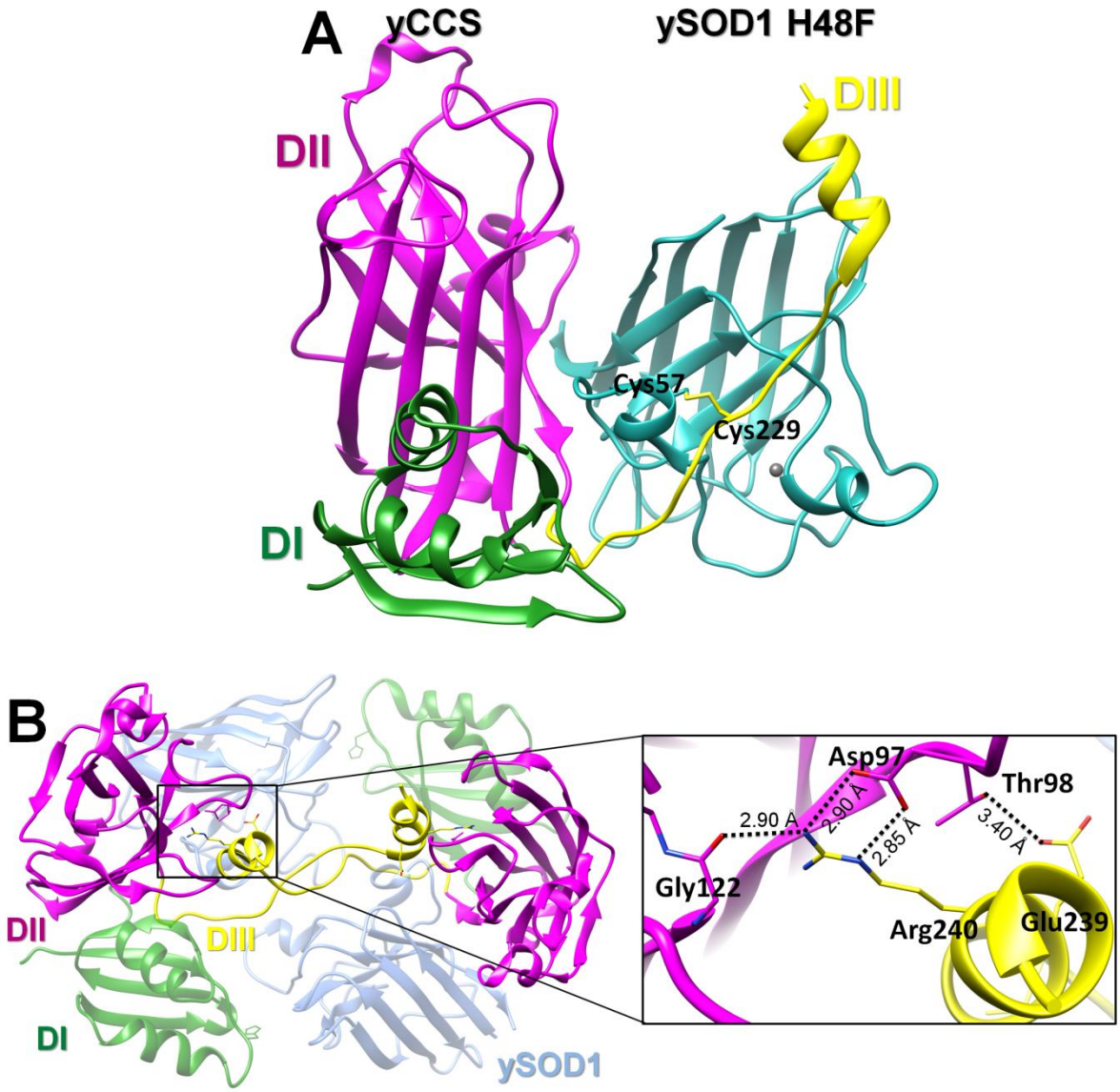

Source from: Own authorship.

Additionally, the yeast heterodimer contains in the asymmetric unit two non-crystallographically related complexes in which the yCCS domain III interacts with the yCCS domain II from the second heterodimer, via hydrogen bond formed between Arg240 and Gly122, Arg240 and Asp97 and Ans239 Thr98, as depicted in Figure 44 B. The role of CCS DIII transferring disulphide to SOD1 is also reinforced by a

pioneer study conducted by Banci and collaborators (BANCI *et al.*, 2012b) where they describe specifically the contribution of each hCCS domain in the series of events that undergo hSOD1 maturation.

Despite the fact that in our structures most of hCCS DIII cannot be localized due to poor electron density, our compact heterodimeric structure is consistent with this hypothesis. It shows the hCCS domain I to stabilize domain III in a position interacting with the SOD1 disulphide loop. This conformation brings the cysteines involved in hCCS-SOD1 disulphide formation into close proximity, and reinforces the direct role of hCCS DIII in catalyzing disulphide bond formation, as previously displayed in Figure 27 C and D. This is emphasized in the representation given in Figure 45.

Figure 45 – Structure of the compact heterodimer. The complex is shown as molecular surface and each domain is coloured differently. hCCS domain III is in a position interacting with the hSOD1 DNT motif.

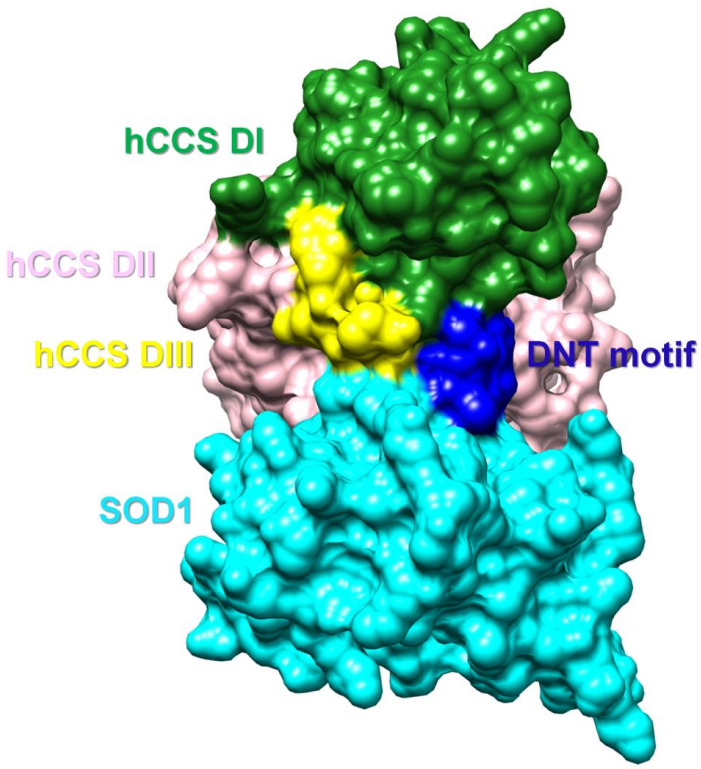

Source from: Own authorship.

In spite of the uncertainty in the details of the CCS-hSOD1 disulphide exchange process, the fact that the heterocomplex dissociates upon thiol oxidation of cys57 and cys146 was extensively observed in the course of this work. To explain

this we propose that once hSOD1 Cys57-Cys146 has been oxidized, the amino acid residue Gly51 accommodate the rearrangement in loop IV by a rotation in carbonyl (torsion angles psi varied from -12° to +49° in hSOD1 reduced state and oxidized state, respectively). In this new position carbonyl causes a steric clash with the side-chain hCCS Ala231 causing repulsion (Figure 46 A). Thus, the heterodimer dissociates and hSOD1 homodimerizes mitigating this repulsion as the hSOD1 has as a counterpart residue a glycine (Gly150). A schematic representation is also shown to better illustrate the mechanism (Figure 46 B).

Figure 46 - SOD1 Gly51 is the pivot of complex dissociation and SOD1 homodimerization on a molecular lever. (A) Oxidation of the disulphide bond causes conformational changes that are accommodated by rotation in Gly51, which projects the carbonyl group toward the interaction interface with hCCS, causing a steric repulsion with Ala231. (B) The mechanism is also represented schematically.

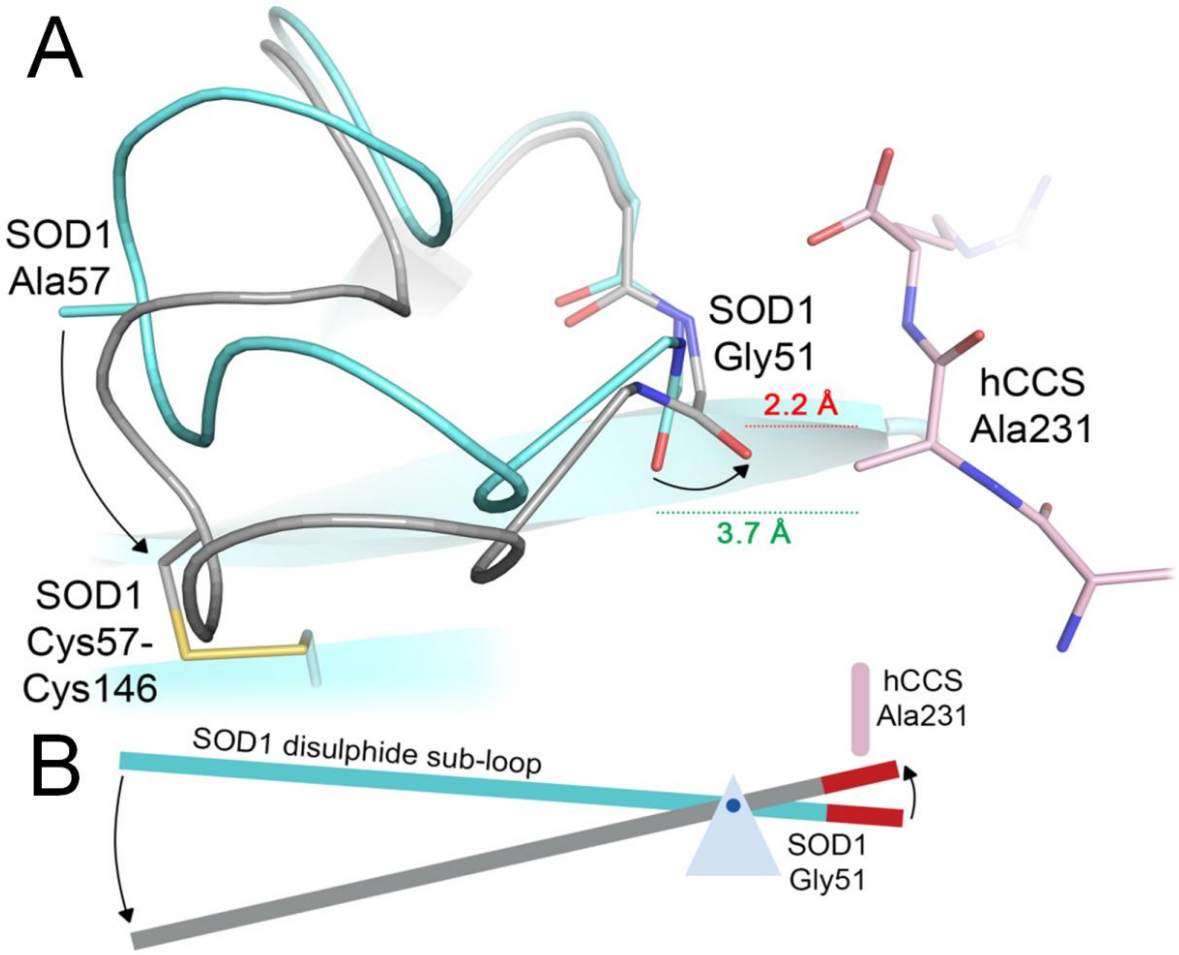

Source from: (SALA *et al.*, 2019).

As a necessity of the similarity of the proteins involved, the affinities that regulate the homodimers dissociation, heterodimer formation and dissociation and finally mature hSOD1 formation are finely balanced. The change on disulphide loop conformation affects directly the interactions. Moreover, we suggest that the hCCS Ala231 methyl dictates the dissociation. Curiously, while hSOD1 disulphide flexibility is related to the pathogenesis of hSOD1-related ALS, here we find that loop IV disordering is an absolute necessity for hCCS-catalysed hSOD1 maturation.

4.5 Membrane association and copper acquisition

So far we have described all the steps of hCCS catalyzed hSOD1 maturation. However, how the hCCS initially acquires its copper? Experimental evidence has suggested a critical role for the C-terminal region of hCTR1 in regulating Cu(I) entry into the cytoplasm and the direct transfer of copper to high affinity metallochaperones, such as hCCS (KAHRA; KOVERMANN; WITTUNG-STAFSHEDE, 2016; SKOPP *et al.*, 2019). In order to locate the membrane bound copper transporter the hCCS has been described to interact with the lipid membrane bilayer, thus minimizing the search space to two dimensions (ALLER; UNGER, 2006; BOYD *et al.*, 2019; POPE; DE FEO; UNGER, 2013).

Hypotheses which have been proposed involve the formation of a transient binary or ternary complex (hCCS-CTR1 or hSOD1-hCCS-CTR1) within the context of the membrane (ARNESANO *et al.*, 2004; BANCI *et al.*, 2012b; BROWN *et al.*, 2004). Motivated by these proposals, we have performed a liposome binding assay to determine whether hCCS or hSOD1-hCCS would engage directly with lipid bilayers to acquire its cargo.

It has been previously described that the yeast CCS interaction with the plasma membrane occurs through positively charged residues in yCCS DII, including Lys89, Ly95, Lys96, Arg101 and Lys167. However these residues are not conserved from yeast to human CCS, as depicted in Figure 47:

Figure 47 – Supposed residues involved in membrane association in yeast and human. Crystal structure of yCCS (PDB ID 1QUP) and hCCS DI, DII and DIII are show in green, magenta and yellow, respectively. The residues hypothesized to be involved in the yeast interaction are show in gray as sticks. The Columbic surface potential was calculated with Chimera, positively and negatively charged residues are displayed in blue and red, respectively (at ± 5kT). In the hCCS structure, from the compact heterodimer, D I, II and III are show in green, pink and yellow, respectively. The positive residues in yeast Domain II are not conserved in human (shown in gray as sticks), and the columbic surface potential is negatively charged in the vicinity.

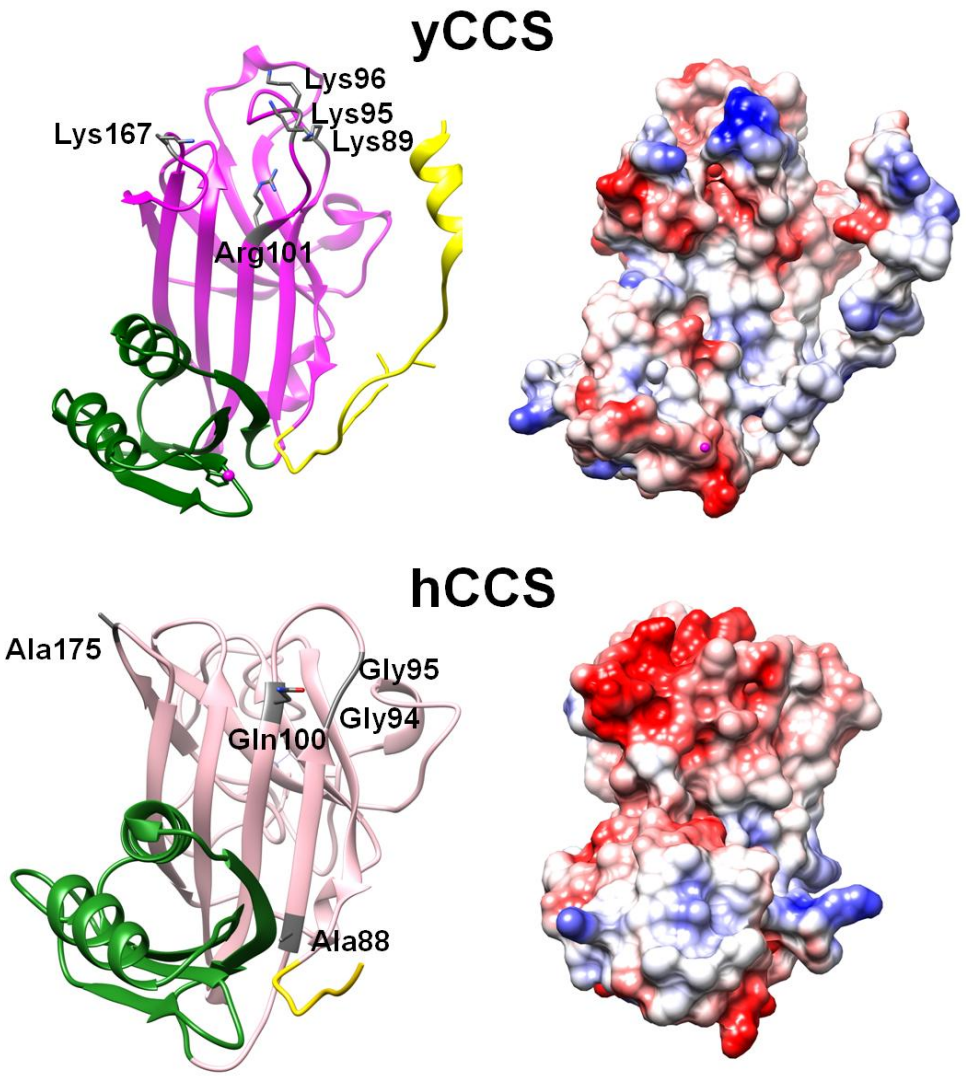

Source from: Own authorship.

In fact, hCCS DII seems to be negatively charged in the region, thus it is unlikely to be the responsible to interact with the negative surface charge in the inner left side of the membrane. Therefore, to investigate what drives the hCCS association in the case of human system we designed a series of mutants, which were either related to: probing the role of individual hCCS domains (hCCS domain I,

hCCS domain II, hCCS domain I,II), its oligomeric state (hCCS A231G) as well as the positively charged residues in hCCS DI (hCCS R30A, K31A) which are conserved from the homolog Atx1 and pointed there as crucial for membrane interaction.

For this experiment, a synthetic lipid substrate was prepared and the experiment was performed as described in section 3.12. Negatively charged lipid bilayers representative of the inner surface of the plasma membrane were used. In the experiment, for each protein we obtained three fractions corresponding to: the first supernatant (after 60 minutes incubation with the liposomes), the washing solution and the pellet. All fractions were loaded onto SDS-PAGE. Only the proteins present in the pellet fractions were considered to indicate membrane interaction. The ImageJ program was used to calculate the percentage of association and the results are shown in Figure 48:

Figure 48 - Liposome binding assay. The percentage of each protein associated with the membrane.

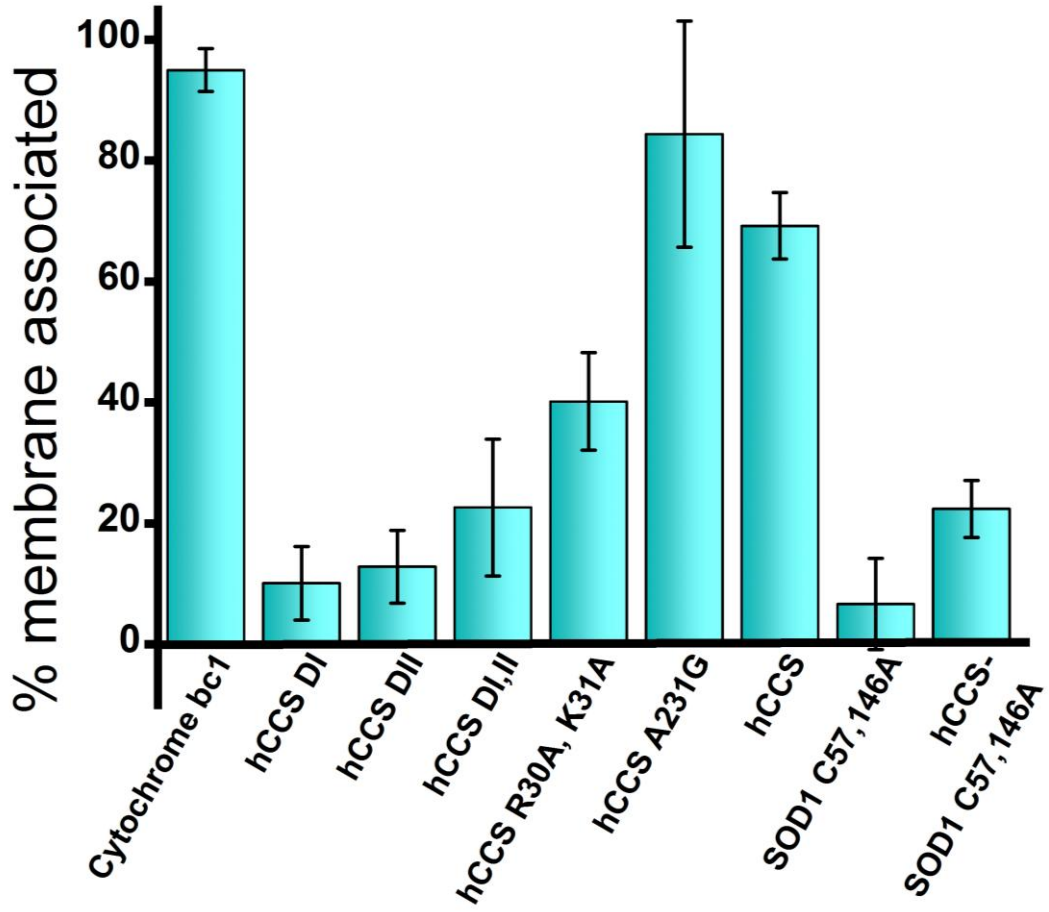

Source from: Own authorship.

The same experimental procedure was applied to all proteins. The cytochrome bc1 complex is well known to associate with the membrane, so it was used here as a quality control for our liposomes. The results revealed a membrane binding of over 90%, attesting the quality of the liposomes.

The full length wt hCCS associated significantly with liposomes, and an increase in the hCCS homodimer affinity (via Ala231 mutation to glycine) further improved its interaction with the membrane. On the other hand, mutations on Arg30 and Lys31, which are located close to the domain I copper site, to neutral alanine resulted in a reduction in lipid binding showing that probably hCCS DI charged residues has a role in association with the membrane, but it is not solely responsible.

hCCS truncations were also tested. The monomeric hCCS DI showed almost no interaction, despite its similarities with the Atx1, which has been proposed to interact with membrane (FLORES; UNGER, 2013). Moreover, differently from the yeast CCS results, the truncation hCCS domain II also revealed low affinity (approximately 15%) (POPE; DE FEO; UNGER, 2013). The combination of these domains (hCCS DI,II) had marginally improved association of roughly 20% to the membrane possibly due a monomer dimer-equilibrium shifted to monomeric species, as previous discussed in section 4.1 and showed in Figure 13. The disulphide reduced wild-type hSOD1 was also assessed and little associate with the lipid membrane while the hCCS-hSOD1 complex showed low levels of association.

In summary, our results showed that positively charged residues in hCCS domain I (i.e., hCCS R30A/K31A) and improvement in hCCS dimer affinity (hCCS A231G) may have some role increasing the electrostatic interaction with the membrane. On the other hand, the reduction of hCCS interacting surface (e.g., upon heterodimer formation) had a more pronounced effect decreasing membrane association. Therefore copper acquisition is likely to occur by hCCS in its homodimeric state prior to complexation with hSOD1. The subsequent activation of hSOD1 is more likely to occur off the lipid bilayer as described in section 4.4.

5 Conclusions

The complexity of cells necessitates an equally complex system of courier proteins to internalize and deliver biologically useful metals such as copper. The human antioxidant enzyme superoxide dismutase 1 (hSOD1) is one of the proteins that require copper. It is well known that hSOD1 acquires its cargo via direct protein-protein interaction with the copper chaperone (hCCS). However, the dependent maturation has never been fully elucidated due to the difficulty in obtaining the human transient SOD1-CCS complexes.

The currently accepted mechanism for maturation of hSOD1 is shown in Figure 49 and involves hCCS membrane association and copper(I) acquisition via interactions with hCTR1. Subsequently, Cu(I)-hCCS forms a stable heterodimer with immature hSOD1 via contacts between the hCCS DII and the immature hSOD1, copper transfer via domain I of hCCS reorientation and hSOD1 Cys57-Cys146 disulphide oxidation presumably via hCCS DIII transfer. Once the disulphide is formed, the heterodimer dissociates, hSOD1 forms a mature, stable and active enzyme while the hCCS is released to restart the cycle (BANCI *et al.*, 2012b).

Figure 49 – Schematic mechanism of the current accepted hCCS-dependent hSOD1 maturation.

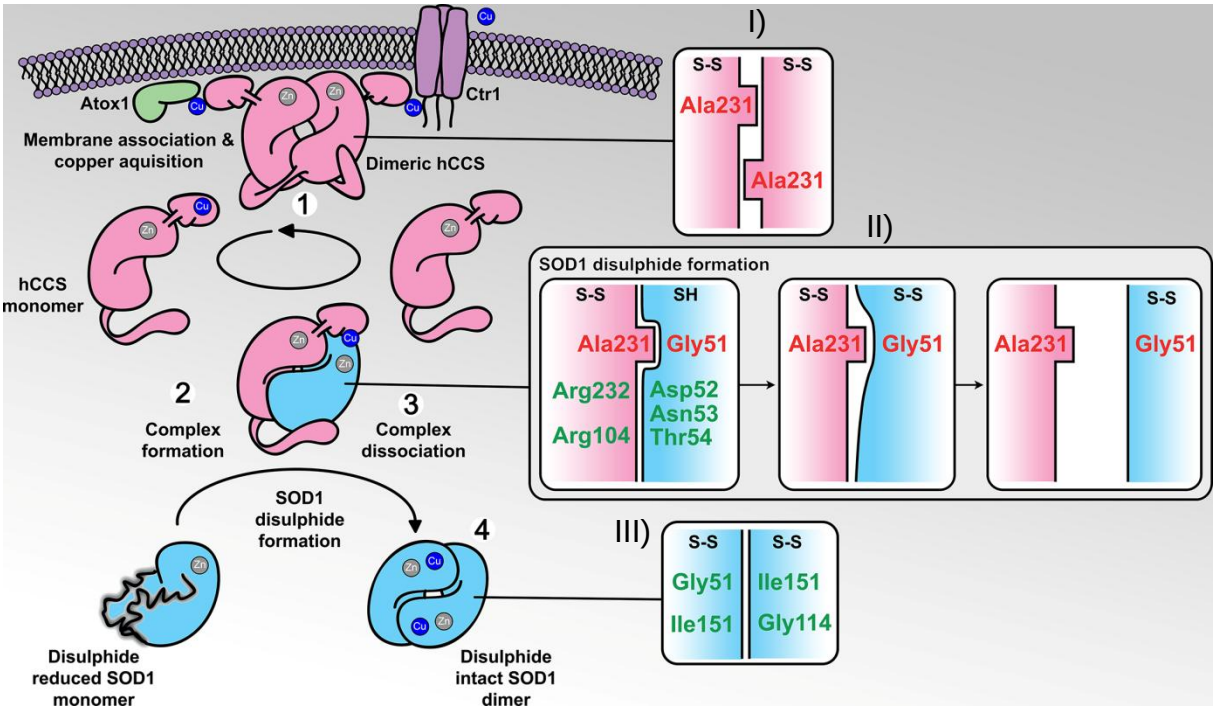

Source from: (SALA *et al.*, 2019).

Overall, our results support the proposed mechanism of CCS-dependent maturation (Figure 7). Specific our contribution to the field was the dissection of some of the atomic details involved in the molecular recognition events and conformational rearrangements that facilitate hCCS-catalysed SOD1 activation shown in Figure 49. In order to do so, we discovered a means to make the human complex amenable to structural studies and characterized, for the first time, the human transient SOD1-hCCS complex in different redox and metallation states using protein crystallography. We also crystallized and solved the structure of immature SOD1 (E,Zn hSOD1 C57,146A) as well as performing a reappraisal of the hCCS DII structure which had been described previously at a much lower resolution (LAMB *et al.*, 2000). Together these structures represent snapshots of reaction precursors, intermediates and products of the hSOD1 maturation pathway.

As shown in step 1 in Figure 49, to initiate the maturation pathway the apo-hCCS DI must acquire the Cu(I) ion from hCTR1, as has been previously suggested (FLORES; UNGER, 2013; POPE; DE FEO; UNGER, 2013; SKOPP *et al.*, 2019). This process could involve hCCS and/or hCCS-hSOD1 interaction with the lipid membrane bilayer. Using liposome binding assay we demonstrated that hSOD1-

hCCS does not engage directly with lipid bilayers, thereby copper acquisition must occur through the formation of a complex between hCTR1 and homodimeric hCCS.

The hSOD1 - Cu(I) hCCS heterodimeric complex formation is most likely to occur in the cytosol. Analyzing our hCCS homodimeric structure sheds light on why the interface is not expected to be highly stable in solution. This comes from the steric repulsion effects involving Ala231 (insert I, Figure 49) and the electrostatic desestabilization caused by Arg232-Arg196 contacts. On the other hand, as previously suggested, fully cysteine depleted hSOD1 has increased conformational freedom in loop IV, located at the homodimeric interface. This suggests that the reduced form of hSOD1 would favour the monomeric species.

Along with others, we have shown that hSOD1 must be disulphide reduced to form a complex with hCCS (CULIK *et al.*, 2018; FURUKAWA; O'HALLORAN, 2006; HÖRNBERG *et al.*, 2007; LINDBERG *et al.*, 2004). It seems that the same region of hSOD1 (loop IV) is involved in disfavouring immature hSOD1 homodimerization and also favouring heterodimer formation. Additionally, our experiments demonstrated that the disulphide formation activates complex dissociation and therefore likely changes the affinity of hCCS for hSOD1. Thus, the state of the SOD1 disulphide is determinant in initiating and terminating contact with hCCS while the chaperone plays a passive role. If hSOD1 disulphide oxidation initiates complex dissociation, how can hCCS prioritize passing copper to hSOD1?

Our heterodimeric structures offered a clue. Upon complexation (Step 2 in Figure 49) hCCS stabilizes hSOD1 loop IV flexibility by hydrogen bond interactions formed across the dimer interface between Arg104, Arg232 and the solvent exposed surface of the opposing disulphide loop (DXT motif). The presences of this interaction stabilized loop IV and pulled Cys 57 and 146 apart, opening the disulphide loop and preventing their oxidation prior to copper transfer.

As a result of the opening of loop IV in the reduced state, Arg143, which is well known to be related to enzyme activity in hSOD1, shifts its positions and interposes between Cys57 and 146 in the space normally occupied by the disulphide sub-loop, creating an inactive enzyme. Subsequently, domain I of hCCS moves to a position which enables copper transfer to the hSOD1. The high positional dynamics of domain I was shown in our crystallographic structures. Once zinc and copper are bound, the flexibility of loop IV is attenuated favouring the conformation observed in the mature hSOD1 homodimer.

We hypothesize this effect is part of the maturation mechanism. The Arg143 side chain inhibits the formation of the hSOD1 disulphide bridge until copper has been acquired, so that interactions which yield inactive or unstable hSOD1 products are minimized. Indeed, we have also addressed complex formation and its stability after copper incorporation. These results were particularly interesting and reinforced the notion that copper incorporation is the first step in the SOD1-hCCS maturation process (BANCI *et al.*, 2012b).

After copper incorporation the Cys57-Cys146 disulphide bridge is suggested to be formed via a process involving a transfer reaction from one of the cysteines from DIII of hCCS to hSOD1 Cys57 (LAMB *et al.*, 2001). However, our *in vitro* results demonstrated that hCCS domain I can speed up hSOD1 disulphide oxidation or be the responsible for to transfer itself in the absence of hCCS DIII. These results reveal that the mechanism of disulphide transfer may be more promiscuous than previous anticipated.

Once the Cys57-Cys146 is formed the heterocomplex disengages (Step 3 in Figure 49). To explain why the heterodimer affinity is weakened upon hSOD1 maturation we demonstrated that once the hSOD1 Cys57-Cys146 has been oxidized, loop IV is rearranged and a rotation in the carbonyl group of hSOD1 Gly51 is required to accommodate this new conformation (insert II, Figure 49) . This causes a steric clash with the side-chain of hCCS Ala231 causing repulsion. As the hSOD1 has, as a counterpart residue, a glycine (Gly150 in place of Ala231), the heterodimer dissociates and hSOD1 homodimerizes attenuating this repulsion and forming four strong hydrogen bonds (insert III, Figure 49) in the interface (Step 4).

In summary, it can be concluded that the novel conformation observed for loop IV possibly orchestrates complex formation, the timing of copper and disulphide transfer, the complex dissociation and finally the mature hSOD1 dimerization. As a consequence of the similarity of the proteins involved, the affinities that regulate the dissociation of the homodimers, and the formation and dissociation of the heterodimers and finally the formation of the mature hSOD1 are delicately balanced.

Interestingly, in ALS associated SOD1 mutations, aggregated proteins are found especially in the reduced and/or apo form (FURUKAWA; TORRES; O'HALLORAN, 2004). In spite of our best efforts SOD1 ALS related mutants cannot efficiently associate with hCCS. This highlights that SOD1 monomerization and

subsequently toxicity acts in concert with the absence of the post translational modifications.

6 Future work

The question of how the copper chaperone initially acquires its cargo remains elusive and further studies are clearly needed. Thus, a new goal would be to understand in depth the interaction and the mechanism of copper transfer from hCTR1 to hCCS and finally to SOD1. Focus would be placed therefore to solve the structure of the putative ternary complex hCTR1-hCCS. Additionally, confocal microscopy experiments for hCTR1, hCCS, hCCS-hSOD1 and hSOD1 would be interesting to corroborate our membrane association experiments.

Finally, a lot remains to be understood regarding how to decrease the toxicity of ALS related mutants. With a better understanding of the hCCS-hSOD1 molecular recognition process, drug discovery efforts that aim to stabilize the heterocomplex until SOD1 acquires post-translational modifications could be an interesting alternative in the fight against neurodegenerative diseases.

Bibliography

ADAMS, P. D.; AFONINE, P. V.; BUNKOCZI, G.; CHEN, V. B.; DAVIS, I. W.; ECHOLS, N.; HEADD, J. J.; HUNG, L. W.; KAPRAL, G. J.; GROSSE-KUNSTLEVE, R. W.; MCCOY, A. J.; MORIARTY, N. W.; OEFFNER, R.; READ, R. J.; RICHARDSON, D. C.; RICHARDSON, J. S.; TERWILLIGER, T. C.; ZWART, P. H. PHENIX: a comprehensive Python-based system for macromolecular structure solution. **Acta Crystallographica Section D:** Biological Crystallography, Malden, v. 66, n. 2, p. 213–221, 2010.

ALLEN, S.; BADARAU, A.; DENNISON, C. Cu(I) affinities of the domain 1 and 3 sites in the human metallochaperone for Cu,Zn-superoxide dismutase. **Biochemistry**, Washington, v. 51, n. 7, p. 1439–1448, 2012.

ALLER, S. G.; UNGER, V. M. Projection structure of the human copper transporter CTR1 at 6-A resolution reveals a compact trimer with a novel channel-like architecture. **Proceedings of the National Academy of Sciences of the United States of America**, Washington, v. 103, n. 11, p. 3627–3632, 2006.

AMIE, K.; ROSENZWEIG, A. C. Structural bioloogy of copper trafficking. **Chemical Reviews**, Washington, v. 109, n. 10, p. 4760–4779, 2009.

ARNESANO, F.; BANCI, L.; BERTINI, I.; MARTINELLI, M.; FURUKAWA, Y.; O'HALLORAN, T. V. The unusually stable quaternary structure of human Cu,Zn-superoxide dismutase 1 is controlled by both metal occupancy and disulfide status. **Journal of Biological Chemistry**, Bethesda, v. 279, n. 46, p. 47998–48003, 2004.

ASSMANN, G.; BREHM, W.; DIEDERICHS, K. Identification of rogue datasets in serial crystallography. **Journal of Applied Crystallography**, Chichester, v. 49, n. 3, p. 1021–1028, 2016.

BANCI, L.; BENEDETTO, M.; BERTINI, I.; DEL CONTE, R.; PICCIOLI, M.; VIEZZOLI, M. S. Solution structure of reduced monomeric Q133M2 copper, zinc superoxide dismutase (SOD). Why is SOD a dimeric enzyme? **Biochemistry**, Washington, v. 37, n. 34, p. 11780–11791, 1998.

BANCI, L.; BERTINI, I.; DURAZO, A.; GIROTTO, S.; GRALLA, E. B.; MARTINELLI, M.; VALENTINE, J. S.; VIERU, M.; WHITELEGGE, J. P. Metal-free superoxide dismutase forms soluble oligomers under physiological conditions: a possible general mechanism for familial ALS. **Proceedings of the National Academy of Sciences of the United States of America**, Washington, v. 104, n. 27, p. 11263–11267, 2007.

BANCI, L.; BERTINI, I.; BOCA, M.; GIROTTO, S.; MARTINELLI, M.; VALENTINE, J. S.; VIERU, M. SOD1 and amyotrophic lateral sclerosis: mutations and oligomerization. **Plos ONE**, San Francisco, v. 3, n. 2, p. 1–8, 2008.

BANCI, L.; BERTINI, I.; CEFARO, C.; CENACCHI, L.; CIOFI-BAFFONI, S.; FELLI, I. C.; GALLO, A.; GONNELLI, L.; LUCHINAT, E.; SIDERIS, D.; TOKATLIDIS, K. Molecular chaperone function of Mia40 triggers consecutive induced folding steps of the substrate in mitochondrial protein import. **Proceedings of the National Academy of Sciences of the United States of America**, Washington, v. 107, n. 47, p. 20190–20195, 2010 a.

BANCI, L.; BERTINI, I.; CIOFI-BAFFONI, S.; KOZYREVA, T.; ZOVO, K.; PALUMAA, P. Affinity gradients drive copper to cellular destinations. **Nature**, London, v. 465, n. 7298, p. 645–648, 2010 b.

BANCI, L.; BERTINI, I.; BLAŽEVITŠ, O.; CALDERONE, V.; CANTINI, F.; MAO, J.; TRAPANANTI, A.; VIERU, M.; AMORI, I.; COZZOLINO, M.; CARRÌ, M. T. Interaction of cisplatin with human superoxide dismutase. **Journal of the American Chemical Society**, Washington, v. 134, n. 16, p. 7009–7014, 2012 a.

BANCI, L.; BERTINI, I.; CANTINI, F.; KOZYREVA, T.; MASSAGNI, C.; PALUMAA, P.; RUBINO, J. T.; ZOVO, K. Human superoxide dismutase 1 (hSOD1) maturation through interaction with human copper chaperone for SOD1 (hCCS). **Proceedings of the National Academy of Sciences of the United States of America**, Washington, v. 109, n. 34, p. 13555–13560, 2012 b.

BANCI, L.; BARBIERI, L.; BERTINI, I.; LUCHINAT, E.; SECCI, E.; ZHAO, Y.; ARICESCU, A. R. Atomic-resolution monitoring of protein maturation in live human cells by NMR. **Nature Chemical Biology**, London, v. 9, n. 5, p. 297–299, 2013 a.

BANCI, L.; CANTINI, F.; KOZYREVA, T.; RUBINO, J. T. Mechanistic aspects of hSOD1 maturation from the solution structure of cui-Loaded hCCS domain 1 and analysis of disulfide-free hSOD1 mutants. **ChemBioChem**, Weinheim, v. 14, n. 14, p. 1839–1844, 2013 b.

BATTYE, T. G. G.; KONTOGIANNIS, L.; JOHNSON, O.; POWELL, H. R.; LESLIE, A. G. W. iMOSFLM: a new graphical interface for diffraction-image processing with MOSFLM. **Acta Crystallographica Section D:** Biological Crystallography, Malden, v. 67, n. 4, p. 271–281, 2011.

BERGFORS, T. Seeds to crystals. **Journal of Structural Biology**, Maryland Heights, v. 142, n. 1, p. 66–76, 2003.

BERTINI, I.; MANGANL, S.; VIEZZOLI, M. S. Structure and properties of copper-zinc superoxide dismutases. **Advances in Inorganic Chemistry**, Maryland Heights, v. 45, p. 127–250, 1998.

BEYER, W. F.; FRIDOVICH, I.; MULLENBACH, G. T.; HALLEWELL, R. Examination of the role of arginine-143 in the human copper and zinc superoxide dismutase by site-specific mutagenesis. **Journal of Biological Chemistry**, Bethesda, v. 262, n. 23, p. 11182–11187, 1987.

BOYD, S. D.; LIU, L.; BULLA, L.; WINKLER, D. D. Quantifying the interaction between copper-zinc superoxide dismutase (Sod1) and its copper chaperone (Ccs1). **Journal of Proteomics & Bioinformatics**, Brussels, v. 11, n. 4, p. 1–14, 2018.

BOYD, S. D.; CALVO, J. S.; LIU, L.; ULLRICH, M. S.; SKOPP, A.; MELONI, G.; WINKLER, D. D. The yeast copper chaperone for copper-zinc superoxide dismutase (CCS1) is a multifunctional chaperone promoting all levels of SOD1 maturation. **Journal of Biological Chemistry**, Bethesda, v. 294, n. 6, p. 1956-1966, 2019.

BROOM, H. R.; RUMFELDT, J. A. O.; VASSALL, K. A.; MEIERING, E. M. Destabilization of the dimer interface is a common consequence of diverse ALS-associated mutations in metal free SOD1. **Protein Science**, Hoboken, v. 24, n. 12, p. 2081–2089, 2015.

BROWN, N. M.; TORRES, A. S.; DOAN, P. E.; O'HALLORAN, T. V. Oxygen and the copper chaperone CCS regulate posttranslational activation of Cu,Zn superoxide dismutase. **Proceedings of the National Academy of Sciences of the United States of America**, Washington, v. 101, n. 15, p. 5518–5523, 2004.

CAPPER, M. J.; WRIGHT, G. S. A.; BARBIERI, L.; LUCHINAT, E.; MERCATELLI, E.; MCALARY, L.; YERBURY, J. J.; O'NEILL, P. M.; ANTONYUK, S. V.; BANCI, L.; HASNAIN, S. S. The cysteine-reactive small molecule ebselen facilitates effective SOD1 maturation. **Nature Communications**, London, v. 9, n. 1, p. 1–9, 2018.

CARRICO, R. J.; DEUTSCH, H. F. The presence of zinc in human cytocuprein and some properties of the apoprotein. **Journal of Biological Chemistry**, Bethesda, v. 245, n. 4, p. 723–727, 1970.

CARROLL, M. C.; OUTTEN, C. E.; PROESCHER, J. B.; ROSENFELD, L.; WALTER, H.; WHITSON, L. J.; HART, P. J.; JENSEN, L. T.; CIZEWSKI, V. The effects of glutaredoxin and copper activation pathways on the disulfide and stability of Cu,Zn superoxide dismutase. **Journal of Biological Chemistry**, Bethesda, v. 281, n. 39, p. 28648–28656, 2009.

CARUANO-YZERMANS, A. L.; BARTNIKAS, T. B.; GITLIN, J. D. Mechanisms of the copper-dependent turnover of the copper chaperone for superoxide dismutase. **Journal of Biological Chemistry**, Bethesda, v. 281, n. 19, p. 13581–13587, 2006.

CASARENO, R. L. B.; WAGGONER, D.; GITLIN, J. D. The copper chaperone CCS directly interacts with copper/zinc superoxide dismutase. **Journal of Biological Chemistry**, Bethesda, v. 273, n. 37, p. 23625–23628, 1998.

CHANG, L. Y.; SLOT, J. W.; GEUZE, H. J.; CRAPO, J. D. Molecular immunocytochemistry of the CuZn superoxide dismutase in rat hepatocytes. **Journal of Cell Biology**, New York, v. 107, n. 6, p. 2169–2179, 1988.

CHATTOPADHYAY, M.; VALENTINE, J. S. Aggregation of copper-zinc superoxide dismutase in familial and sporadic ALS. **Antioxidants and Redox Signaling**, New Rochelle, v. 11, n. 7, p. 1603–1614, 2009.

CHEN, V. B.; ARENDALL, W. B.; HEADD, J. J.; KEEDY, D. A.; IMMORMINO, R. M.; KAPRAL, G. J.; MURRAY, L. W.; RICHARDSON, J. S.; RICHARDSON, D. C. MolProbity: all-atom structure validation for macromolecular crystallography. **Acta Crystallographica Section D:** Biological Crystallography, Malden, v. 66, n. 1, p. 12–21, 2010.

CLABBERS, M. T. B.; GRUENE, T.; PARKHURST, J. M.; ABRAHAMS, J. P.; WATERMAN, D. G. Electron diffraction data processing with DIALS. **Acta Crystallographica Section D:** Structural Biology, Malden, v. 74, n. 6, p. 506–518, 2018.

CLEVELAND, D. W.; ROTHSTEIN, J. D. From charcot to lou gehrig: deciphering selective motor neuron death in als. **Nature Reviews Neuroscience**, London, v. 2, n. 11, p. 806–819, 2001.

CULIK, R. M.; SEKHAR, A.; NAGESH, J.; DEOL, H.; RUMFELDT, J. A. O.; MEIERING, E. M.; KAY, L. E. Effects of maturation on the conformational free-energy landscape of SOD1. **Proceedings of the National Academy of Sciences of the United States of America**, Washington, v. 115, n. 11, p. E2546–E2555, 2018.

CULOTTA, V. C.; KLOMP, L. W. J.; STRAIN, J.; CASARENO, R. L. B.; KREMS, B.; GITLIN, J. D. The copper chaperone for superoxide dismutase. **Journal of Biological Chemistry**, Bethesda, v. 272, n. 38, p. 23469–23472, 1997.

D'ARCY, A.; BERGFORS, T.; COWAN-JACOB, S. W.; MARSH, M. Microseed matrix screening for optimization in protein crystallization: what have we learned? **Acta Crystallographica Section F:** Structural Biology Communications, Hoboken, v. 70, p. 1117–1126, 2014.

DIEDERICHS, K.; KARPLUS, A. Assessing and maximizing data quality in macromolecular crystallography. **Current Opinion in Structural Biology**, Kidlington, v. 34, p. 60–68, 2015.

DUPEYRAT, F.; VIDAUD, C.; LORPHELIN, A.; BERTHOMIEU, C. Long distance charge redistribution upon Cu,Zn-superoxide dismutase reduction: significance for dismutase function. **Journal of Biological Chemistry**, Bethesda, v. 279, n. 46, p. 48091–48101, 2004.

EMSLEY, P.; LOHKAMP, B.; SCOTT, W. G.; COWTAN, K. Features and development of coot. **Acta Crystallographica Section D:** Biological Crystallography, Malden, v. 66, n. 4, p. 486–501, 2010.

EVANS, P. Scaling and assessment of data quality. **Acta Crystallographica Section D:** Biological Crystallography, Malden, v. 62, n. 1, p. 72–82, 2006.

FESTA, R. A.; THIELE, D. J. Copper: an essential metal in biology. **Current Biology**, Cambridge, v. 21, n. 21, p. 877–883, 2011.

FETHEROLF, M.; BOYD, S. D.; WINKLER, D. D.; WINGE, D. R. Oxygen-dependent activation of Cu,Zn-superoxide dismutase-1. **Metallomics**, Cambridge, v. 9, n. 8, p. 1047–1059, 2017 a.

FETHEROLF, M. M.; BOYD, S. D.; TAYLOR, A. B.; KIM, H. J.; WOHLSCHLEGEL, J. A.; BLACKBURN, N. J.; HART, P. J.; WINGE, D. R.; WINKLER, D. D. Copper-zinc superoxide dismutase is activated through a sulfenic acid intermediate at a copper ion entry site. **Journal of Biological Chemistry**, Bethesda, v. 292, n. 29, p. 12025–12040, 2017 b.

FLORES, A. G.; UNGER, V. M. Atox1 contains positive residues that mediate membrane association and aid subsequent copper loading. **Journal of Membrane Biology**, New York, v. 246, n. 12, p. 903–913, 2013.

FURUKAWA, Y.; O'HALLORAN, T. V. Amyotrophic lateral sclerosis mutations have the greatest destabilizing effect on the apo- and reduced form of SOD1, leading to unfolding and oxidative aggregation. **Journal of Biological Chemistry**, Bethesda, v. 280, n. 17, p. 17266–17274, 2005.

FURUKAWA, Y.; O'HALLORAN, T. V. Posttranslational modifications in Cu,Zn-superoxide dismutase and mutations associated with amyptrophic lateral sclerosis. **Antioxidants and Redox Signaling**, New Rochelle, v. 8, n. 5–6, p. 847–867, 2006.

FURUKAWA, Y.; TORRES, A. S.; O'HALLORAN, T. V. Oxygen-induced maturation of SOD1: a key role for disulfide formation by the copper chaperone CCS. **EMBO Journal**, Chichester, v. 23, n. 14, p. 2872–2881, 2004.

GERTSMAN, I.; WUU, J.; MCALONIS-DOWNES, M.; GHASSEMIAN, M.; LING, K.; RIGO, F.; BENNETT, F.; BENATAR, M.; MILLER, T. M.; DA CRUZ, S. An endogenous peptide marker differentiates SOD1 stability and facilitates pharmacodynamic monitoring in SOD1 amyotrophic lateral sclerosis. **JCI Insight**, Michigan, v. 4, n. 10, p. e122768, 2019.

GETZOFF, E. D.; TAINER, J. A.; WEINER, P. K.; KOLLMAN, P. A.; RICHARDSON, J. S.; RICHARDSON, D. C. Electrostatic recognition between superoxide and copper, zinc superoxide dismutase. **Nature**, London, v. 306, n. 5940, p. 287–290, 1983.

HALL, L. T.; SANCHEZ, R. J.; HOLLOWAY, S. P.; ZHU, H.; STINE, J. E.; LYONS, T. J.; DEMELER, B.; SCHIRF, V.; HANSEN, J. C.; NERSISSIAN, A. M.; VALENTINE, J. S.; HART, P. J. X-ray crystallographic and analytical ultracentrifugation analyses of truncated and full-length yeast copper chaperones for SOD (LYS7): a dimer- dimer model of LYS7-SOD association and copper delivery. **Biochemistry**, Washington, v. 39, n. 13, p. 3611–3623, 2000.

HARTZ, J. W.; DEUTSCH, H. F. Subunit structure of human superoxide dismutase. **Journal of Biological Chemistry**, Bethesda, v. 247, n. 21, p. 7043–7050, 1972.

HIPP, M. S.; PARK, S. H.; HARTL, U. U. Proteostasis impairment in protein-misfolding and -aggregation diseases. **Trends in Cell Biology**, Kidlington, v. 24, n. 9, p. 506–514, 2014.

HÖRNBERG, A.; LOGAN, D. T.; MARKLUND, S. L.; OLIVEBERG, M. The coupling between disulphide status, metallation and dimer interface strength in Cu/Zn superoxide dismutase. **Journal of Molecular Biology**, London, v. 365, n. 2, p. 333–342, 2007.

HOUGH, M. A.; GROSSMANN, J. G.; ANTONYUK, S. V.; STRANGE, R. W.; DOUCETTE, P. A.; RODRIGUEZ, J. A.; WHITSON, L. J.; HART, P. J.; HAYWARD, L. J.; VALENTINE, J. S.; HASNAIN, S. S. Dimer destabilization in superoxide dismutase may result in disease-causing properties: structures of motor neuron disease mutants. **Proceedings of the National Academy of Sciences of the United States of America**, Washington, v. 101, n. 16, p. 5976–5981, 2004.

JEN, A.; MERKLE, H. P. Diamonds in the rough: protein crystals from a formulation perspective. **Pharmaceutical Research**, New York, v. 18, n. 11, p. 1483–1488, 2001.

KABSCH, W. XDS. **Acta Crystallographica Section D:** Biological Crystallography, Malden, v. 66, n. 2, p. 125–132, 2010.

KAHRA, D.; KOVERMANN, M.; WITTUNG-STAFSHEDE, P. The C-Terminus of human copper importer Ctr1 acts as a binding site and transfers copper to Atox1. **Biophysical Journal**, Saint Louis, v. 110, n. 1, p. 95–102, 2016.

KARCH, C. M.; PRUDENCIO, M.; WINKLER, D. D.; HART, P. J.; BORCHELT, D. R. Role of mutant SOD1 disulfide oxidation and aggregation in the pathogenesis of familial ALS. **Proceedings of the National Academy of Sciences of the United States of America**, Washington, v. 106, n. 19, p. 7774–7779, 2009.

KEELE, B. B.; MCCORD, J. M.; FRIDOVICH, I. Further characterization of bovine superoxide dismutase and its isolation from bovine heart. **Journal of Biological Chemistry**, Bethesda, v. 246, n. 9, p. 2875–2880, 1971.

KRAUSS, I. R.; MERLINO, A.; VERGARA, A.; SICA, F. An overview of biological macromolecule crystallization. **International Journal of Molecular Sciences**, Basel, v. 14, n. 6, p. 11643–11691, 2013.

KRISSINEL, E.; HENRICK, K. Inference of Macromolecular Assemblies from Crystalline State. **Journal of Molecular Biology**, London, v. 372, n. 3, p. 774–797, 2007.

LAMB, A. L.; WERNIMONT, A. K.; PUFAHL, R. A.; O'HALLORAN, T. V.; ROSENZWEIG, A. C. Crystal structure of the copper chaperone for superoxide dismutase. **Nature Structural Biology**, London, v. 6, n. 8, p. 724–729, 1999.

LAMB, A. L.; WERNIMONT, A. K.; PUFAHL, R. A.; O'HALLORAN, T. V.; ROSENZWEIG, A. C. Crystal structure of the second domain of the human copper chaperone for superoxide dismutase. **Biochemistry**, Washington, v. 39, n. 7, p. 1589–1595, 2000.

LAMB, A. L.; TORRES, A. S.; O'HALLORAN, T. V.; ROSENZWEIG, A. C. Heterodimeric structure of superoxide dismutase in complex with its metallochaperone. **Nature Structural Biology**, London, v. 8, n. 9, p. 751–755, 2001.

LEE, J.; PETRIS, M. J.; THIELE, D. J. Characterization of mouse embryonic cells deficient in the Ctr1 high affinity copper transporter: identification of a Ctr1-independent copper transport system. **Journal of Biological Chemistry**, Bethesda, v. 277, n. 43, p. 40253–40259, 2002.

LINDBERG, M. J.; NORMARK, J.; HOLMGREN, A.; OLIVEBERG, M. Folding of human superoxide dismutase: disulfide reduction prevents dimerization and produces marginally stable monomers. **Proceedings of the National Academy of Sciences of the United States of America**, Washington, v. 101, n. 45, p. 15893–15898, 2004.

MACDIARMID, C. W. Zinc transporters that regulate vacuolar zinc storage in Saccharomyces cerevisiae. **The EMBO Journal**, Chichester, v. 19, n. 12, p. 2845–2855, 2000.

MANN, T.; KEILIN, D. Haemocuprein and hepatocuprein, copper-protein compounds of blood and liver in mammals. **Proceedings of the Royal Society of London B Biological Sciences**, Washington, v. 126, n. 844, p. 303–315, 1938.

MCALARY, L.; PLOTKIN, S. S.; YERBURY, J. J.; CASHMAN, N. Prion-like propagation of protein misfolding and aggregation in amyotrophic lateral sclerosis. **Frontiers in Molecular Neuroscience**, Lausanne, v. 12, n. 262, p. 1–21, 2019.

MCCORD, J. M.; FRIDOVICH, I. Superoxide dismutase an enzyme function for erythrocuprein. **The Journal of Biological Chemistry**, Bethesda, v. 244, n. 22, p. 6094–6055, 1969.

MCCOY, A. J.; GROSSE-KUNSTLEVE, R. W.; ADAMS, P. D.; WINN, M. D.; STORONI, L. C.; READ, R. J. Phaser crystallographic software. **Journal of Applied Crystallography**, Chichester, v. 40, n. 4, p. 658–674, 2007.

MOHAMED, M. S.; GREENBERG, D. M. Isolation of purified copper protein from horse liver. **The Journal of General Physiology**, New York, v. 37, n. 4, p. 433–439, 1954.

MÜNCH, C.; BERTOLOTTI, A. Exposure of hydrophobic surfaces initiates aggregation of diverse ALS-causing superoxide dismutase-1 mutants. **Journal of Molecular Biology**, London, v. 399, n. 3, p. 512–525, 2010.

MURPHY, R. M. Static and dynamic light scattering of biological macromolecules: what can we learn? **Current Opinion in Biotechnology**, Kidlington, v. 8, n. 1, p. 25–30, 1997.

MURSHUDOV, G. N.; SKUBÁK, P.; LEBEDEV, A. A.; PANNU, N. S.; STEINER, R. A.; NICHOLLS, R. A.; WINN, M. D.; LONG, F.; VAGIN, A. A. REFMAC5 for the refinement of macromolecular crystal structures. **Acta Crystallographica Section D:** Biological Crystallography, Malden, v. 67, n. 4, p. 355–367, 2011.

O'HALLORAN, T. V.; CULOTTA, V. C. Metallochaperones, an intracellular shuttle service for metal ions. **Journal of Biological Chemistry**, Bethesda, v. 275, n. 10, p. 25057–25060, 2000.

OCHI, T.; BOLANOS-GARCIA, V. M.; STOJANOFF, V.; MORENO, A. Perspectives on protein crystallisation. **Progress in Biophysics and Molecular Biology**, Oxford, v. 101, n. 1–3, p. 56–63, 2009.

OKADO-MATSUMOTO, A.; FRIDOVICH, I. Subcellular distribution of Superoxide Dismutases (SOD). **Journal of Biological Chemistry**, Bethesda, v. 276, n. 42, p. 38388–38393, 2001.

OUTTEN, C. E.; O'HALLORAN, T. V. Femtomolar sensitivity of metalloregulatory proteins controlling zinc homeostasis. **Science**, Washington, v. 292, n. 5526, p. 2488–2492, 2001.

PANTOLIANO, M. W.; VALENTINE, J. S.; BURGER, A. R.; LIPPARD, S. J. A pH-dependent superoxide dismutase activity for zinc-free bovine erythrocuprein. Reexamination of the role of zinc in the holoprotein. **Journal of Inorganic Biochemistry**, Philadelphia, v. 17, n. 4, p. 325–341, 1982.

PARGE, H. E.; HALLEWELL, R. A; TAINER, J. A. Atomic structures of wild-type and thermostable mutant recombinant human Cu,Zn superoxide dismutase. **Proceedings of the National Academy of Sciences of the United States of America**, Washington, v. 89, n. July, p. 6109–6113, 1992.

PETTERSEN, E. F.; GODDARD, T. D.; HUANG, C. C.; COUCH, G. S.; GREENBLATT, D. M.; MENG, E. C.; FERRIN, T. E. UCSF Chimera - a visualization system for exploratory research and analysis. **Journal of Computational Chemistry**, Hoboken, v. 25, n. 13, p. 1605–1612, 2004.

POPE, C. R.; DE FEO, C. J.; UNGER, V. M. Cellular distribution of copper to superoxide dismutase involves scaffolding by membranes. **Proceedings of the National Academy of Sciences of the United States of America**, Washington, v. 110, n. 51, p. 20491–20496, 2013.

RAE, T. D.; SCHMIDT, P. J.; PUFAHL, R. A.; CULOTTA, V. C.; O'HALLORAN, T. V. Undetectable intracellular free copper: the requirement of a copper chaperone for superoxide dismutase. **Science**, Washington, v. 284, n. 5415, p. 805–808, 1999.

RAE, T. D.; TORRES, A. S.; PUFAHL, R. A.; O'HALLORAN, T. V. Mechanism of Cu,Zn-superoxide dismutase activation by the human metallochaperone hCCS. **Journal of Biological Chemistry**, Bethesda, v. 276, n. 7, p. 5166–5176, 2001.

RAKHIT, R.; CHAKRABARTTY, A. Structure, folding, and misfolding of Cu,Zn superoxide dismutase in amyotrophic lateral sclerosis. **Biochimica et Biophysica Acta:** Molecular Basis of Disease, Amsterdam, v. 1762, n. 11–12, p. 1025–1037, 2006.

RHODES, G. **Crystallograhy made crystal clear**. 3. ed. San Diego: Elsevier, 2006.

ROBINETT, N. G.; PETERSON, R. L.; CULOTTA, V. C. Eukaryotic copper-only superoxide dismutases (SODs): a new class of SOD enzymes and SOD-like protein domains. **Journal of Biological Chemistry**, Bethesda, v. 293, n. 13, p. 4636–4643, 2018.

ROBINSON, N. J.; WINGE, D. R. Copper metallochaperones. **Annual Review of Biochemistry**, Palo Alto, v. 79, p. 537–562, 2010.

RODRIGUEZ, J. A.; SHAW, B. F.; DURAZO, A.; SOHN, S. H.; DOUCETTE, P. A.; NERSISSIAN, A. M.; FAULL, K. F.; EGGERS, D. K.; TIWARI, A.; HAYWARD, L. J.; VALENTINE, J. S. Destabilization of apoprotein is insufficient to explain Cu,Zn-superoxide dismutase-linked ALS pathogenesis. **Proceedings of the National Academy of Sciences of the United States of America**, Washington, v. 102, n. 30, p. 10516–10521, 2005.

RUPP, B. **Biomolecular crystallography:** principles, practice, and ppplication to structural biology. New York: Garland Science, 2010.

SACCON, R. A.; BUNTON-STASYSHYN, R. K. A.; FISHER, E. M. C.; FRATTA, P. Is SOD1 loss of function involved in amyotrophic lateral sclerosis? **Brain**, Oxford, v. 136, n. 8, p. 2342–2358, 2013.

SALA, F. A.; WRIGHT, G. S. A.; ANTONYUK, S. V.; GARRATT, R. C.; HASNAIN, S. S. Molecular recognition and maturation of sod1 by its evolutionarily destabilised cognate chaperone hCCS. **Plos Biology**, San Francisco, v. 17, n. 2, p. 1–22, 2019.

SCHMIDT, P. J.; RAE, T. D.; PUFAHL, R. A.; HAMMA, T.; STRAIN, J.; O'HALLORAN, T. V.; CULOTTA, V. C. Multiple protein domains contribute to the action of the copper chaperone for superoxide dismutase. **Journal of Biological Chemistry**, Bethesda, v. 274, n. 34, p. 23719–23725, 1999.

SEA, K.; SOHN, S. H.; DURAZO, A.; SHENG, Y.; SHAW, B. F.; CAO, X.; TAYLOR, A. B.; WHITSON, L. J.; HOLLOWAY, S. P.; HART, P. J.; CABELLI, D. E.; GRALLA, E. B.; VALENTINE, J. S. Insights into the role of the unusual disulfide bond in copper-zinc superoxide dismutase. **Journal of Biological Chemistry**, Bethesda, v. 290, n. 4, p. 2405–2418, 2015.

SKOPP, A.; BOYD, S. D.; ULLRICH, M. S.; LIU, L.; WINKLER, D. D. Copper–zinc superoxide dismutase (Sod1) activation terminates interaction between its copper chaperone (Ccs) and the cytosolic metal-binding domain of the copper importer Ctr1. **BioMetals**, Dordrecht, v. 3, p. 695–705, 2019.

SLOTBOOM, D. J.; DUURKENS, R. H.; OLIEMAN, K. E.; GUUS, B. Static light scattering to characterize membrane proteins in detergent solution. **Methods**, Maryland Heights, v. 46, n. 2, p. 73–82, 2008.

SMITH, M. W.; DOOLITTLE, R. F. A comparison of evolutionary rates of the two major kinds of superoxide dismutase. **Journal of Molecular Evolution**, New York, v. 34, n. 2, p. 175–184, 1992.

STATHOPULOS, P. B.; RUMFELDT, J. A. O.; KARBASSI, F.; SIDDALL, C. A.; LEPOCK, J. R.; MEIERING, E. M. Calorimetric analysis of thermodynamic stability and aggregation for Apo and Holo amyotrophic lateral sclerosis-associated Gly-93 mutants of superoxide dismutase. **Journal of Biological Chemistry**, Bethesda, v. 281, n. 10, p. 6184–6193, 2006.

STRANGE, R. W.; ANTONYUK, S. V.; HOUGH, M. A.; DOUCETTE, P. A.; VALENTINE, J. S.; HASNAIN, S. S. Variable metallation of human superoxide dismutase: atomic resolution crystal structures of Cu-Zn, Zn-Zn and as-isolated wild-type enzymes. **Journal of Molecular Biology**, London, v. 356, n. 5, p. 1152–1162, 2006.

SUHY, D. A.; SIMON, K. D.; LINZER, D. I. H.; O'HALLORAN, T. V. Metallothionein is part of a zinc-scavenging mechanism for cell survival under conditions of extreme zinc deprivation. **Journal of Biological Chemistry**, Bethesda v. 274, n. 14, p. 9183–9192, 1999.

TAINER, J. A.; GETZOFF, E. D.; BEEM, K. M.; RICHARDSON, J. S.; RICHARDSON, D. C. Determination and analysis of the 2 Å structure of copper, zinc superoxide dismutase. **Journal of Molecular Biology**, London, v. 160, n. 2, p. 181–217, 1982.

TAINER, J. A.; GETZOFF, E. D.; RICHARDSON, J. S.; RICHARDSON, D. C. Structure and mechanism of copper, zinc superoxide dismutase. **Nature**, London, v. 306, n. 5940, p. 284–287, 1983.

TARAZONA, M. P.; SAIZ, E. Combination of SEC/MALS experimental procedures and theoretical analysis for studying the solution properties of macromolecules. **Journal of Biochemical and Biophysical Methods**, Amsterdam, v. 56, n. 1–3, p. 95–116, 2003.

TOKUDA, E.; FURUKAWA, Y. Copper homeostasis as a therapeutic target in amyotrophic lateral sclerosis with SOD1 mutations. **International Journal of Molecular Sciences**, Basel, v. 17, n. 5, p. 1–14, 2016.

TRUMBULL, K. A.; BECKMAN, J. S. A role for copper in the toxicity of zinc-deficient superoxide dismutase to motor neurons in amyotrophic lateral sclerosis. **Antioxidants and Redox Signaling**, New Rochelle, v. 11, n. 7, p. 1627–1639, 2009.

TYLER, D. D. Polarographic assay and intracellular distribution of superoxide dismutase in rat liver. **Biochemical Journal**, London, v. 147, p. 493–504, 1975.

VASSALL, K. A.; STUBBS, H. R.; PRIMMER, H. A.; TONG, M. S.; SULLIVAN, S. M.; SOBERING, R.; SRINIVASAN, S.; BRIERE, L. A. K.; DUNN, S. D.; COLÓN, W.; MEIERING, E. M. Decreased stability and increased formation of soluble aggregates by immature superoxide dismutase do not account for disease severity in ALS. **Proceedings of the National Academy of Sciences of the United States of America**, Washington, v. 108, n. 6, p. 2210–2215, 2011.

VEHVILÄINEN, P.; KOISTINAHO, J.; GOLDSTEINS, G. Mechanisms of mutant SOD1 induced mitochondrial toxicity in amyotrophic lateral sclerosis. **Frontiers in Cellular Neuroscience**, Lausanne, v. 8, n. 126, p. 1–7, 2014.

WATERHOUSE, A.; PROCTER, J. B.; MARTIN, D. M. A.; CLAMP, M.; BARTON, G. J. Jalview Version 2-A multiple sequence alignment editor and analysis workbench. **Bioinformatics**, Oxford, v. 25, n. 9, p. 1189–1191, 2009.

WEISIGER, R. A.; FRIDOVICH, I. Mitochondrial superoxide simutase. Site of synthesis and intramitochondrial localization. **The Journal of Biological Chemistry**, Bethesda, v. 248, n. 13, p. 4793–4796, 1973.

WILCOX, K. C.; ZHOU, L.; JORDON, J. K.; HUANG, Y.; YU, Y.; REDLER, R. L.; CHEN, X.; CAPLOW, M.; DOKHOLYAN, N. V. Modifications of superoxide dismutase (SOD1) in human erythrocytes: a possible role in amyotrophic lateral sclerosis. **Journal of Biological Chemistry**, Bethesda, v. 284, n. 20, p. 13940–13947, 2009.

WLODAWER, A.; MINOR, W.; DAUTER, Z.; JASKOLSKI, M. Protein crystallography for non-crystallographers, or how to get the best (but not more) from published macromolecular structures. **FEBS Journal**, Chichester, v. 275, n. 1, p. 1–21, 2008.

WONG, P. C.; WONG, P. C.; WAGGONER, D.; SUBRAMANIAM, J. R.; TESSAROLLO, L.; BARTNIKAS, T. B.; CULOTTA, V. C.; PRICE, D. L.; ROTHSTEIN, J.; GITLIN, J. D. Copper chaperone for superoxide dismutase is essential to activate mammalian Cu/Zn superoxide dismutase. **Proceedings of the National Academy of Sciences of the United States of America**, Washington, v. 97, n. 6, p. 2886–2891, 2000.

WRIGHT, G. S. A.; ANTONYUK, S. V.; KERSHAW, N. M.; STRANGE, R. W.; HASNAIN, S. S. Ligand binding and aggregation of pathogenic SOD1. **Nature Communications**, London, v. 4, p. 1710–1758, 2013.

WRIGHT, G. S. A.; ANTONYUK, S. V.; HASNAIN, S. S. A faulty interaction between SOD1 and hCCS in neurodegenerative disease. **Scientific Reports**, London, v. 6, p. 1–9, 2016.

WRIGHT, G. S. A.; ANTONYUK, S. V.; HASNAIN, S. S. The biophysics of superoxide dismutase-1 and amyotrophic lateral sclerosis. **Quarterly reviews of biophysics**, Cambridge, v. 52, n. e12, p. 1–39, 2019.

WRIGHT, G. S. A.; HASNAIN, S. S.; GROSSMANN, J. G. The structural plasticity of the human copper chaperone for SOD1: insights from combined size-exclusion chromatographic and solution X-ray scattering studies. **Biochemical Journal**, London, v. 439, n. 1, p. 39–44, 2011.

WYATT, P. J. Mean square radius of molecules and secondary instrumental broadening. **Journal of Chromatography A**, Amsterdam, v. 648, n. 1, p. 27–32, 1993.

YERBURY, J. J.; OOI, L.; DILLIN, A.; SAUNDERS, D. N.; HATTERS, D. M.; BEART, P. M.; CASHMAN, N. R.; WILSON, M. R.; ECROYD, H. Walking the tightrope: proteostasis and neurodegenerative disease. **Journal of Neurochemistry**, Chichester, v. 137, n. 4, p. 489–505, 2016.

YOUN, H. D.; KIM, E. J.; ROE, J. H.; HAH, Y. C.; KANG, S. O. A novel nickel-containing superoxide dismutase from Streptomyces spp. **Biochemical Journal**, London, v. 318, n. 3, p. 889–896, 1996.

ZIMM, Bruno H. The scattering of light and the radial distribution function of high polymer solutions. **The Journal of Chemical Physics**, Melville, v. 16, n. 12, p. 1093–1099, 1948.